UNIVERSITY OF OKLAHOMA

GRADUATE COLLEGE

INVESTIGATION OF CASING DEFORMATION DURING HYDRAULIC FRACTURING CONSIDERING WELLBORE CENTRALIZATION AND CEMENT VOIDS

A THESIS

SUBMITTED TO THE GRADUATE FACULTY

in partial fulfillment of the requirements for the

Degree of

MASTER OF SCIENCE

By

MICHAEL FERNANDO MENDEZ RESTREPO
Norman, Oklahoma
2018

INVESTIGATION OF CASING DEFORMATION DURING HYDRAULIC FRACTURING CONSIDERING WELLBORE CENTRALIZATION AND CEMENT VOIDS

A THESIS APPROVED FOR THE
MEWBOURNE SCHOOL OF PETROLEUM AND GEOLOGICAL ENGINEERING

BY

Dr. Catalin Teodoriu, Chair

Dr. Xingru Wu

Dr. Saeed Salehi

This work is dedicated to my father, mother and brother whose unconditional support have helped me to accomplish all the goals during this journey.

Acknowledgements

I would like to express my deepest gratitude to my advisor Dr. Catalin Teodoriu for his guidance and mentoring throughout this work and my master studies. To Dr. Xingru Wu that allowed me to work in this research and provided his continued guidance throughout all the process. To Dr. Saeed Salehi for his support and recommendations in this work.

To my friend Yuliana Zapata who helped me in the edition and formatting of this work. To my friend Ruben Gonzales who helped me editing and improving several graphs developed in this study.

To my friends Ziyi Xu and Xiaye Wu who shared information regarding this project and help me translating information from a different language.

To my friends Laura Hernandez, Any Ordoñez, Andrea Lopez, Antonio Marquez and Adonis-Costin Ichim for the continuous support during this project, and all other friends who directly or indirectly supported me to accomplish my goals during my master degree.

Table of Contents

List of Tables

List of Figures

Abstract

The fast growth of shale gas development through horizontal drilling and hydraulic fracturing has expanded the extraction of hydrocarbon resources in countries such as the United States, China, and Argentina. Even though the technology of fracturing low permeable shale can be replicated in different reservoirs, factors such as flow regime, high horizontal stress anisotropy, formation temperature and quantity of natural fractures will dictate several changes and considerations in the completion design.

High rates and pressures applied during hydraulic fracturing in a long horizontal section could induce wellbore integrity issues. This work will focus on researching how the integrity of the cement and casing is affected during these operations. A finite element analysis (FEA) was performed in order to study the stress concentration in casing and cement. The yield criterion of equivalent von Mises stress was applied in order to verify if the stresses were exceeding the casing yield strength and the cement compressive strength. The majority of the input parameters were based on a real case of casing deformation during hydraulic fracturing in a shale gas play in China.

The effect of wellbore centralization in wellbore integrity was the main parameter modeled in this work. It was demonstrated that a poor centralization that contributes to the formation of drilling fluid voids in the cement will induce casing failure during hydraulic fracturing operations. The equivalent maximum stress can increase from three to four times in casing and cement from a concentric case to an eccentric case in a cement sheath with voids. Boundary conditions were also studied in order to evaluate if the stress impact on the casing and cement are different and significant.

1. Introduction

1.1 Motivation

Successful production of hydrocarbons from the reservoirs in a safe, cost efficient, and environmental friendly way is the primarily goal in the oil and gas industry. The most critical process for accomplish this objective comes with the drilling and completion operations of the well since it represents the most expensive portion of its life cycle. These high costs are associate to rig day rental and hydraulic fracturing operations.

Horizontal drilling and hydraulic fracturing are fundamental in order to develop oil and gas shale worldwide. Rotary drilling consists of the mechanical energy transfer from the top to the drilling bit with the rotation of the drilling pipe by the rotary system. The rotary system applies the torque to rotate the entire string and drilling bit, and the weight-on-bit is controlled by the hosting system. All the rock cuttings are lift by the drilling fluids. All this is developed in a vertical, curve and horizontal section.

Hydraulic fracturing comes after drilling and consist of injecting high volumes at high pressure to do an extensive fracturing in the rock in order to create new paths for the oil to displace to the well. Since shales wells are low in permeability, this is the only technique available to produce oil and gas from them for now.

The optimization and effectiveness of the drilling and completion process depends upon many factors such as the technology available at the area of operations, depth of the target reservoir, geological and rock mechanics properties, production requirement to be economically sustainable, human factor, among others. One of the most critical factor or possibly the most critical one is wellbore integrity since it carries environmental implications.

Well integrity defects increase the risk of uncontrolled release of formation fluids throughout the life cycle of a wells. If the defect occurs in early stages such as hydraulic fracturing operations, it might not allow the entire process to be completed since completion tools won't be able to access the casing or injected fluids won't be reach their destination.

1.2 Problem Statement

Increase in energy demand impulse by the economic growth of emergent nations makes oil, natural gas along with nuclear power to play the major role in this unprecedented increase. Therefore, countries who do not possess extensive conventional reservoirs are moving to unconventional reservoir such as thigh gas, and shale oil and gas.

The development of shale plays requires new and improved technology such as horizontal drilling and extensive hydraulic fracturing. Most of the recent research has been focus on the development of these plays not only because their current demand but also for their cost and complexity. Producing from this wells could be two or three times more expensive than conventional wells since formation properties are different such as permeability (low values), hence the reservoir contact needs to be higher and new paths (fractures) needs to be created. Any delayed, difficulty or failure during these activities will have a strong impact in the well expenses, especially when the wellbore integrity is involved

The interaction between casing, cement, and formation strongly influence the integrity of a wellbore, and makes the understanding of the mechanical properties of all wellbore components vital. The long-term wellbore integrity depends on several factors that includes the eccentricity of the casing in the wellbore and the annular clearance between casing and wellbore wall - usually called standoff, with 100% standoff when the casing and the wellbore are concentric, and 0% standoff when the casing touches the borehole or the previous casing (Figure 1).

The eccentricity of the wellbore mainly depends on the forces around the casing, such as material weight and applied tension or compression. Therefore, the casing will be in different positions throughout the wellbore trajectory, as shown in Figure 1.

With the need of long horizontal sections, eccentricity will be more frequent if a proper centralization is not present. The casing will tend to lay in the bottom part of the wellbore because of its material weight. In addition, tortuosity might be present as well during the horizontal trajectory making more tedious a good centralization.

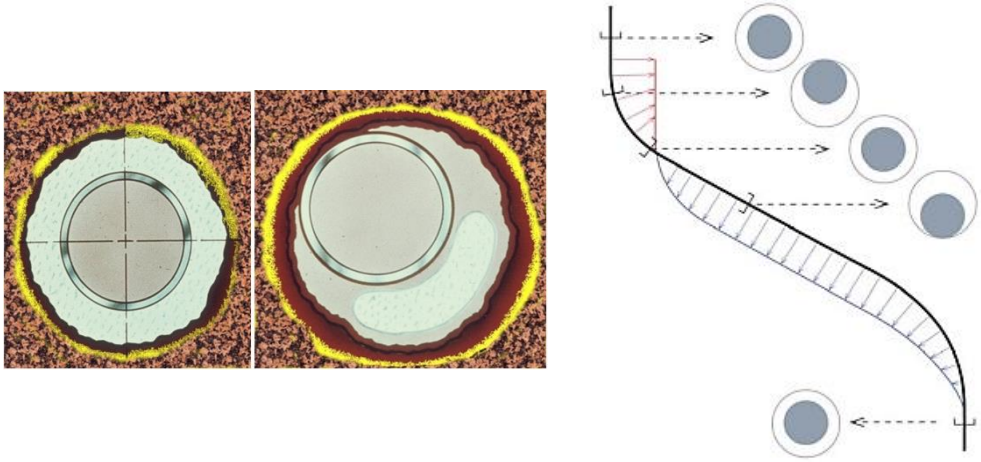

Figure 1. Wellbore eccentricity and casing standoff (Farley & Scott, 2011) and (G. Liu & Weber, 2012)

If eccentricity is present in the wellbore, there is a high chance of having a poor cementation. Even for a concentric casing, there is still a chance of formation of voids and channels, so the chances of happening in an eccentric casing are much higher (Lavrov, Todorovic, & Torsæter, 2016). When the cement is being pumped to displace the drilling mud in the wellbore in an eccentric casing, some drilling mud will remain in the area where the annular space between the casing and the cement is lower, as shown in Figure 2. Therefore, the cement sheath will not be complete. Logs run in different fields around the world have confirmed this concept.

Figure 3 shows a real case of a well in the Changning-Weiyuan shale gas field where channeling was observed in a narrower side of the annulus (Xi, Li, Liu, Cha, & Fu, 2017). Casing deformation is observed at the same location which confirms the importance of a deep analysis in the effect of standoff in casing integrity.

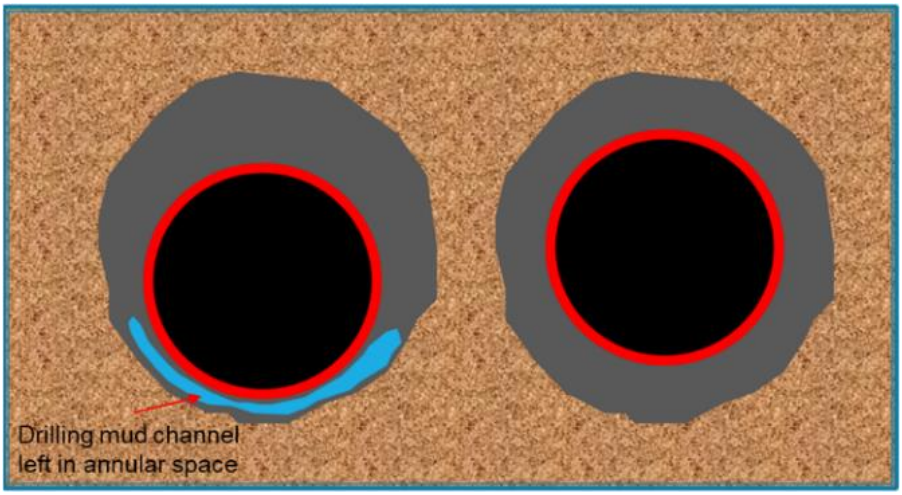

Figure 2. Drilling mud channels left in the cement sheath

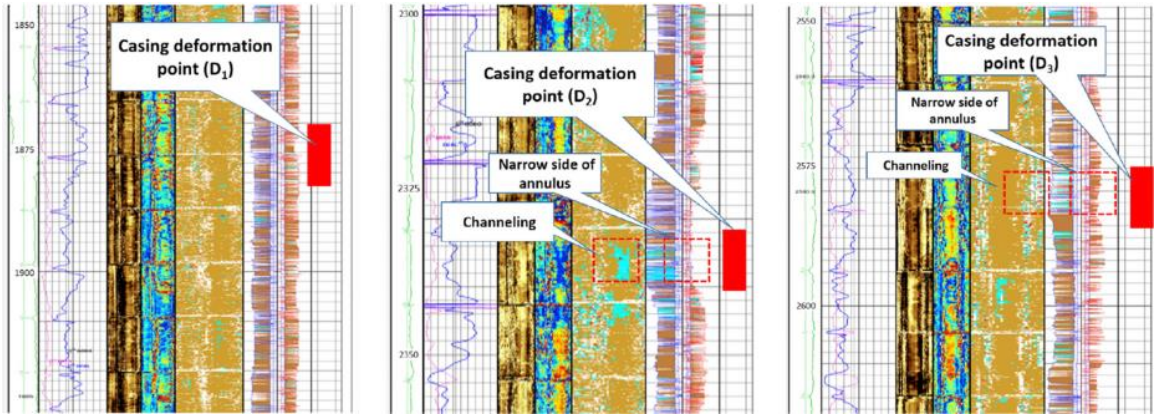

Figure 3. Image logging of H601-1 Well (Xi et al., 2017)

Casing centralization in the wellbore or in another casing string is usually expressed as percentage standoff (%). This is calculated as $Standoff$=C/(A−B) * 100, where C is the shortest distance between the pipe wall and the wellbore, A is the hole diameter and B the pipe outer diameter, expressed in units of length (Figure 4).

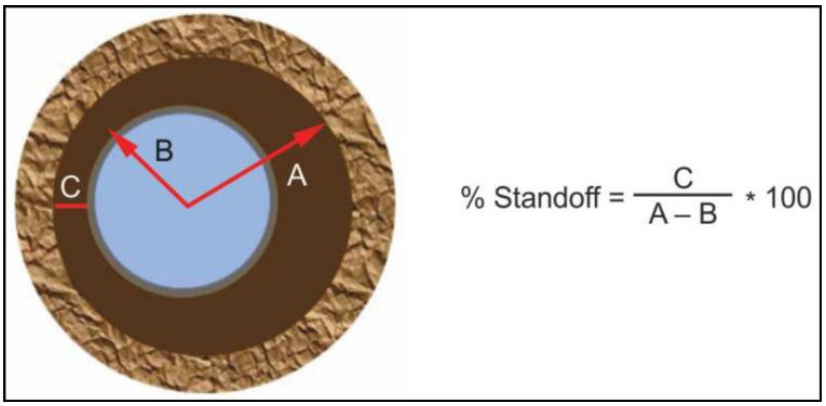

Figure 4. Standoff ratio (Fry & Pruett, 2015)

1.3 Objective

The main objective of this thesis is to study the reason of casing deformation during hydraulic fracturing in some shale oil and gas wells. This study will be performed trough finite element analysis considering all the good practices of a good wellbore integrity. The input parameters will be based primarily in a real case of casing deformation in the Changning-Weiyuan (C-W) shale gas play (Sichuan Basin of China) operated by China National Petroleum Company (CNPC) [cite the reference papers]. Recommendations about good practices during drilling and completion operations and suggestions in the well planning stage to reduce casing deformation in these reservoirs will be provided based on the results of this study.

2. State of Art

2.1 Hydraulic fracturing basics

According to (Gandossi, 2013), hydraulic fracturing has been used for reservoir stimulation since 1949, so it is not a new technique for hydrocarbon extraction. Gandossi also mentioned that the use of high volumes of hydraulic fracturing fluids compare to conventional procedures started in 1968. Later, it was accompanied with horizontal drilling in the late 1980s, and the use of chemicals known as "slickwater fracturing" from 1997.

Currently, because of technology advances that have allowed producing gas and oil from unconventional reservoirs (tight sands, coal beds and shale formations), hydraulic fracturing has become a very frequent and popular technique, especially in the United States, China and Argentine. For instance, development of multi-well pad along with horizontal drilling and hydraulic fracturing has made gas production technically and economically feasible in those plays (Gandossi, 2013).

The technique of hydraulic fracturing consists of pumping liquid at high pressure to fracture the reservoir rocks. The pressure needs to be enough to exceed the fracture strength of the rock but not too high to do not lose control over the fracture length and width. The liquid is usually a water based fluid with small portions of chemicals also known as "additives" such as surfactants, clay-stabilizing agents, among others, and solid particles known as "proppants" as seen in Figure 5 (Goverment of Western Australia, 2015).

The hydraulic fracture design depends enormously on the permeability of the reservoir. Therefore, the hydraulic fracture significantly adds both to well productivity and to the well reserves in low-permeability reservoirs (less than 1 md for oil and 0.01 md for gas) in comparison to moderate permeability ones. Every hydraulic fracture can be characterized by its length,

conductivity, and related equivalent skin effect. (Economides, Hill, Ehlig-Economides, & Zhu, 2013)

The magnitude and direction of the in-situ stresses also plays an important in the hydraulic fracturing designed. The completion program might consider if it is required a specific shape of the hydraulic fracture such as transverse or longitudinal (Figure 6). Fractures will tend to open in the direction of the minimum stress that could be the minimum horizontal stress or the vertical stress depending of the fault regime.

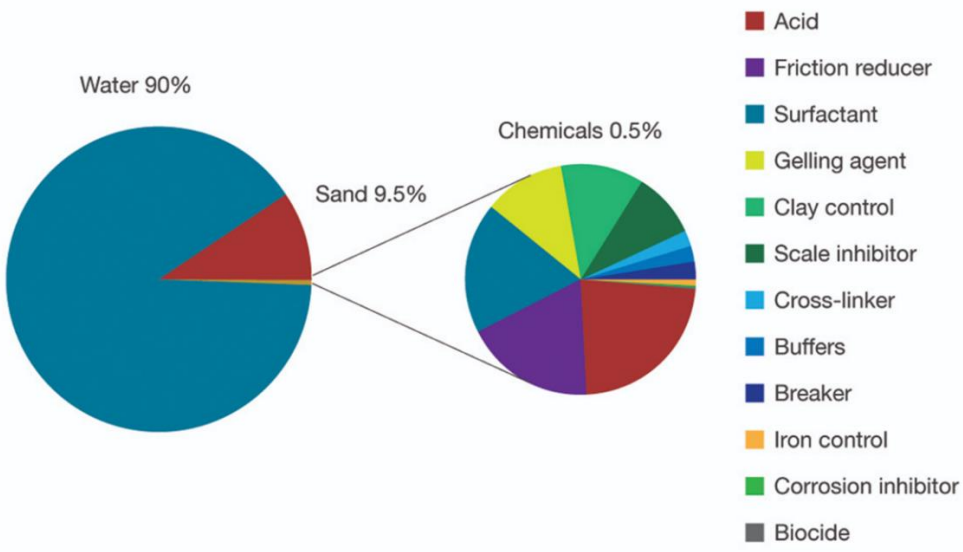

Figure 5. Typical fracture fluid composition (Goverment of Western Australia, 2015)

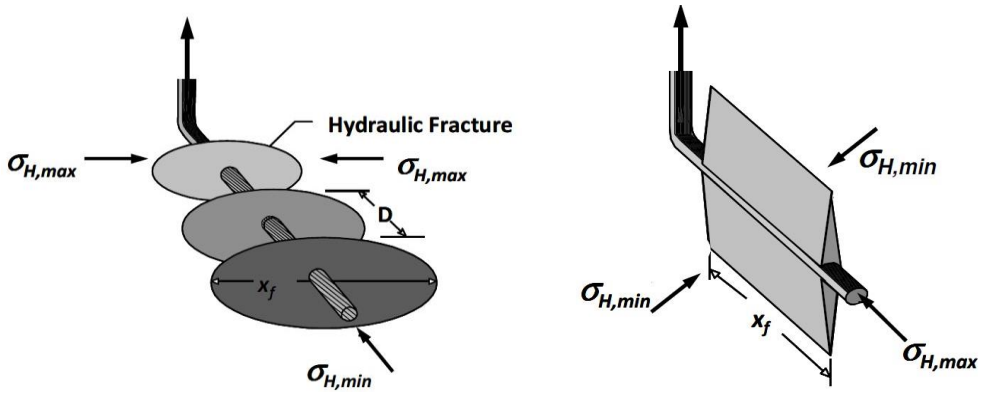

Figure 6. Transverse or longitudinal hydraulic fractures

2.2 Completion of horizontal wells in shales

High viscosity fluids (cross-linked gel), low viscosity fluids (linear gel and slick water) and energized fluids (liquefied CO2 and N2) can be used for hydraulic fracturing operation in very tight shale reservoir. Nevertheless, the primary effort is always to fracture the entire target zone by setting up different mechanisms, or the combination of two or more fracturing fluids. Instead, very low permeability reservoirs need multistage fracturing of long horizontal wells with long fractures to increase the production rate after the fracture.

Slick water high rate injection which is a low viscosity fracturing fluid generates a long fracture but barely forces the fracture along the height. On the other hand, multistage injection that creates several fractures along the height may cover the entire target thickness, and connect some natural fractures in some cases (Figure 7). Nevertheless, the contrast in stress and rock properties within the target zone dictates the achieving of multiple long fractures.

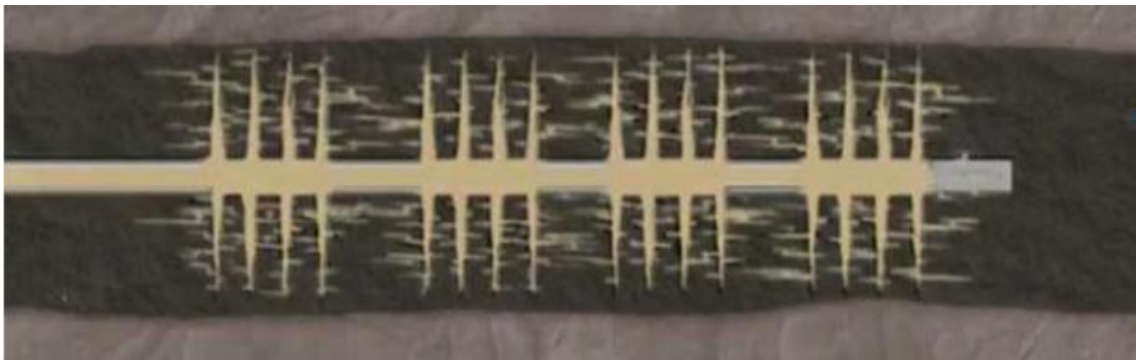

Figure 7. Example of intersection of hydraulic fractures with horizontal natural fractures in a multi-stage horizontal well (Bai, 2012).

Plug and perf and sliding sleeve with a cemented or non-cemented casing are the most common techniques in multi-stage fracturing. Either one is chosen depending of stress and rock properties and production objective. For instance, sliding sleeve has widely been used in the Bakken shale of the Williston Basin whereas Plug and Perf is commonly used in the Barnet shale of the Permian Basin. As an estimate at 2012, 30% of oil shale completions uses sliding sleeve while 70% of oil shale completions uses plug and perf. On the other hand, nearly 100% of gas shale completions uses the plug and perf technique. (Pearson, 2013)

The process of Plug and Perf involves pumping e-line perforating guns with a fracturing plug downhole. The guns are activated to perforate a sequence of spaced perforation clusters within each lateral stage and then extracted from the hole. Then, in order to allow the hydraulic fracture fluids to be pumped through the exposed perforations above the plug, a ball is sent downhole to seal against the upper part of the plug which had been set. The procedure is repeated with new stages until the entire distance of the horizontal section is fractured. The plugs are then drilled out using coiled tubing or jointed pipe. Even tough different length of perforated stages had been undertaking, a range between 200 ft. to 500 ft. is typically completed.

Plug and perf can be performed in cemented or non-cemented casing with an unlimited number of prospective zones. Multiple perforated cluster can be completed per stage. The process is slow since each stage is perforated and stimulated, taking up to 5 hours per cycle. Since sometimes the basic assumption is that all perforation cluster would be treated equally regarding formation characteristic, inconsistencies in production results and post fracturing job will be occurring. Therefore, as mentioned previously, formation properties play an important role over the efficiency of plug and perf completions.

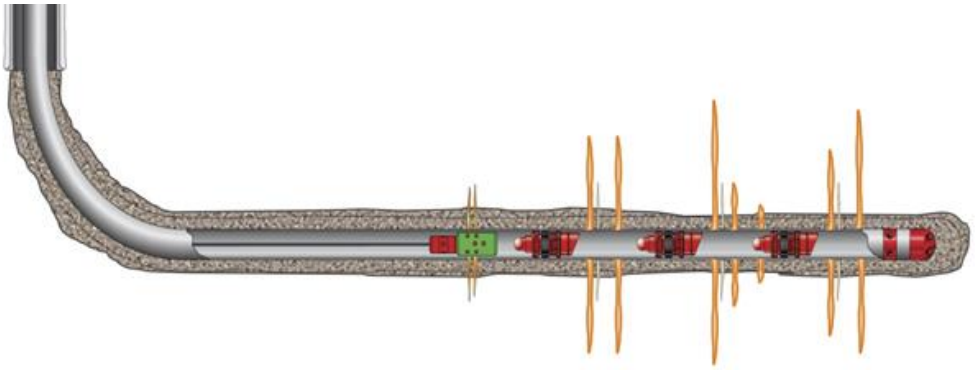

Figure 8. Plug and perf completion schematic (Stegent, 2016)

Ball-actuated sliding sleeves also known as mechanical isolators can be run in the openhole or inside a liner. The system consists of ported sleeves installed between isolation packers on a single liner string. Completion packers isolate the horizontal section into several stages. After the packers are set up, a ball is pumped within the fluid down the string seating in the mechanical sleeve. Then, the sleeve will open exposing the ports and diverting the fluid to the formation, which creates a hydraulic fracture within the isolated zone. Larger sized balls will progressively be pumped and the sleeves will be operated from the toe to the heel of the horizontal section. The balls and ball seats can be drilled out with coiled tubing. The well is cleaned out from the fluids inject by flow back operation naturally or artificially induced.

The plug and perf technique is typically limited to 20 stages and one opening per stage. Failure of balls and seats in the opening of the sliding sleeves along with the potential for limited insertion of the tool string are the challenges of this technology. It is faster in compare to the plug and perf method since allows for a quick and efficient fracture stimulation operation by minimizing fluid use, limiting trips downhole, and streamlining the pumping operation. The timing is driven by the completion designed and it takes between 1 to 2 hours per cycle.

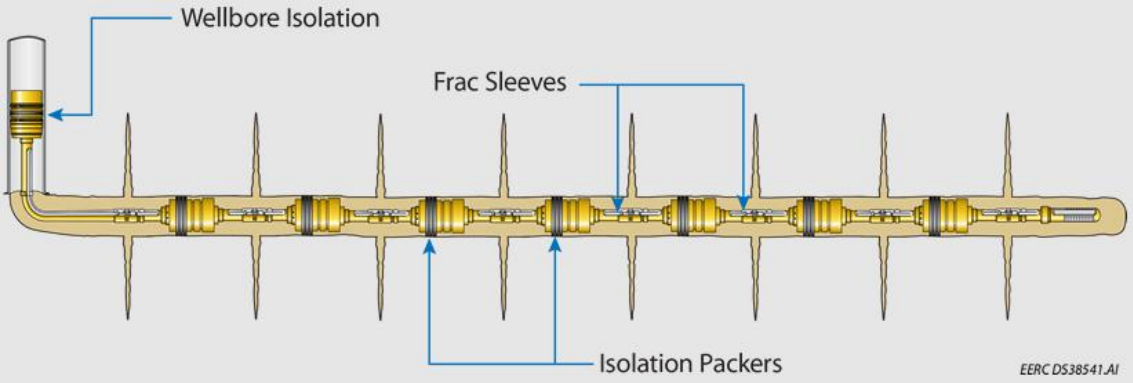

Figure 9. Sliding sleeve completion schematic (University of North Dakota EERC, 2014)

2.3 Conditions associated with casing failures during hydraulic fracturing

Casing's yield properties and fatigue limits are the main parameters that need to be considered when a casing fails. Table 1 shows the yield strength of several casing grades used in the industry. Hence, casing will fail if applied stresses and operating conditions exceeds those parameters. There are a lot of conditions that affect casing stress such as casing/hole configurations, fluid properties and surface operations.

Table 1. API casing grades (API Spec 5CT, 2011)

API Grade	Yield Strength	
	(Psi)	(MPa)
H-40	40000	276
J-55	55000	379
K-55	55000	379
N-80	80000	552
L-80	80000	552
C-90	90000	620
C-95	95000	655
T-95	95000	655
P-110	110000	758
Q-125	125000	862
P-140	140000	965

Well profile, dog-leg severity, cement height in the annulus, well components sizes, properties of annular fluids and corrosion are included in hole configurations. Pump rate, pressure and wellhead vibrations are included in surface operations. Temperature, type, size and quantity of proppants and acid concentration are included in fluid properties. Fluid mechanics such as internal fluid velocities, pressure and erosion are affected also by casing and coupling geometries. Bending, ballooning and buckling of the casing influence casing stress. Vibrations, dampening effects of the wellbore and cyclic operations affect the fatigue limit.

In order to successfully analyzed casing failure, it is necessary to quantify individually the conditions discuss previously that generate stresses, and then consequently combine them. Buckling, bending, ballooning, temperature changes can be quantified by equations available in the literature, but variables such as vibrations and fatigue are almost impossible to quantify nowadays. (Adams, Services, Mitchell, Eustes, & Sampaio, 2017)

2.3.1 Pump rate and pressure

Pump rates and pressure in hydraulic fracturing operations are unique and critical for casing failure since their high values are only experience during these operations. Pump rates are usually quite high in hydraulic fracturing operations reaching rates between 11 m3/min and 16 m3/min (70 bbl/min and 100 bbl/min). Vibrations will be generated at these high fluid rates affecting all the equipment going from surface to the last casing string. Pressures are also quite high since a downhole pressure of 110 MPa (16000 psi) might be needed in order to create a fracture in the formation

2.3.2 Temperature

The casing is exposed to dynamic temperature loads during hydraulic fracturing operations. In some fields worldwide the formation temperature can be 100°C or higher whereas the surface temperature can be 10°C. The hydraulic fracturing fluids are stored in frack tanks at rig location, therefore their temperature will be similar to 10°C or even lower. At the moment they are injected at high velocities, variations from the fluid's cooling effect can cause considerable stress increase or decrease in the casing. In addition, casing temperature will not be constant during hydraulic fracturing operation because pump rates variates during the operation or when the shut-down periods occurs, hence cooling and heating will be observed during the operations.

Thermal loads might induce casing failure. Casing will expand or contract in different sections at different rates. The difficulty of evaluating casing failure by thermal loads lies on the fact that casing cracks are similar in how it looks to fatigue or brittle cracks. A lot of research on thermal loads is ongoing, and this is the one of the primaries reasons this work will consider to analyze casing deformation under thermal load.

2.3.2.1 Cement voids in the cement

As mentioned earlier, voids or channels are left in the annular space between the casing and the wellbore, especially if the casing is not centralized, leading to a poor displacement of drilling fluids when the cementation is performed. These confined spaces are left with a respective fluid pressure similar to the hydrostatic pressure at the respective depth or to the pore pressure depending of the reservoir.

Annular pressure buildup (APB) is a concept that has been commonly experienced in offshore wells subjected to thermal heating (Sugden et al., 2012).When a hot fluid is produced or injected, heat will transfer through the casing, and then to the fluids in the voids. This transfer will increase the temperature of the fluids in the confined space creating fluid expansion and since the fluids are trapped, the pressure build up cannot be relieving. This pressure will add an additional load to the casing increasing casing stress.

A similar concept occurs during hydraulic fracturing.**(**Bellarby, Kofoed, Marketz, & Oil, 2013). As mention before, hydraulic fracturing fluids have temperature close to the surface temperature (4°C to 30°C) depending of the operation location. On the other hand, formations could have temperatures higher than 100°C where casing and cement can exhibit the same temperature since they are in contact with the formation. The fluid is injected at high rates and a heat transfer occurs cooling the casing and surroundings. The drilling fluid inside the cement voids will shrink due to the decrease in temperature since formation fluids will not migrate to compensate the pressure loss due to the extremely low permeability in shale formations. This action will result in loss of back up pressure and aggravate severe burst loads (Sugden et al., 2012)

Several authors have already discus this problematic and assigned pressure values to the voids in the cement. For instance, Sugden based the calculations on deep and high temperature

plays such as Haynesville and Eagle ford. Since horizontal section in shales are drill with oil base mud (OBM) and vertical section with water base mud (WBM), the results were presented for both as seen in Table 2

Table 2. Pressure drop of voids in the cement for OBM and WBM (Sugden et al., 2012)

Inlet temperature (ºC)	Temperature drop at reservoir depth (ºC)	Pressure drop for OBM in void (MPa)	Pressure drop for WBM in void (MPa)
4	131	-78	-42
10	126	-78	-42
16	120	-78	-42

Jandhyala & Chiney (2014) developed a finite element approach to predict the effect of APB in the wellbore. In his worked, the pressure drop of an unconstrained fluid is calculating by the following considerations. When the fluid in a confined space is cooled or heated through decrease or increase of temperature (ΔT) respectively, the fluid volume increase is described by

$$V = V_o(1+\propto \Delta T) \quad (1)$$

Where $\propto$ is the thermal expansion coefficient of the fluid.

Since the fluids in the annulus are confined, any attempt to change the volumetric quantity of fluids leads to a decrease or increase of pressure. Therefore, the pressure change is given by

$$\Delta P = \frac{(V - V_o)}{V_o B_N} \quad (2)$$

Where V is the volume after expansion, V_o is the initial volume and B_N is the fluid compressibility. The pressure drop from Eq. 2 is based in the fact that there are not any leak paths, otherwise, results will be lower.

The fluid temperature in the constrained space is the same of a formation temperature of 100ºC. After several stages fractured, the temperature of the fluid in the constrained space reduces

to 60°C. Since the water thermal expansion coefficient changes with temperature, a coefficient value of $\propto = 0.000522$ at 60°C is applied, and under low pressure (a pressure below 400 MPa), the water compressibility coefficient is B_N is $4.5\ x\ 10^{-4}$. Considering all these parameters in the equations, the pressure drop for a water based mud is 46 MPa which is in the range of values calculated by (Sugden et al., 2012).

2.3.3 Erosion

Proppant, a sand or artificial particle with variable sizes and shapes is injected along with the fracturing fluid in order to keep the fracture open when the production phase starts. During the injection, high rates and velocities are reached inside the casing. This process may erode the inside part of the casing if factors such as roughness and straightness of the inner tube wall, hardness and angularity of the proppant, and fluid velocity are not well considering in the casing design. Encana, a North American energy company, reported severe erosion during hydraulic fracturing operations performed in several wells at a shale gas field in British Columbia, Canada (Farahani et al., 2011). They occurred close to the tubing hanger and the first casing connection below the wellhead

Figure 10. Eroded connection from field under hydraulic fracturing operations (Farahani et al., 2011)

2.3.4 Buckling

Buckling also affects casing stress but it does not fail the casing if the pipe's yield properties are not exceeded. It is a function of several variables including thermal and pressure load that produces compressive loads, section length and external support from cement or the wellbore. The occurrence of buckling might be common since long horizontal section and high pressures are experienced during hydraulic fracturing operations. Different types of buckling are experienced throughout the wellbore trajectory which is composed of a vertical, build-up, and horizontal section as seen in Figure 11. Sinusoidal buckling usually occurs in horizontal sections and during hydraulic fracturing is the most experienced one. (Lubinski, 1950), (Mitchell, 2006).

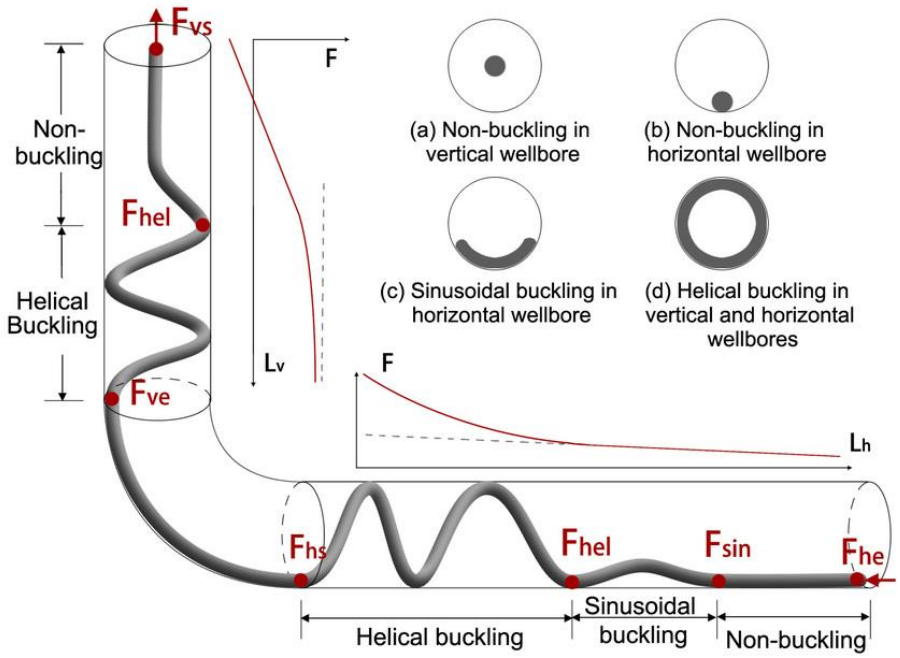

Figure 11. Different types of buckling in a wellbore (Huang, Gao, & Liu, 2018)

2.3.5 Ballooning

Plug and perf or sliding sleeve are completion options that can be performed in cemented or non-cemented casing. If the casing is cemented, it will restrain casing's movement axially. Ballooning occurs when the fluid pressure is applied internally to the casing and it becomes critical when the casing is restrained increasing casing stress (Clark, 1987). Due to the variation of pump pressure, ballooning will be a dynamic process that increases fatigue wear. Figure 12 shows an example of how ballooning changes tubing length, which is similar to the effect of hydraulic fracture pressure in casing.

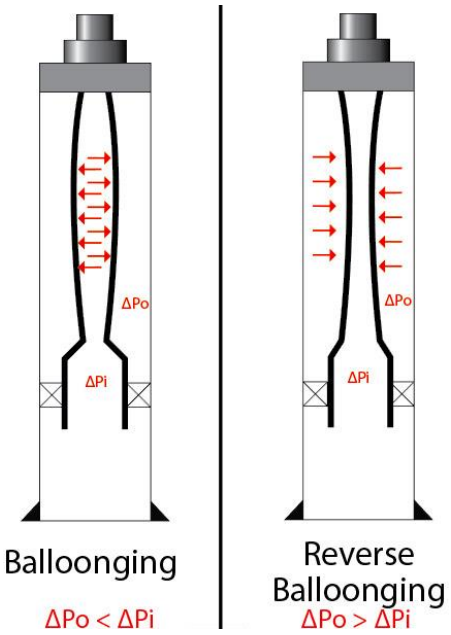

Figure 12. Example of tubing length change due to ballooning (J & Coleman, 2016)

2.3.6 Bending

Similar to buckling, bending does not fail the casing if the pipe's yield properties are not exceeded. It is the summation of the initial axial stress and the bending-related stress. Bending is common in horizontal wells since the dog-leg generated during the curve causes a stress increase on one side of the casing and it equally decrease the stress in the opposite side. Bending also occurs in vertical wells. Microdoglegs as seen in Figure 13 are a natural result of any vertical or directional well that generates bending stress and can explain an extensive diversity of downhole problems.

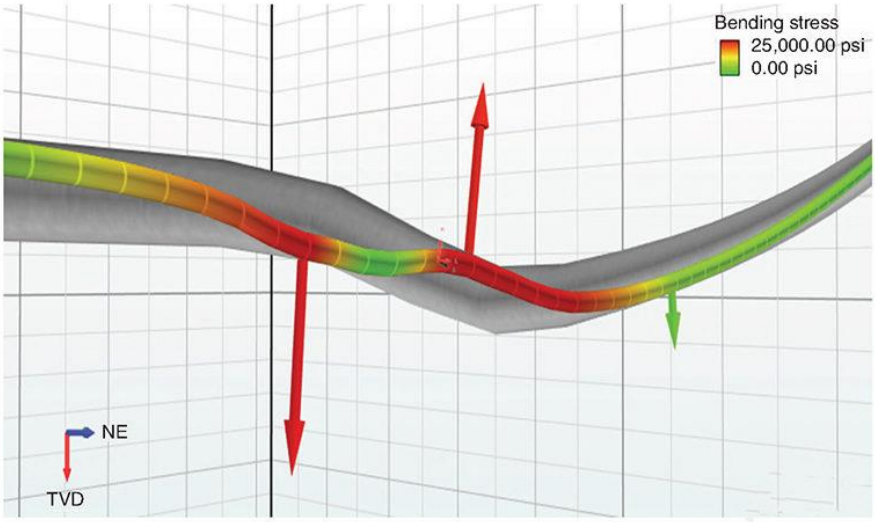

Figure 13. 3D view of pipe in borehole dogleg (Mills, Menand, & Suarez, 2016)

2.3.7 Fatigue

Fatigue is defined as the progressive and localized structural damage that happens when a material is exposed to cyclic loading (A. F. Liu, 2005). Fatigue failure is critical since the values that causes fatigue are much lower than the yield strength of the material, hence it must be consider during the design phase. However, considering fatigue failure in the design is quite difficult. The mechanism of why it occurs are still not well understood. Some research has advanced in this matter showing that the alternating stress component is, for instance, the most critical variable in defining the number of load cycles a material can withstand before fracture. Most casing failures are associate with fatigue in the couplings although new casing were run in the wells (Figure 14).

2.3.8 Brittle Failures

Brittle failure is another type of failure that occur at a lower stress than the yield strength of the material. The ability to resist brittle failure and to absorb energy is defined as toughness. Brittle materials experience only small plastic deformations before fracture, so they have low toughness. Generally brittle fracture occurs in high grade casings since toughness decreases with increasing

yield strength. Decreasing temperature and pH, increases the changes of brittle failure. Since tensile stress is high in a coupling due to high hoop stress, increasing tensile stress will increase chances of brittle fracture in couplings. And, if the exposure time to any of this conditions is high, higher probability of brittle fracture will be present.

Figure 14. Coupling fatigue (Adams et al., 2017)

2.3.9 Manufacturing issues

It might sound unrealistic, but casing failures have occurred because the casing was not manufacture properly. Visual casing inspections before running the casing are required since casing might have suffered stress load during transportation to the well side. However, it is difficult to visually determine if the casing was properly manufactured. A laboratory analysis is required for these cases. It includes the visual inspection and a metallurgical testing. The API' Specification 5CT "Specification for Casing and Tubing" provides the basis for dictate if the casing was under the correct design parameters. Improperly quenched and tempered when manufacturing or tensile measurement outside API's acceptable range are for instance two available case histories found in the literature. (API TR 5C3, 2008)

2.4 Overview of casing deformation cases during hydraulic fracturing in shales

2.4.1 United States shale fields

Only a few cases of casing failure during hydraulic fracturing in the United States shale fields has been reported in the literature. Casing coupling failures in a P110 casing grade, split failures near heel after multiple frack jobs, jewelry failures in the lateral section, and crack in casing wall at last engaged thread of frack head are some of the failures reported by Magill (2013). Cross threading while running API connections that also occurs in non-frack wells is another reported cause of casing deformation while hydraulic fracturing. The well location and operator in charge during the failure are usually not specified.

Couplings in a P110 casing experienced a longitudinal split that could be associated with brittle failure. There was no evidence of abuse or improper makeup. Sometimes theses failures are associate with presence of H2S, but it is not required to generate them. It is an often cause for stage fracturing abort.

Figure 15. Connection failure (Magill, 2013)

Some failures found in the horizontal section are associate with a sliding sleeve completions (Figure 9). The failure occurs in the packer and/or sliding sleeve. It is often diagnosed

a mandrel failure that is a pipe component of a packer and/or sliding sleeves. The reason can be brittle failure due to product design issue.

Crack in casing well at last engaged thread of the frack head are commonly cause by vibration that induced fatigue. Jobs are aborted since there is an uncontrolled release of fluids in surface. The vibrations are generated by pressure or rate pulsations from pumps that cause lines to cycle back and forth. The frack tree also moves back and forth. These vibrations create a low cycle fatigue crack initiated at thread root (notch).

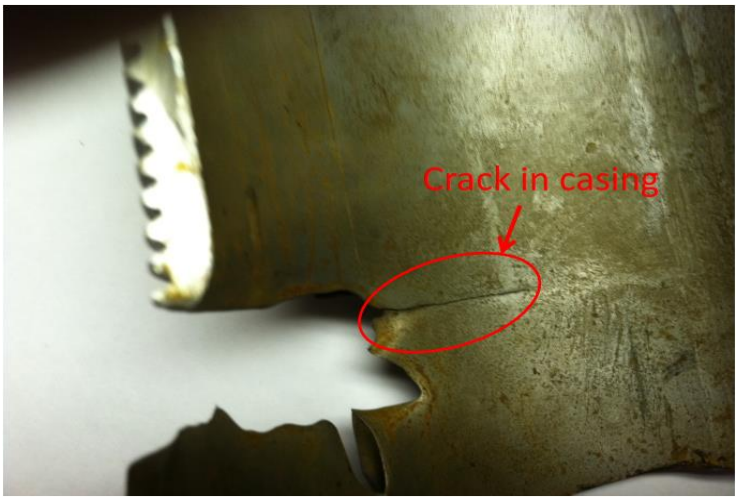

Figure 16. Crack in casing at last engaged thread of the frack head (Magill, 2013)

Split failures near the heel of the horizontal section usually occurs after multiple frack treatments at high pressure and high rates. They are mostly found in P110 casing grade. It is associate with acid that can cause sulfide stress cracking in the casing and a repeated exposure to hydrogen chloride gas (HCL) under low temperature and high pressure that allow atomic hydrogen to be absorbed by the steel. Similar to coupling failure, high yield strength appears to make the casing vulnerable to brittle failure. Therefore, if the H2S content is too high, P110 casing grade is not appropriate in the well. The below historic case described in more detailed a casing failure in the heel of the horizontal section

Figure 17. Example of split failures in casing (Magill, 2013)

A casing failure occur in an Oklahoma shale field during the 15th stage. A 16th stage was developing when the drilling crew realizes about the pressure loss. A tubing with a packer were run to diagnose that the failure occurred at 7550 ft. The location deformation is at the heel of the horizontal section in the buildup section according to the wellbore schematic (Figure 18).

The reason of casing failure is unclear. Fracturing conditions are quite aggressive compare to other operations in the fields, but the internal pressure (8550 psi) is still lower than the casing's burst rating of 10690 psi for a P110 grade casing, 4.5 in. Since severe dogleg might be a reason for casing failure due to bending stress, survey data was used to validate if the ranges were abnormal. Doglegs in the build section were higher that 16.5 degrees, which are quite alarming but still lower than 30 degrees that has been historically reported without experiencing casing failure. Preliminarily investigation from the case did not associated the dogleg severity of the well with the casing failure

The investment of the well could not be lost since an estimate of 1.5 million dollars was already expended in drilling cost to the time the hydraulic fracturing began. The initial plan was to frack 34th stages and almost half of them were already performed. Also, it was not possible to

recover the casing for lab analysis because the build section was cemented. Therefore, the determination was to put the well into production even though the casing failure was not squeezed. Fortunately, sucker rod pump was successfully installed to produce the well.

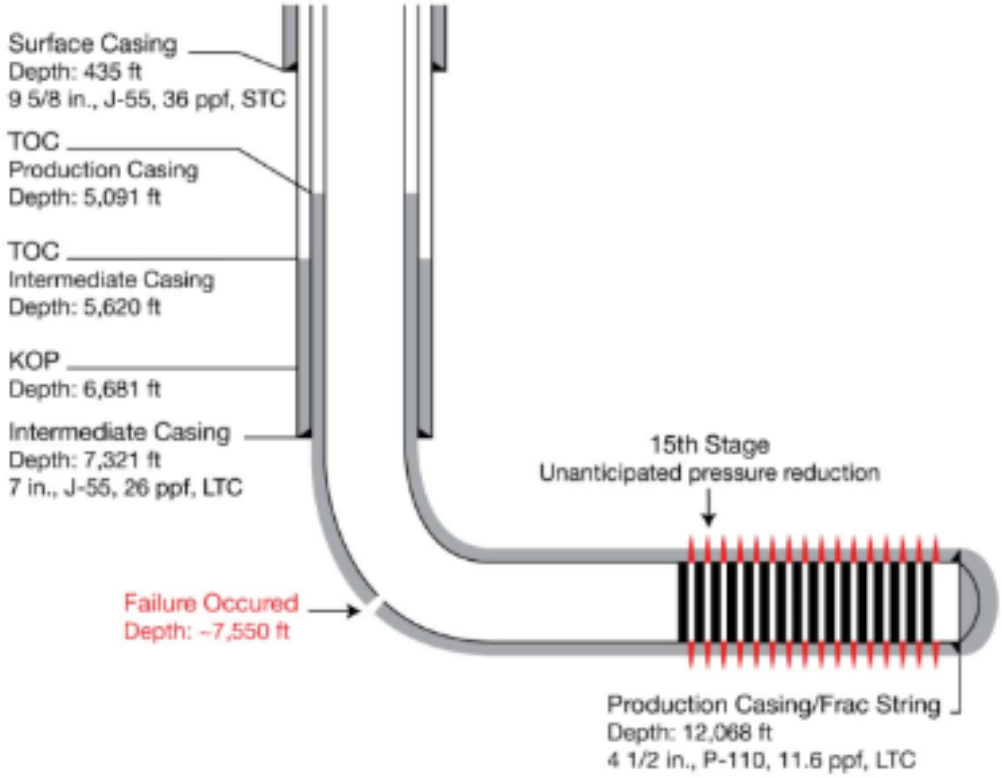

Figure 18. Wellbore schematic of a casing failure case in United States (Adams et al., 2017)

2.4.2 China shale fields

Changning-Weiyuan shale gas play exhibits a high rate of casing failure during hydraulic fracturing. The average casing failure rate was 50% by 2011(Xu, 2018). Some basic design improvements were made such as higher casing grade; thicker wall thickness, increase well logging and well trajectory optimization. Operational improvements were also made such as a stricter pressure monitor. With all this the casing failure rate decreases to 23.2% by 2017 (Xu, 2018). However, the rate is still critical considering that developing a shale gas field without casing failure is still quite expensive. In addition, casing failure occurs during hydraulic fracturing

impacting the subsequent operations and production efficiency. In a great number of cases, fracturing stages could not be finished since wells were leaving with a lower number of intervals as it was planned.

The average vertical depth of the wells is around 2440 m. Oil base mud is used with a fluid density of 2-2.2 g/cm3 when the horizontal section is drilled. The casing grade used in the wells goes from a low P95S to a high P140V with outside diameters (OD) going from 4.5 in to 5.5 in. Borehole diameters going from 6 in to 8.5 can also be found. For each respective wellbore configuration, casing deformation was reported. Plug and perf is the completion technique used, and after the deformation occurs, bridge plugs and completion tools have a difficult time accessing the deformation section for future fracturing operations (following stages).

The main reason of casing failure remains unsolved. Formation properties and regional stresses of the Changning-Weiyuan shale gas play are quite different from other develop shale fields such as United States shales fields. This fact makes it more complicated since a comparison with shale fields that do not present this elevate rate of casing failure can barely be made. For instance, regional stresses are quite high in comparison with other develop shale formations, minimum horizontal stress gradient is 2.3-2.4 MPa/100 m, and the maximum horizontal stress gradient is higher than 3 MPa/100 m. The temperature gradient is between 2.4-3.6 ^{o}C/100 m.

Three fault regimes, Normal, Strike-Slip and Reverse or Thrust exist in different oil and gas fields around the world (Figure 19). Normal regime is the most common in shale oil and gas in United States, so the majority of completion and drilling operations techniques are performed under this stress regime. Changning-Weiyuan shale gas play experiences strike-slip and reverse fault regime since in some wells the vertical stress is higher than the principal horizontal stresses and in others the vertical stress is only higher than the principal minimum stress. The anisotropy

of the principal horizontal stresses, minimum and maximum, is often very high. (Table 3) (Xu, 2018)

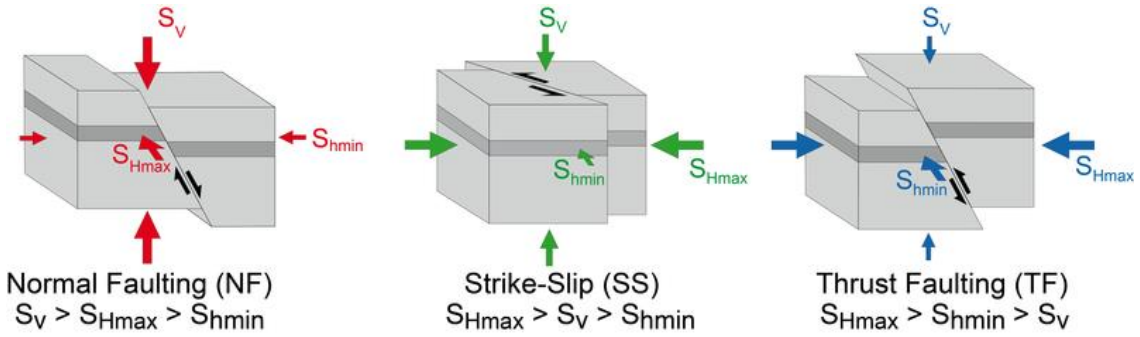

Figure 19. Fault Regimes (World Stress Map, 2016)

Table 3. Magnitude of in situ stresses and fault regime for some wells (Xu, 2018)

Well No.	TVD (m)	Maximum horizontal stress (MPa)	Minimum horizontal stress (MPa)	Vertical stress (MPa)	Horizontal stress difference (MPa)	Fault regime
N201-H1	2500	86	57.8	57	28	Reverse
NH3-1	2492	86	57.8	57	28.2	Reverse
N201	2500	86	57.8	57	28	Reverse
N206	1876	84	66	50	18	Reverse
W201-H1	1157	48	29	35	19	Strike-slip
W201-H3	2679	67	46	61	21	Strike-slip

The casing failures location varies quite a lot in the wells. Location points are found throughout the wellbore trajectory. Some of them are in the buildup section and others in the horizontal section. 30 horizontal wells out of 90 had casing failure by 2016. The casing failure location are shown in Figure 20. Around 47% (14 wells) casing failure happened in the region X while the other 53% (16 wells) occurred in the region Y. (Yan et al., 2016)

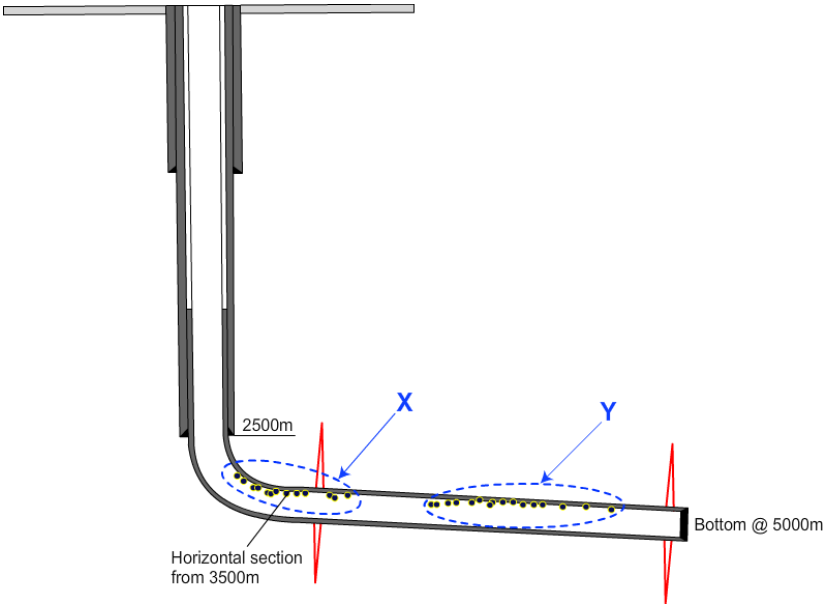

Figure 20.Schematic of casing failure locations (Yan et al., 2016)

Another singularity of the casing failure location is that they usually are not located close to the perforations which is the area where the casing strength decreases. Information about the deformation location in the wellbore and the nearest perforation section to that deformation of 6 wells in Changning-Weiyuan shale gas play are shown in Table 4

Table 4. Distance from deformation point nearest perforation

Well No.	Deformation point (m)	Nearest perforation section (m)	Distance to nearest perforation (m)
A-1	2727	3051-3052	324
	2789.48	3051-3052	261.52
	3247.6	3370-3371	123.4
A-2	2470	2701-2702	231
	2587.74	2701-2702	113.26
	2974	3094-3095	120
A-3	2967	2953-2954	12
A-4	2924	2860-2861	63
A-5	2834	2750-2751	83
B-1	2331.5	2318-2316.5	13.5
	1882.74	1888.5-1886.5	3.8

Different mechanism has been studied independently in the wells to get a better approach of the reason of casing failure. As mentioned previously increasing the grade of the casing from P110 to P140 which is the highest grade available in the market, did not solve the problem since deformation incidents still occurred. The dog-leg severity of horizontal wells introduces bending stress on casing. However, after placing the data of a couple of wells and observing that the deformation positions are not in the place where largest dog-leg severity is, bending stress might be a deciding factor of casing deformation.

The shale reservoir in Sichuan Basin is highly naturally fractured and the deformation locations usually occur close to a natural fracture. Base on the hypothesis that during hydraulic fracturing, the artificially induce fractures interact with the surrounding natural fractures, rock slippage might occur leading to casing deformation. This mechanism might be one of the reason of casing deformation in Changning-Weiyuan shale gas play (Yin et al., 2018).

Another mechanism that might be a reason for casing deformation, according to (Yan et al., 2016) and (Xi et al., 2017) is an incomplete cement sheath that occurs when the casing is touching the bottom of the wellbore combine with several factors such as decrease of temperature in casing and cement, formation properties, internal pressure, lithology interface, among others. Well logs show that locations in wellbore trajectory where the casing was eccentric, casing deformation points were encountered as seen in Figure 3.

3. Analytical Model and Input Parameters

3.1 Finite Element Analysis Concept

The mathematical modelling of the problem in Finite Element Analysis (FEA) is very engaging due to its formulation in a system of algebraic equations instead of requiring to solve systems of differential equations. It is done by dividing the problem into small pieces whose performance can be modelled simply in finite (size) elements.

The interactions among each neighboring element and node are controlled in order that, taken as a whole, the "Mesh" of finite elements approaches to the original problem. In other words, the system is solved for each element and node to associate and integrate the global result contrary to solving the problem for the entire system in a unique step. (Logan, 2012)

The objective of FEA is to mathematically model a physical problem that cannot be solved adequately by other methods. Trying to find the solution in typical problems can go for a deficient physical model, very expensive lab test or mathematical modelling of other methods that cannot represent the problem precisely. FEA has been extensively used in solving structural, mechanical, heat transfer, and fluid dynamics problems, among others.

The behavior of the material under external load requires to establish constitutive models that represents mathematical descriptions. This models are made by constituting relationship between the stress tensor and strain tensor and represent an idealized that is a close description of real behavior. Ideally-elastic and ideally-plastic are the most common models that describe material properties. Although the models almost never meet the conditions of real materials, they were, especially due to their simplicity, indispensable for the industry. Thanks to advances of the plasticity theory, new elastic-plastic models have developed describing closer to reality the non-linear characteristics of steel and various granular (friction) materials, such as concrete and rock.

For a linear static structural analysis, the displacements (x) are solved in the matrix equation below. This results are under several assumptions related to the analysis. K is essentially constant, so a linear elastic material behavior is assumed with the small deflection theory and some nonlinear conditions may be included. F is statically applied, hence the forces are considering constant and inertial effect are not included (mass, damping).

$$[K]\{x\} = \{F\} \quad (3)$$

In the case of a nonlinear behavior, different materials and space state of stress and strain are present. ANSYS R18.2 Academic is a general-purpose software that allows the application of different treatment of the plastic behavior of materials by applying more rheological models. Table 5 shows a summary of different plasticity options.

In the linear structural analysis, the displacement (x) at which the equilibrium of external and internal forces is established can be determined directly by solving the corresponding system of equations as mentioned before. In the nonlinear finite element analysis, the relationship between force F and displacement (x) is not linear, hence it is solving by discretization in space (a network of finite elements) and time (time increments).

The basis of incremental procedure for solving non-linear material problems is that the nonlinear behavior approximates linear in small steps where the linear material behavior law is applied. Equilibrium during each increment is accomplished by iterative procedures that combined are called the incremental-iterative procedure. ANSYS uses Newton-Raphson's process in order to solve nonlinear problems, where the total load is divided into a series of incremental loads, and each incremental load into several load steps. (Bonic, Vacev, Prolovic, Mijalkovic, & Dancevic, 2010)

Table 5. Some plasticity options in ANSYS

Name	Yield Criterion	Flow Rule	Hardening Rule	Material Response
Bilinear Isotropic Hardening	von Mises/Hill	associative	work hardening	bilinear
Nonlinear Isotropic Hardening	von Mises/Hill	associative	work hardening	nonlinear
Bilinear Kinematic Hardening	von Mises/Hill	associative	kinematic hardening	bilinear
Nonlinear Kinematic Hardening	von Mises/Hill	associative	kinematic hardening	nonlinear
Anisotropic	modified von Mises	associative	work hardening	bilinear, each direction & tens & comp different
Drucker-Prager	Mises-dependence on hydrostatic stress	associative or non- associative	none	elastic- perfectly plastic

The Newton-Raphson's method is used in order to calculate a vector of unbalanced load before each iteration, which represents the difference between the applied load and load corresponding to stress in element. Then, ANSYS enforces linear resolution using unbalanced load and tests the convergence of solution. Except that the convergence criterion is satisfied, the unbalanced load vector is re-determined, stiffness matrix is calculated again and the new solution is acquired. This iterative procedure continues up to solution converge. (Bonic, Vacev, et al., 2010)

The stress level at which yielding starts is determined by the yield criterion. It is represented as a functions of the individual components, $f(\{\sigma\})$ where $\{\sigma\}$ is stress vector, for multi-component stresses, that can be understood as an equivalent stress

$$\sigma_e = f(\{\sigma\}) \tag{4}$$

Von Mises's yield criterion concludes that material starts to yield when the second invariant of stress deviator reaches the critical value

$$I_2 = -K_M^2 \tag{5}$$

That written in the derived form

$$I_2 = -\frac{1}{6}[(\sigma_{11} - \sigma_{22})^2 + (\sigma_{11} - \sigma_{22})^2 + (\sigma_{11} - \sigma_{22})^2 + 6(\sigma_{12}^2 + \sigma_{12}^2 + \sigma_{12}^2)] = -k_M^2 \tag{6}$$

Where k_M is the yield constant that can be determine from the pure shear test for comparison reasons.

The flow rule defines the direction of plastic straining and is given as:

$$\{d\varepsilon^{pl}\} = \lambda\{\frac{\partial Q}{\partial \sigma}\} \tag{7}$$

λ is the plastic multiplier that defines the amount of plastic straining and Q, a function of stress named the plastic potential that defines the direction of plastic straining. The flow rule is named associative and the plastic strains occur in a direction normal to yield surface if Q is the yield function. (SharcNet, 2016)

The hardening effect in elasto-plastic materials describes how from an initial yield surface in the space of main stresses, changes shape and size in the course of plastic deformation. the material can be with isotropic (working) hardening, kinematic hardening and mixed (anisotropic hardening) depending on the way of change of the yield surfaces.

In materials with kinematic hardening, the initial yield surface space retains the original size and shape during the plastic deformation but changes position in main stresses. On the other hand, isotropic hardening materials changes size since the initial yield surface expands in the main stresses space, but remains geometrically related to the initial one, in other words, it does not change shape during the yield of material. A combination of these hardening effects brings mixed hardening materials.

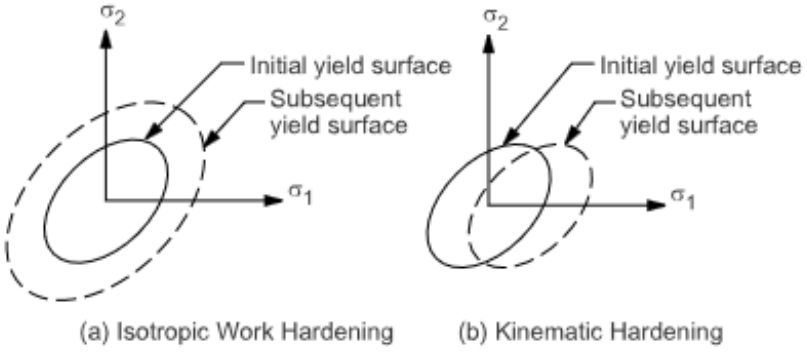

Figure 21. Types of hardening rules (Bonic, Prolovic, & Mladenovic, 2010)

3.2 Model and Input Parameters

In order to demonstrate the importance of appropriate standoff on casing and cement stress distribution, a finite element analysis (FEA) study was performed in a 2D model by using the plane strain function of ANSYS R18.2 Academic. A segment of a horizontal well of unit thickness was built in a two-dimensional plain strain element, since the cement, casing and formation are constrained axially at both ends and the casing internal pressure is uniform.

For an accurate depiction of the influence of standoff on wellbore integrity, five different standoff instances were modeled as shown in Table 6. Figure 22 shows the physical model for a 100 %, 70% and 1 % standoff. The 70% standoff is important to be modeled because the mechanical properties of centralizers are tested to a minimum standoff of 67% according to the American Petroleum Institute (API) Specification 10D (API Spec 10D, 1995)**.** This is the lowest value accepted by the API 10D specification and should be regarded as a minimum recommendation to ensure that the centralizer is not efficient.

Based on the consideration discuss previously that some drilling mud will remain where the annular space between the casing and the cement is lower, it was modeled another model with the same five standoff instances and the addition of voids filled of liquid in the bottom part as

shown in Figure 23. 100% and 70% were modeled only for comparison reasons since we believe that the gap between the casing and wellbore is enough to allow a full cement sheath in the annular space.

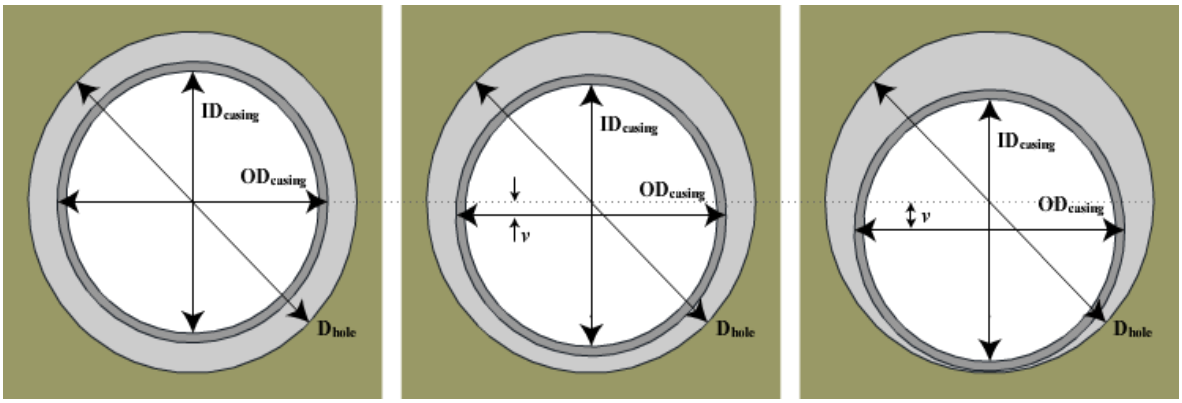

100% Standoff 70% Standoff 1% Standoff

Figure 22. Three cases used for finite element analysis

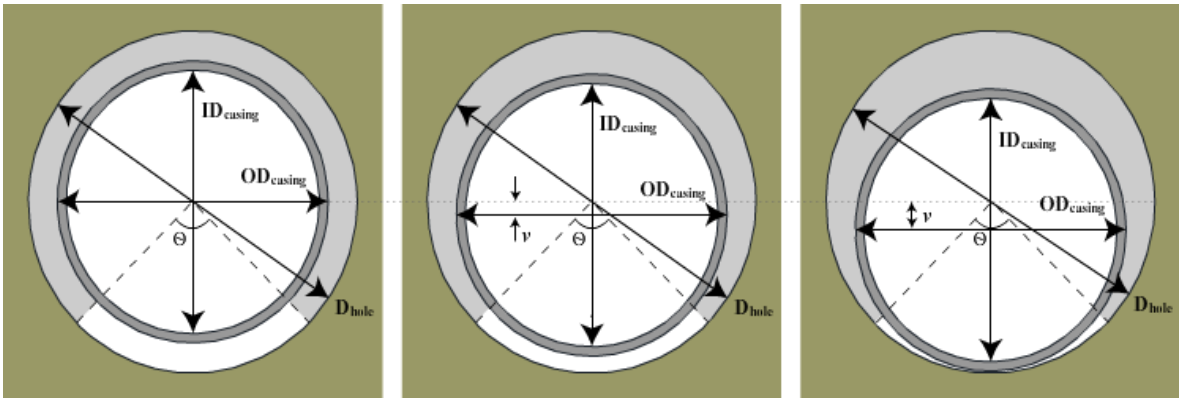

100% Standoff 70% Standoff 1% Standoff

Figure 23. Three cases with voids used for finite element analysis

Table 6. Geometry used for finite element analysis cases

Case	100% Standoff	70% Standoff	40% Standoff	10% Standoff	1% Standoff
Casing offset from hole center, v (in.)	**0**	**0.17**	**0.33**	**0.50**	**0.55**

Table 7 shows the material properties for the three components. The casing, cement and formation are assumed to have an isotropic elasticity. It is also assumed that deformation obeys the pure elastic model.

Table 7. Material Properties

Material	Elastic modulus GPa	Poisson's Ratio -	Density kg/m^3
Casing	**210**	**0.3**	**7850**
Cement	**10**	**0.17**	**3100**
Formation	**22**	**0.23**	**2600**

For all the models, the borehole outer diameter was 6 5/8 in. (168.2 mm) and the cement layer inner diameter was 5.5 in. (139.7 mm), equal to the casing outer diameter. The casing inner diameter is 5 in. (127 mm), so its wall thickness is 1 in. (25.4 mm). The casing offset from the hole center (v in Figure 22, expressed in inches) corresponds to the percent standoff and is used in the sketch to ensure accuracy. 0% standoff is not possible to be modeled since this would lead to an intersection of the two faces. The void's length in Figure 23 is determined by the angle θ. It was more practical for the model to vary the length of the void with the angle (θ) formed between the two edges of the void with respect to the center of the wellbore

The formation boundary was a 70" by 70" (1778 mm x 1778 mm) square with a size more than tenfold the size of the borehole, in order to avoid the influence of boundary effects on stress. For boundary conditions, an internal pressure of 11,600 psi (80 MPa) was applied uniformly over the casing interior face. The vertical stress is 54 MPa and the horizontal stress is 82 MPa which reflects the most common particularity of the fault regime in the Weiyuan-Changning shale field. The mesh element size for the formation was 10 mm, 1 mm was assigned for the cement and 0.7 mm was assigned for the casing.

Unless otherwise mentioned, the default temperature (22°C) of ANSYS will be kept for the entire system (formation, cement and casing) since the effect of wellbore eccentricity in the stress concentration wants to be analyzed in a simpler and generic model. Later, a chapter dedicated to analyzed the impact of different temperatures in the system will be discuss in detail. Appendix A shows all the simulations performed in ANSYS R18.2 for all different cases studied.

The results from the model can be compare with field evidences such as well logs or completion tools. However, numerical modeling methods introduce errors and might not accurately match a well-known analytical solution if the meshing of the model is not carefully assigned (Lee, Eckert, & Nygaard, 2011). Therefore, the model considering merely the formation (size, meshing and material properties) with the borehole along with the boundaries conditions (in-situ stresses and internal pressure) was validated using an analytical solution for wellbore stresses.

The rock stresses are under equilibrium before the borehole is drill and they can be characterized by the three in-situ principal stresses. They are the vertical stress and two far field horizontal stresses according to Andersonian state of stress (Pollard & Fletcher, 2004). The borehole rock is extracted in drilling and the adjacent rock around the wellbore compensate the exerted loads. Local stress concentrations take place in the proximity area of the hole after the redistribution of the stresses is done. Kirsh (1898) initially derived the linear elastic solution that describes the concentration of radial and tangential stresses around a wellbore. Zhang et al. (2006) extended the approach including pore pressure and fluid pressure in the wellbore. If a constant pore pressure and a Biot's coefficient of 1 are assumed, the effective stresses around the wellbore for a vertical well can be obtained:

$$\sigma_{rr} = \frac{(\sigma_H + \sigma_h - 2P_p)}{2}\left(1 - \frac{R_W^2}{r^2}\right) - \frac{(\sigma_H - \sigma_h)}{2}\left(1 - \frac{4R_W^2}{r^2} + \frac{3R_W^4}{r^4}\right)cos2\theta + (P_m - P_p)\frac{R_W^2}{r^2} \quad (8)$$

$$\sigma_{\theta\theta} = \frac{(\sigma_H + \sigma_h - 2P_p)}{2}\left(1 + \frac{R_W^2}{r^2}\right) - \frac{(\sigma_H - \sigma_h)}{2}\left(1 + \frac{3R_W^4}{r^4}\right)cos2\theta - (P_m - P_p)\frac{R_W^2}{r^2} \quad (9)$$

The results for the radial stress and the hoop stress for the model and the analytical solution are seen in Figure 24. The model results of the hoop stress at 0° with respect the σ_H or the radial stress at 90°, and the hoop stress at 90° or the radial stress at 0° matches quite close with the analytical solution. There is a discrepancy of 1.5 MPa at the borehole wall. However, at locations further from the borehole wall, the discrepancy reduces at values lower than 0 MPa implying that the formation size, mesh and boundary condition are properly assigned.

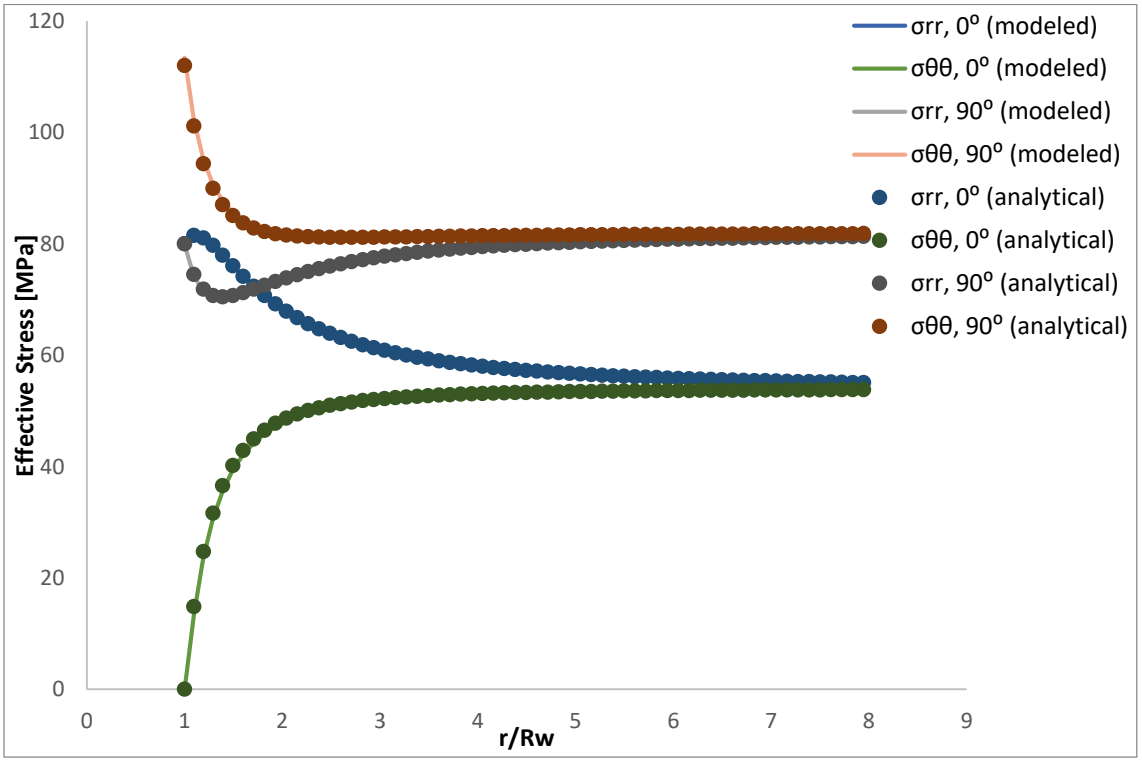

Figure 24. Comparison between modeled results and the analytical solution.

4. Results

Complete cement sheath

A maximum stress of 278 MPa occurs at 100% standoff, and a maximum stress of 340 MPa occurs at 1% standoff. There is an increase of almost 22% from the best to the worst centralization (Figure 26). The orientation of the maximum stresses also changes with a standoff decrease; a shift being observed toward the lower part of the casing. An explanation is the lack of cement sheath at that specific point, and thus, closer contact with formation. On the other hand, the minimum stress changes insignificantly.

If a close look to the cement is made, a maximum stress of 87 MPa occurs at 100% standoff, and a maximum stress of 94 MPa occurs at 1% standoff. There is an increase of 12% from the best to the worst centralization. In addition, a steep stress changes of approximately 18 MPa occurs in the cement within a short distance for the worst centralization (Figure 26). These steep stress changes in the cement are also observed in a model designed to study the effect of wellbore centralization in geothermal wells (Mendez, Ichim, & Teodoriu, 2018). The slope of the graph for lower standoff values becomes higher, which means that the maximum stress variations increase more when the centralization is worse.

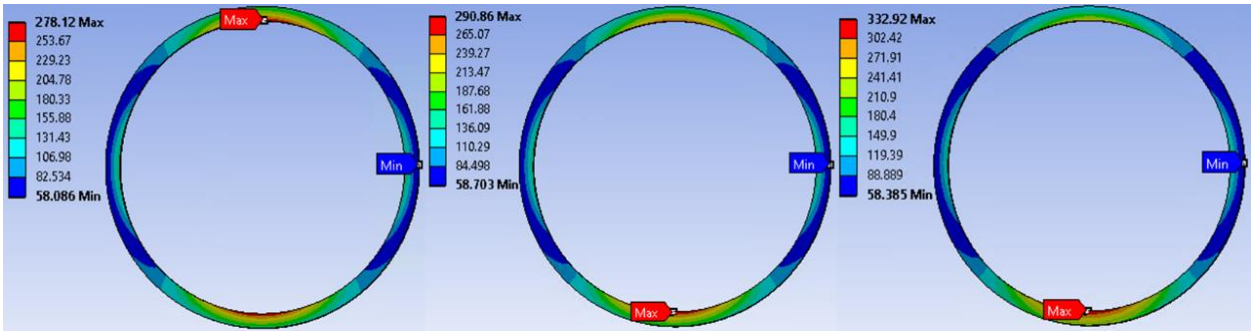

Figure 25. Stress distribution with 100% standoff (left), 70% standoff (center), and 10% standoff (right).

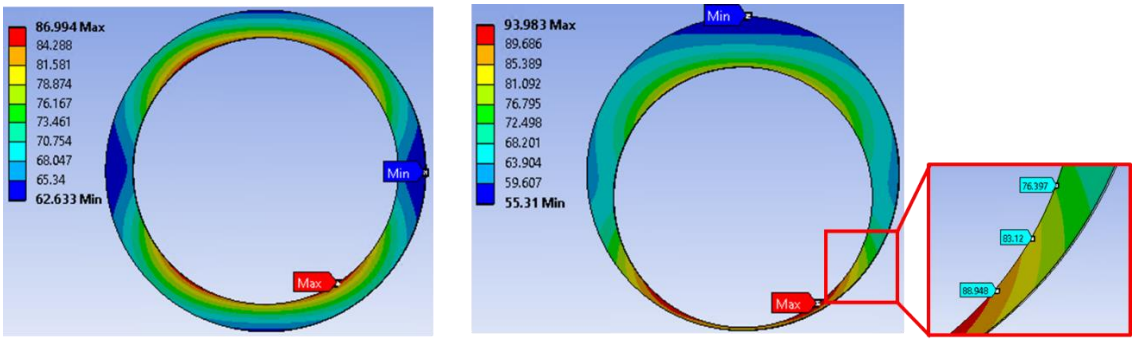

Figure 26. Stress distribution in the cement sheath for 100% left and 1% standoff (right).

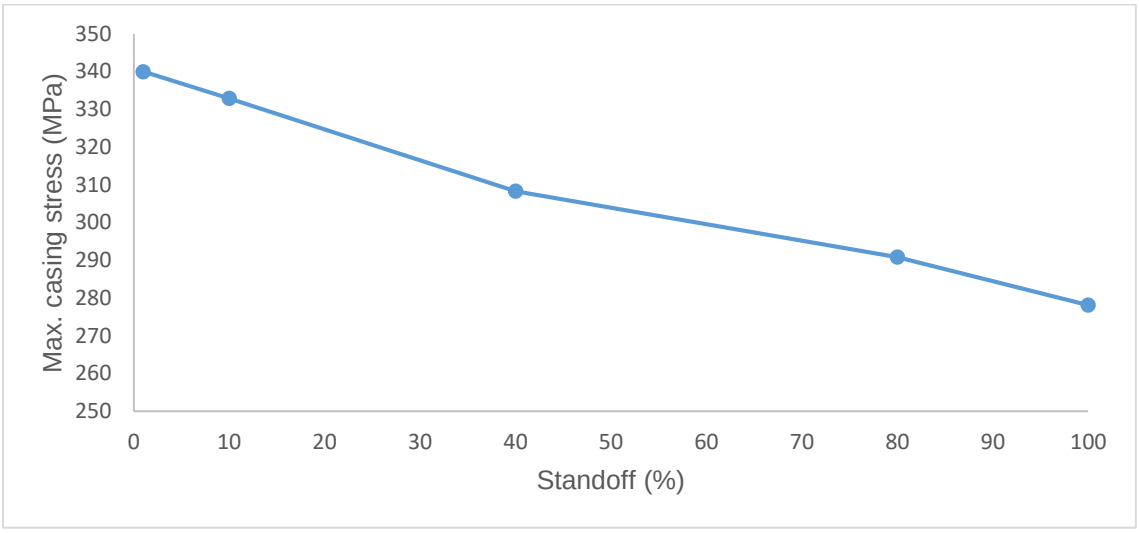

Figure 27. Maximum stress at different standoff.

Cement sheath with voids

In order to correctly evaluate the influence of voids in the cement sheath, it is necessary to consider two variables, void pressure and void length; from now on, void length will be called void angle and it will measure in degrees as shown in Figure 23.

Since it is difficult to set up a specific void pressure and void length considering that the formation of voids at each section of the wellbore trajectory will be different, a sensitive analysis was made to evaluate under what conditions of void pressure and void angle the stresses around the casing becomes more critical.

Figure 28 and Figure 29 show the results of maximum casing stress under the influence of void pressure and void angle for 10% and 100% standoff. As mentioned before, 100% standoff is modeled only for comparison reasons since the chances of getting a void when the casing is centralized are very low.

The magnitude and tendency of the results are similar for both standoff except when the void pressure is 80 MPa. The void angle more critical is 60º and the void pressure more critical is 0 MPa. In order to evaluate if casing deformation did or didn't occur, a reference line of 965 MPa which is the yield strength of the TP140 (highest available casing grade) will be drawn in some figures for now on.

Void pressure of 40 MPa, 20 MPa and 0 MPa will exceed the yield strength of the TP140 at a respective void angle. Figure 32 shows the stress distribution in the casing for 10% standoff and VP=20 MPa at void angles of 60º, 90º, and 120º. There are approximately two to three points were casing deformation might occur and they are located in the proximity to the contact area between the void and the casing.

Figure 33 shows the cement stress distribution for 10% standoff and VP=20 MPa at void angle of 60º and 120º. 580 MPa and 360 MPa are the maximum stresses for 60º and 120º respectively and they occur at the intersection between the cement and the void formed in the cement sheath.

There are more chances of casing deformation at a void pressure of 0 MPa. At 40 MPa there are less chances of casing deformation because the range of void angle decreases; However, it is more likely to obtained voids at angles between 20 and 90 degrees than the others. The use of any lower grade such as P110 and P95 that are more economically accessible will not be recommended because casing deformation will happen also at a void pressure of 60 MPa.

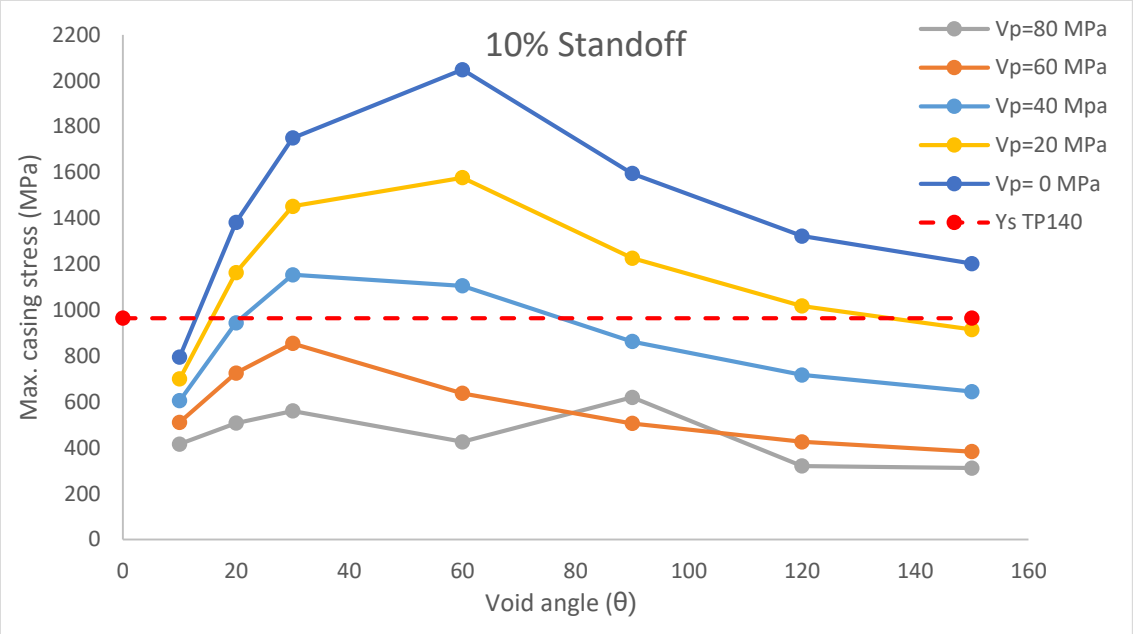

Figure 28. Effect of void angle and void pressure on casing stress at 10% Standoff

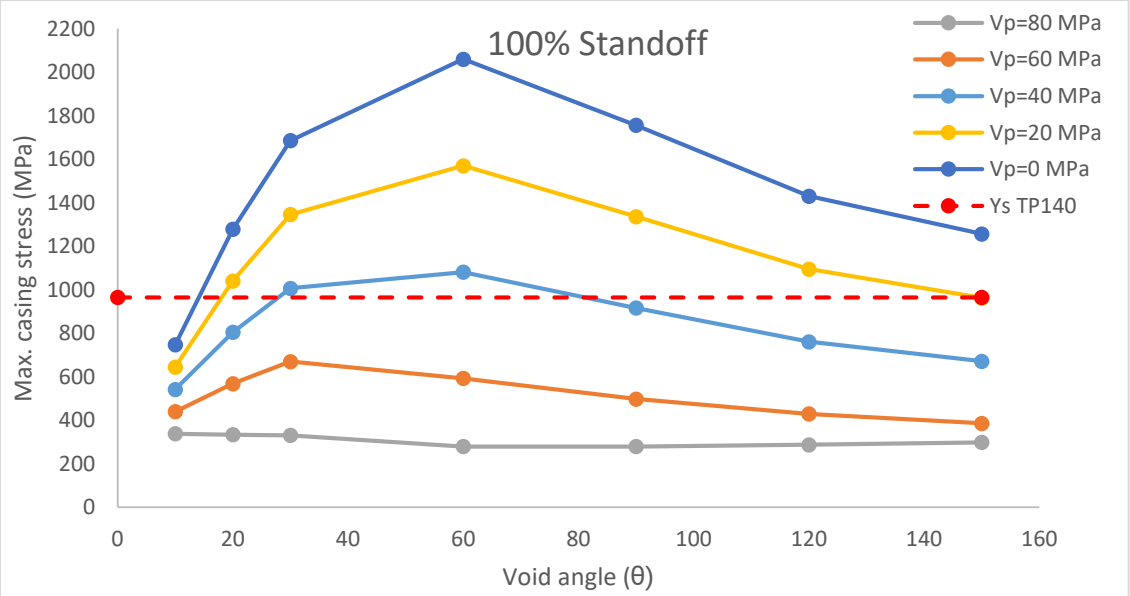

Figure 29. Effect of void angle and void pressure on casing stress at 100% Standoff

The high value of 2000 MPa is disturbing since we are considering the pure elastic model. Now, if we include a non-linear solution such as bilinear isotropic hardening in the model, the result will be closer to the reality because as soon as casing failed, the behavior will be plastic.

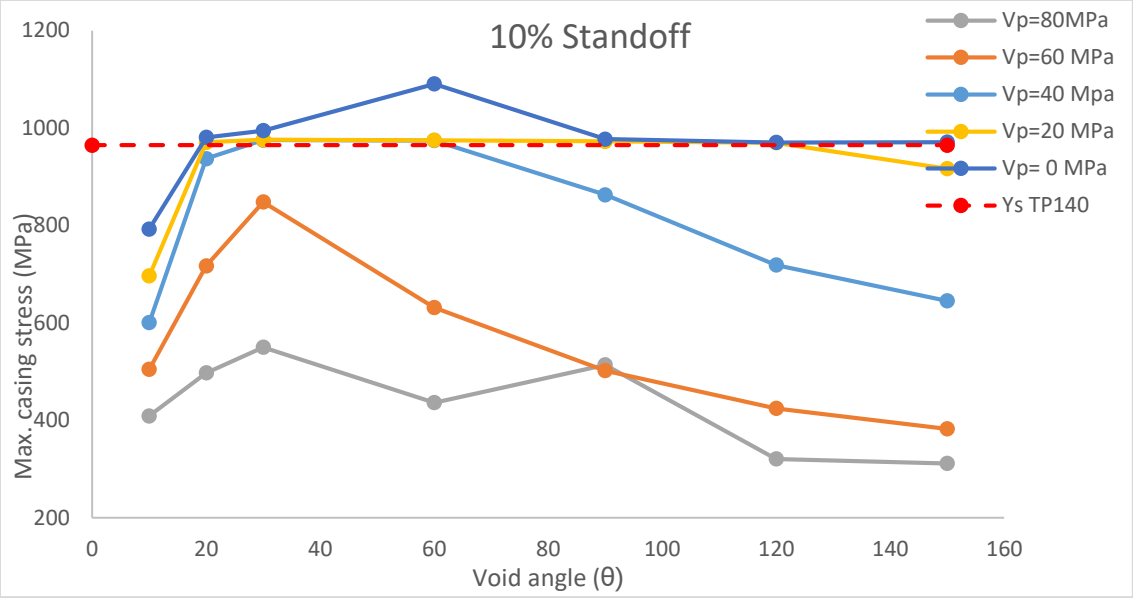

Figure 30. Effect of void angle and void pressure on casing stress at 10% Standoff (including bilinear concept)

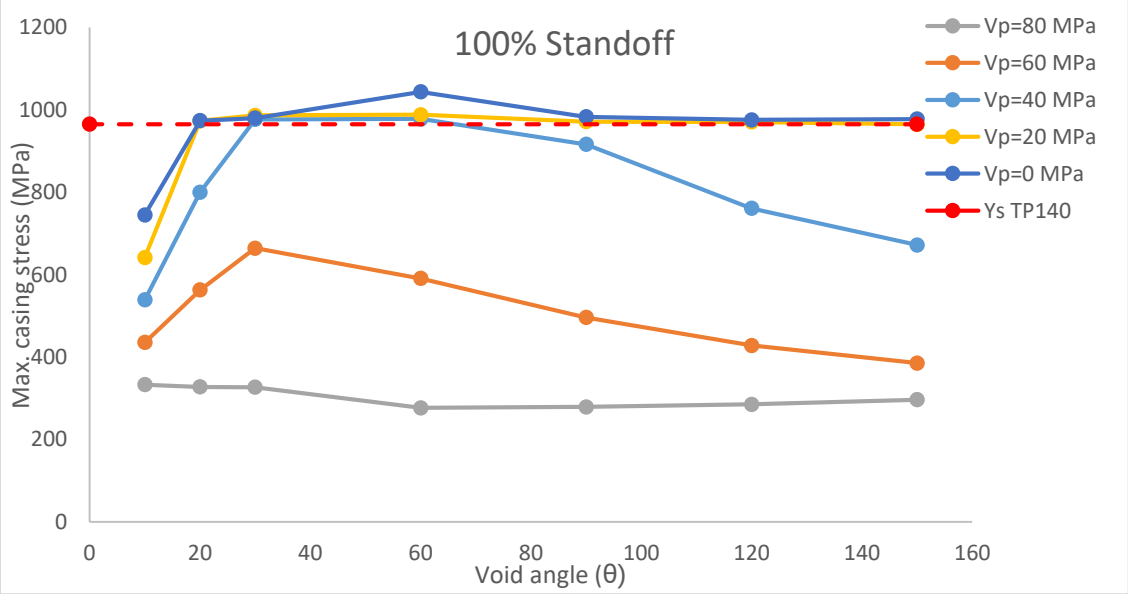

Figure 31. Effect of void angle and void pressure on casing stress at 100% Standoff (including bilinear concept)

As it is seen in Figure 30 and Figure 31, the results are the same except when the maximum casing stress reach the yield strength of the TP140 casing grade (965 MPa). At that point, deformation

occur and the behavior is not linear anymore. We will include the bilinear isotropic hardening concept in the model hereafter.

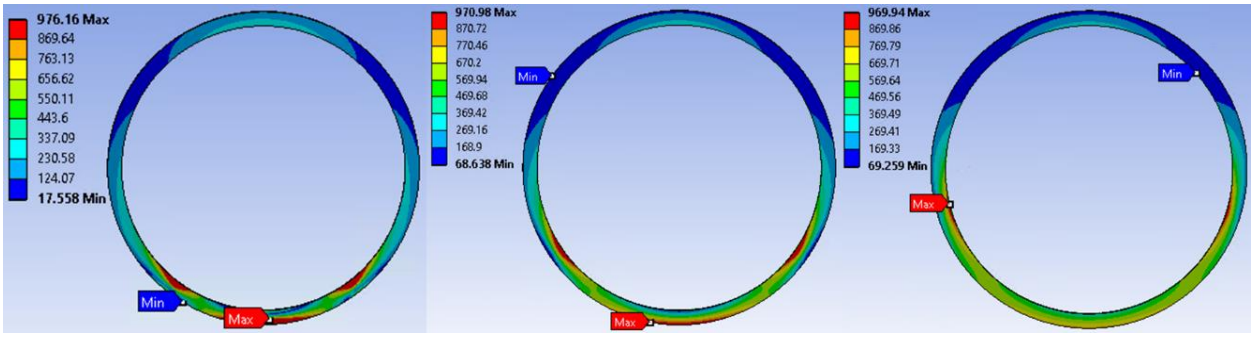

Figure 32. Casing stress distribution for 10% standoff and VP=20 MPa at void angle of 60º(left), 90º(center), and 120º(right)

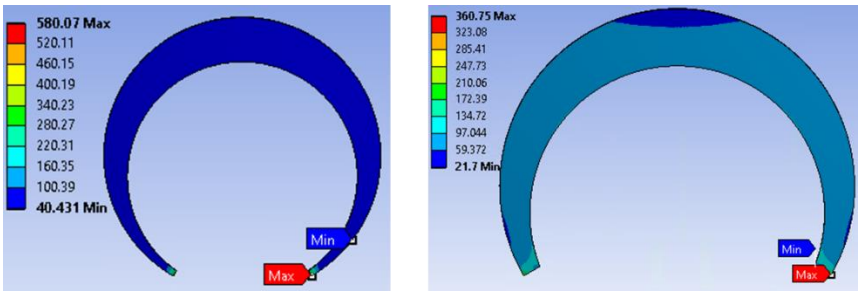

Figure 33. Cement stress distribution for 10% standoff and VP=20 MPa at void angle of 60º(left) and 120º(right)

It seems that the difference of maximum casing stress is low between 10% and 100% standoff. However, it is required a more detail evaluation of the impact of standoff at different void pressure. All the void pressure analyzed previously were included in the simulations with the exception of 80 MPa since it might not lead for casing deformation even for a P95 grade casing.

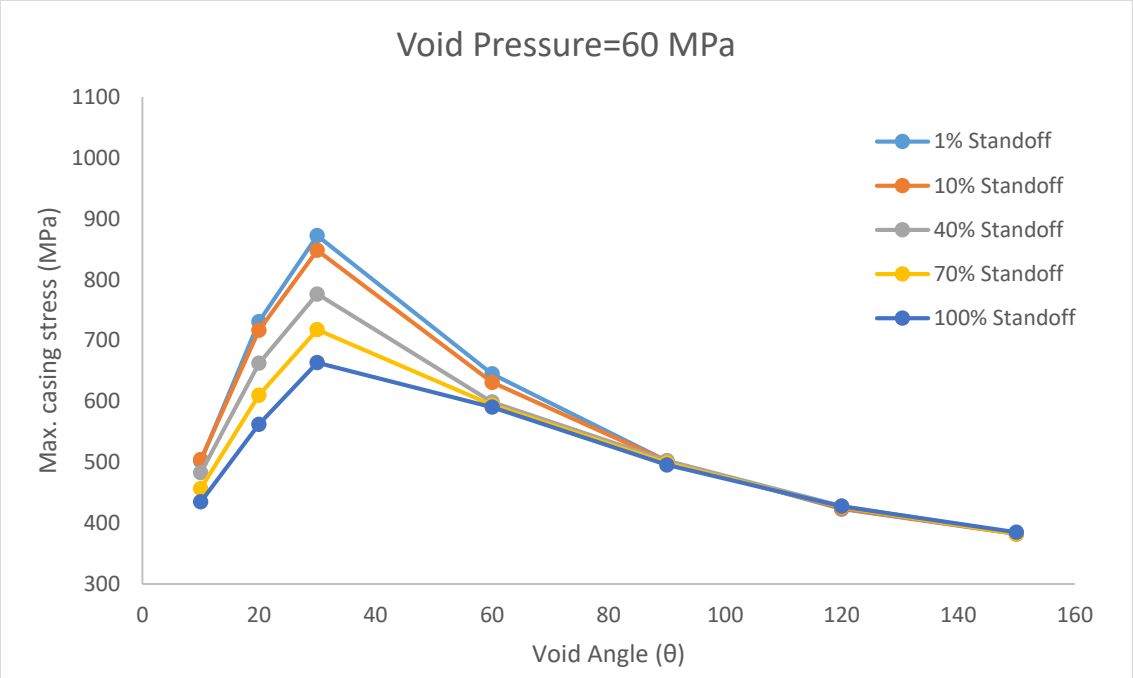

Figure 34. Standoff effect over casing stress in an incomplete cement sheath with a void pressure of 60 MPa

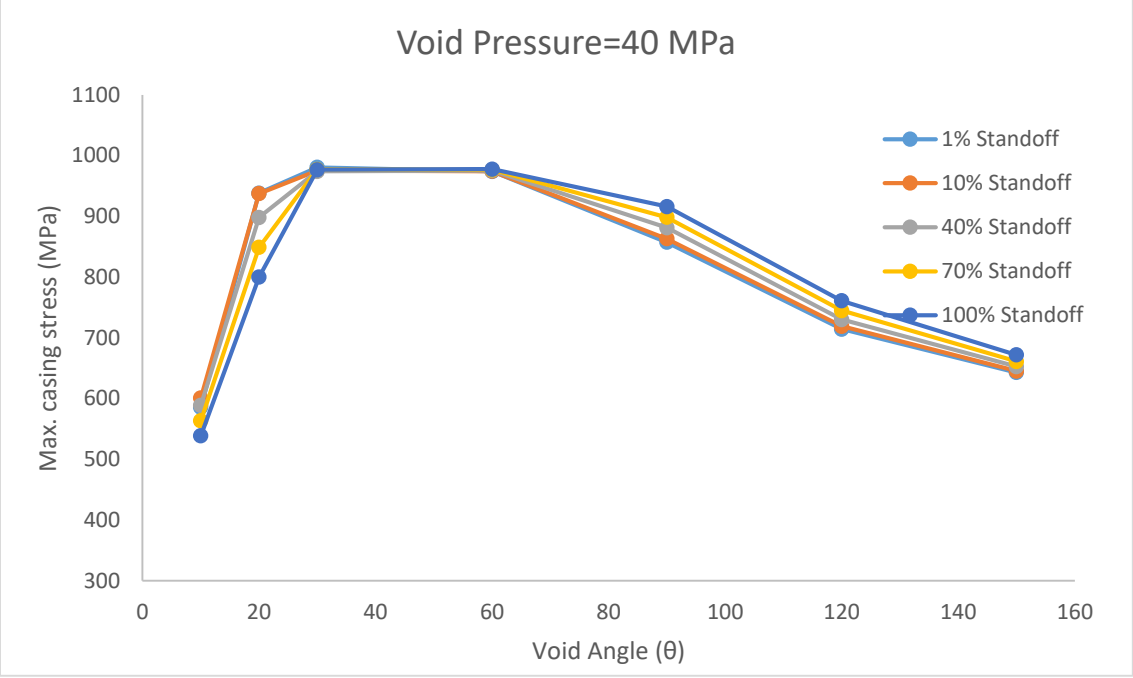

Figure 35. Standoff effect over casing stress in an incomplete cement sheath with a void pressure of 40 MPa

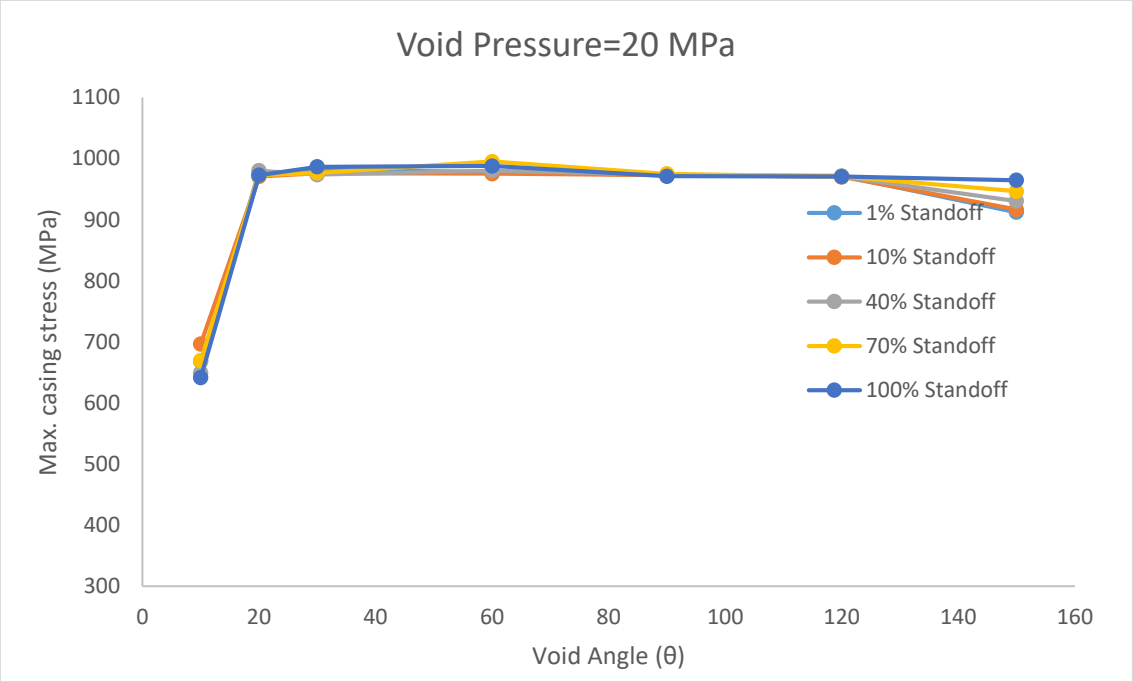

Figure 36. Standoff effect over casing stress in an incomplete cement sheath with a void pressure of 20 MPa

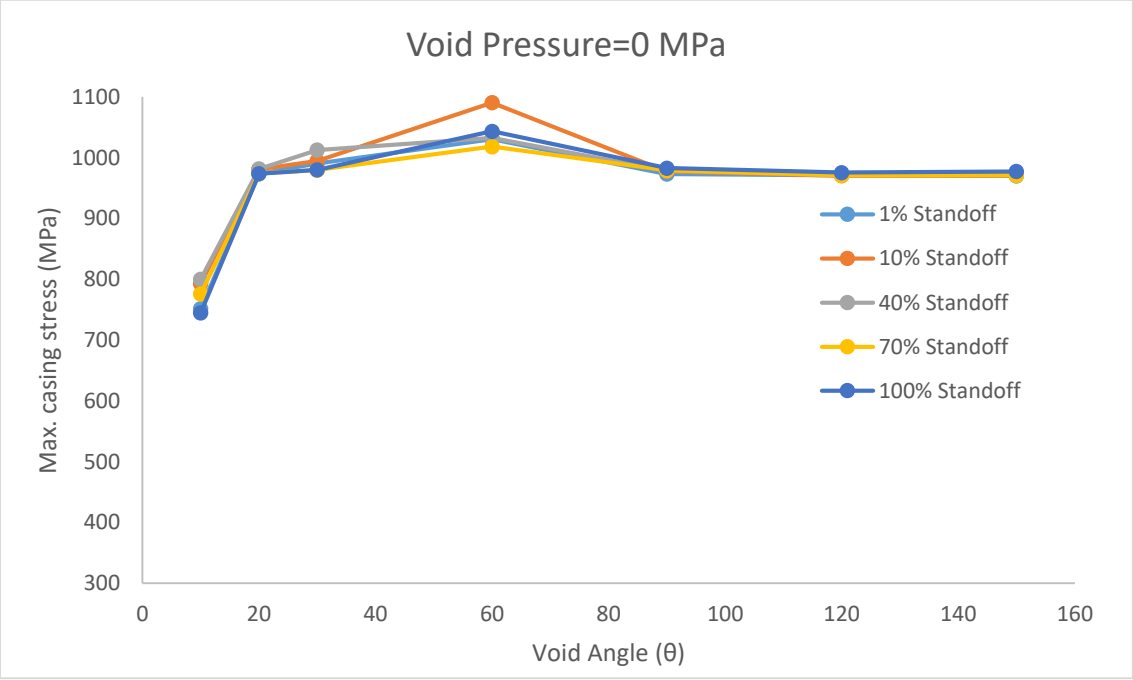

Figure 37. Standoff effect over casing stress in an incomplete cement sheath with a void pressure of 0 MPa

For 60 MPa at void angles over 90º, the maximum casing stress will be the same no matter what standoff is present. Under 90º, lower standoff reflects higher maximum stress on casing. 10% and 1% reflects almost the same value of casing maximum stress. The chances of casing deformation are high at void angles between 20º and 50º for standoff lower than 40%.

For 40 MPa, casing deformation will occur for void angles between 30º and 60º at all standoff values. At a void angle lower than 30%, casing deformation is more likely to happen at lower standoff where 10% and 1% have almost the same values. On the other hand, casing deformation is more likely to happen at higher standoff values at void angles higher than 60º.

For 20 MPa, casing deformation will occur for void angles between 20º and 120º at all standoff values. It might also occur for values higher than 120º with the exception of 100% standoff that is certainly happening. At a void angle lower than 20º, the chances of casing deformation reduced.

For 0 MPa, casing deformation will occur for void angles higher than 20º at all standoff values. However, there is still a high chance of casing deformation for void angle lower than 20º. In conclusion, casing deformation is likely to occur even running a casing of TP140 at any standoff when the void pressure is lower than 20 MPa. At a void pressure of 40 MPa, the probability of casing deformation reduced for void angles lower than 20º and higher than 60º. And, at 60 MPa the chances of casing deformation are almost zero using a standoff higher than 70%. Even though the yield strength of TP140 casing is not reach for values lower than 70%, the values are still high and a great safety factor must be used for casing design.

4.1 Effect of in-situ stresses and internal casing pressure

All these results were obtained under the same model parameters as mentioned in chapter 3 and Table 7. However, reservoir properties and therefore drilling and completion designed might be different from well to well. The regional stresses and the internal pressure might impact differently and significantly the stress distribution over the casing and the cement especially when the casing is not centralized throughout the wellbore trajectory.

There are different fault regimes; Normal, Reverse, or Strike-Slip (Figure 19**)** as mentioned before. Even though regional stresses are intrinsic variables to the reservoir, it is important to know which combination is worse for the wellbore integrity in order to be more cautioning during the drilling and completion operation or to look for unconventional drilling or completion technologies that could mitigate the problem. In addition, it would help to compare among basins where wellbore integrity issues were or weren't encountered. In other words, a standardized well completion might work for wells in the Permian Basin of the United States but they might not work for wells in the Sichuan Basin of China. They might work for both cases but a non-proper centralization could be more critical in the Sichuan Basin than in the Permian Basin.

The internal casing pressure is a variable that depends strongly from reservoir properties such as rock hardness, permeability or pore pressure. It also depends of the well production required to make it commercially exploitable. Therefore, the magnitude oscillation of this variable is low. However, if under certain value of internal casing pressure exists a high risk of casing deformation, a completion redesign must be made to evaluate the pros and cons of reducing or increasing this variable.

Based on all this, an extensive study of cases under different regional stresses and internal pressure will be made below.

4.1.1 In-Situ Stresses

A common distribution of the in-situ stresses in the Sichuan Basin of China where the vertical stress (54 MPa) is lower than the horizontal stress (82 MPa) based on (Xi et al., 2017) has already been modeled. Other three different external boundary conditions were chosen in order to analyze under what in-situ stress or fault regime, the standoff has a major impact over the casing and cement stress distribution.

For the case 1, the vertical stress is higher that the horizontal maximum stress keeping the same high geo stress tendency from the base case ($\sigma_v = 54MPa \ \ \sigma_H = 82\ MPa$). Case 2 reflects the case of isotropic in situ-stress. It means that the vertical stress is the same that the maximum horizontal stress. It is possible to find very similar in-situ stress in some basins but not equal, so this case was chosen mainly for modeling and comparison reasons. Case 3 represents a similar fault regime to the base case, but the magnitude of the stresses is around 30 MPa lower. Case 4 presents again the normal fault regime of case 1 ($\sigma_v = 82MPa \ \ \sigma_H = 54\ MPa$) but the magnitude is around 30 MPa lower.

Complete cement sheath

Case 1: $\boldsymbol{\sigma_v = 82\ MPa\ \sigma_H = 54\ MPa}$

A maximum stress of 278 MPa occurs at 100% standoff, and a maximum stress of 284.2 MPa occurs at 1% standoff. There is an increase of almost 2.5% from the best to the worst centralization. The orientation of the maximum stresses remains constant over the side of the casing. The minimum stress changes insignificantly (Figure 38).

There is not a significant change of the maximum stress from the best to the worst centralization in the cement. It is less than 1%. Also, there isn't a remarkable steep stress changes of the cement within a short distance for the worst centralization (Figure 39). The slope of the

graph for lower standoff values remains almost constant, which means that the maximum stress variations are negligible when the centralization is worse.

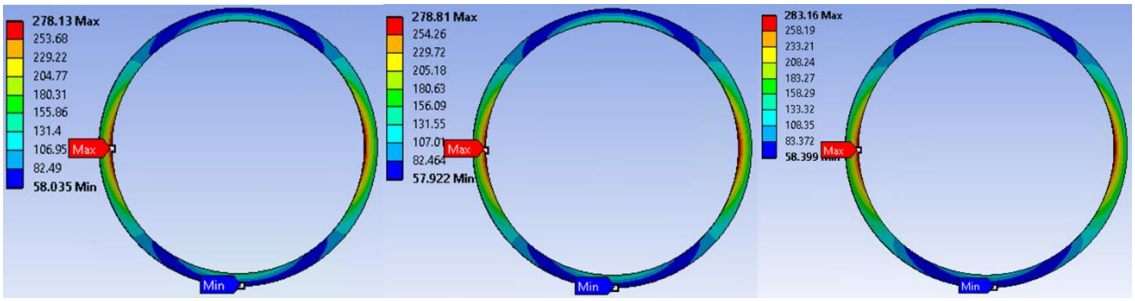

Figure 38. Casing stress distribution with 100% standoff (left), 70% standoff (center), and 10% standoff (right) in case 1.

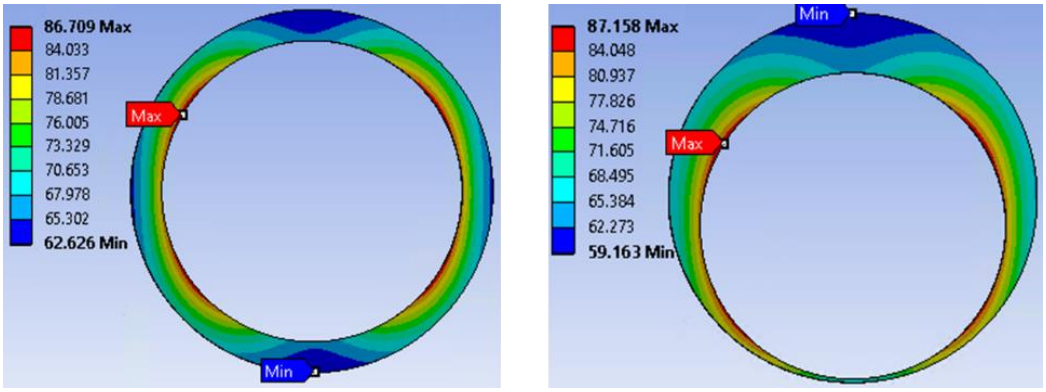

Figure 39. Stress distribution in the cement sheath for 100% left and 1% standoff (right) in case 1

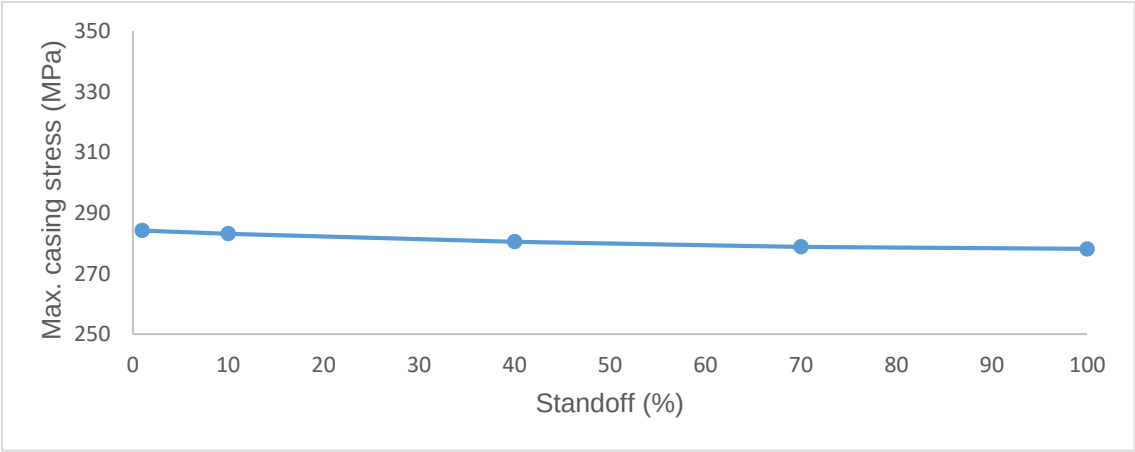

Figure 40. Maximum stress at different standoff for case 1.

Case 2: $\sigma_v = 54\ MPa\ \sigma_H = 54\ MPa$

A maximum stress of 97.2 MPa occurs at 100% standoff, and a maximum stress of 113.5 MPa occurs at 1% standoff. There is an increase of 15% from the best to the worst centralization. The orientation of the maximum stresses also changes with a standoff decrease; a shift being observed toward the higher part of the casing (Figure 41).

A closer look again only to the cement, a maximum stress of 86.7 MPa occurs at 100% standoff, and a maximum stress of 87.2 MPa occurs at 1% standoff. There is an increase of less than 1% from the best to the worst centralization. There isn't a remarkable steep stress changes of the cement within a short distance for the worst centralization (Figure 42). The changes of equivalent stress are more progressive. The slope of the graph for lower standoff values becomes higher, which means that the maximum stress variations increase more when the centralization is worse.

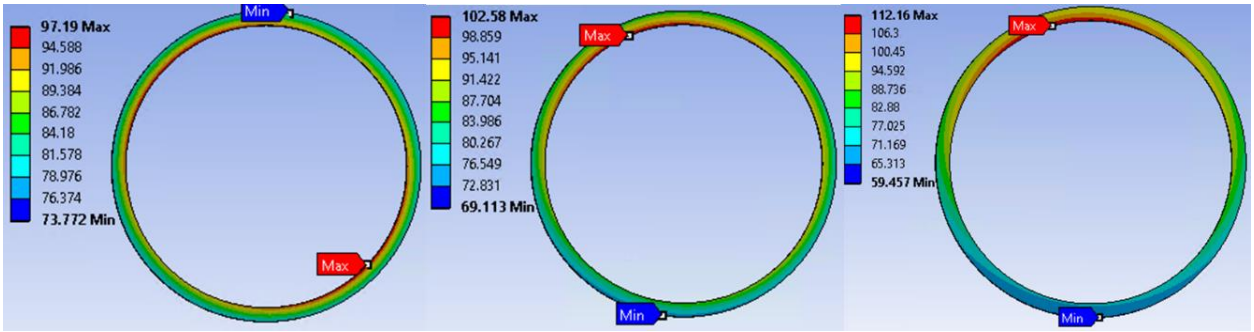

Figure 41. Casing stress distribution with 100% standoff (left), 70% standoff (center), and 10% standoff (right) in case 2.

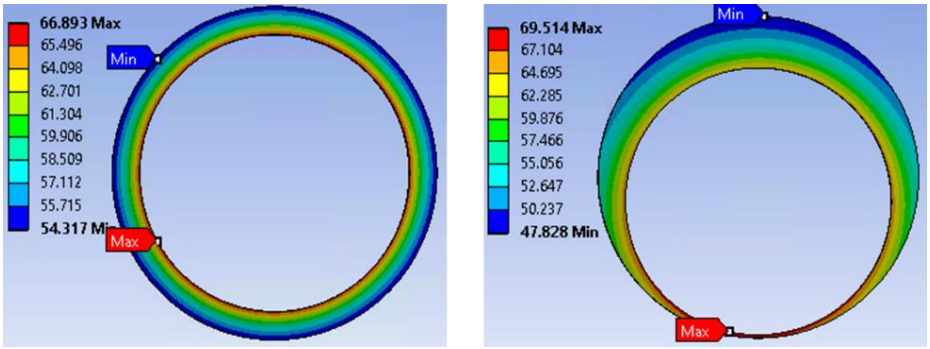

Figure 42. Stress distribution in the cement sheath for 100% left and 10% standoff (right) in case 2.

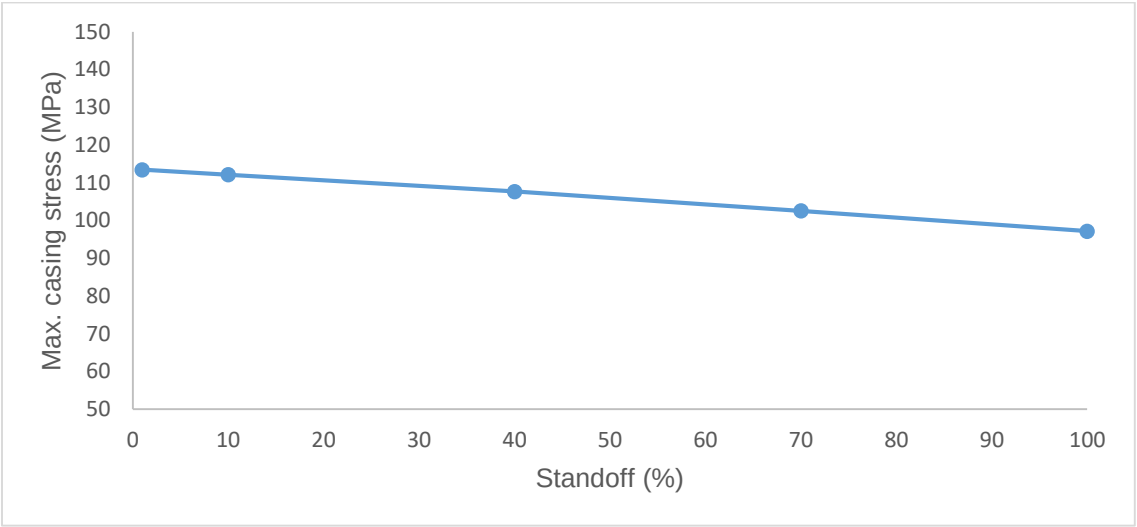

Figure 43. Maximum stress at different standoff for case 3.

Case 3: $\sigma_v = 24MPa$ $\sigma_H = 52\ MPa$

A maximum stress of 422.68 MPa occurs at 100% standoff, and a maximum stress of 425.67 MPa occurs at 1% standoff. There is an increase of less than 1% from the best to the worst centralization. The orientation of the maximum stresses also changes with a standoff decrease as the base case.

For the cement, a maximum stress of 72.17 MPa occurs at 100% standoff, and a maximum stress of 80.454 MPa occurs at 1% standoff. There is an increase of 11% from the best to the worst centralization, which represents a different tendency from the one with casing stress. Similar to

base case, there is a remarkable steep stress changes of the cement within a short distance for the worst centralization.

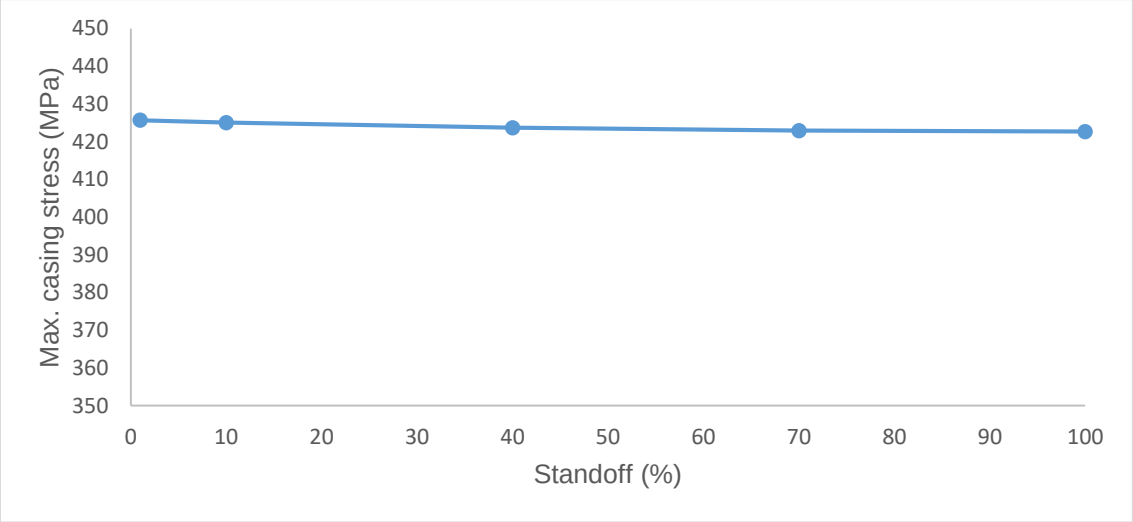

Figure 44. Maximum stress at different standoff for case 3

Case 4: $\sigma_v = 52MPa\ \sigma_H = 24\ MPa$

A maximum stress of 422.67 MPa occurs at 100% standoff, and a maximum stress of 441.42 MPa occurs at 1% standoff. There is an increase of around 4% from the best to the worst centralization. The orientation of the maximum stresses also changes with a standoff decrease as case 2.

For the cement, a maximum stress of 72.13 MPa occurs at 100% standoff, and a maximum stress of 72.642 MPa occurs at 1% standoff. There is an increase of less than 1% from the best to the worst centralization, which represents a different tendency from the one with casing stress. Similar to case 1, there isn't a remarkable steep stress changes of the cement within a short distance for the worst centralization The changes of equivalent stress in the cement sheath are more progressive.

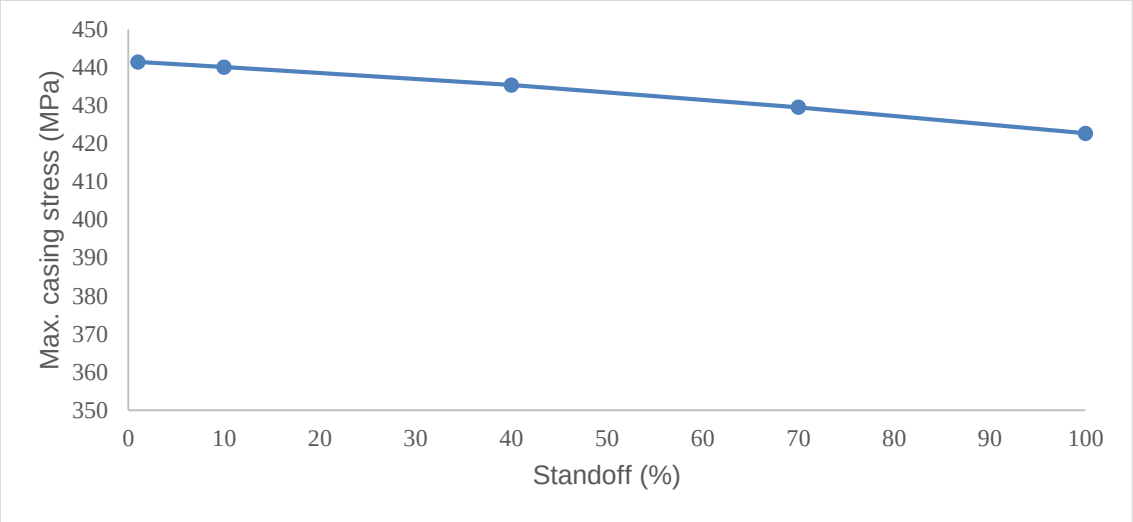

Figure 45. Maximum stress at different standoff for case 4

Cement sheath with voids

For this model, it was only considered a void pressure of 20 MPa and 40 MPa. Even though a void pressure of 0 MPa is more critical, it is less likely to occur during hydraulic fracturing operations. The simulations were run for 10% and 100% standoff.

Case 1: $\sigma_v = 82\ MPa\ \sigma_H = 54\ MPa$

A maximum stress around 970 MPa that would lead to casing deformation in a TP140 casing grade occurs at a void angle between 30º and 90º for a void pressure of 20 MPa. 835 MPa is the highest maximum stress obtained for a void pressure of 40 MPa at a void angle of 60º. The results are similar for the ones obtained from 100% standoff especially when the void angle is higher than 20º. There is a representative difference of 80 MPa between 10% and 100% standoff when the void angle is 30º for a void pressure of 20 MPa.

Figure 46 shows the stress distribution in the casing for 10% standoff and VP=20 MPa at void angle of 60º, 90º, and 120º. There are approximately two to three points were casing deformation might occur and they are located in the proximity to the contact area between the void and the casing. At a void angle of 120º, the maximum stress occurs at the contact area between the

casing and almost the end of curvature of the void. Figure 47 shows the cement stress distribution for 10% standoff and VP=20 MPa at void angle of 60º and 120º. 715.7 MPa and 711 MPa are the maximum stresses for 60º and 120º respectively, and they occur at the intersection between the cement and the void formed in the cement sheath. The location of maximum stress in the cement is the same for all the cases.

Figure 46. Casing stress distribution for 10% standoff and VP=20 MPa at void angle of 60º(left), 90º(center), and 120º(right) in case 1

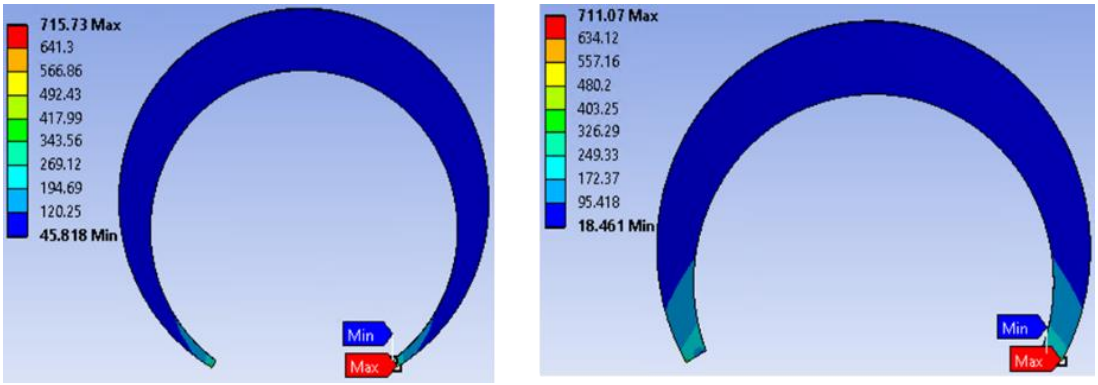

Figure 47. Cement stress distribution for 10% standoff and VP=20 MPa at void angle of 60º(left) and 120º(right) in case 1

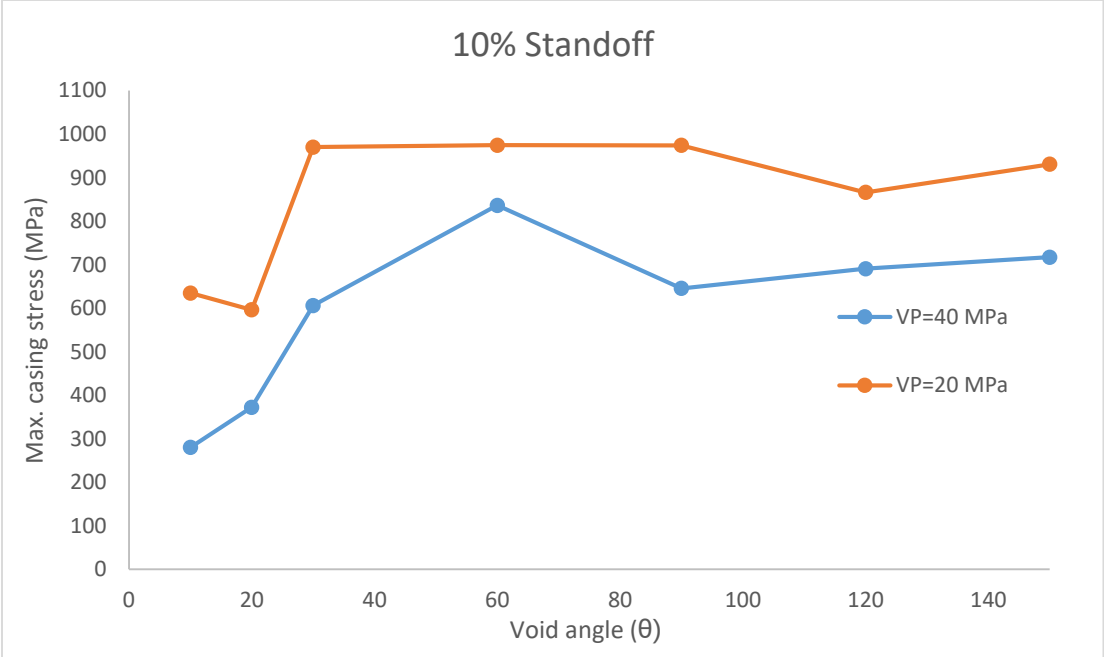

Figure 48. Maximum stress at 10% standoff for a void pressure of 40 MPa and 20 MPa for case 1

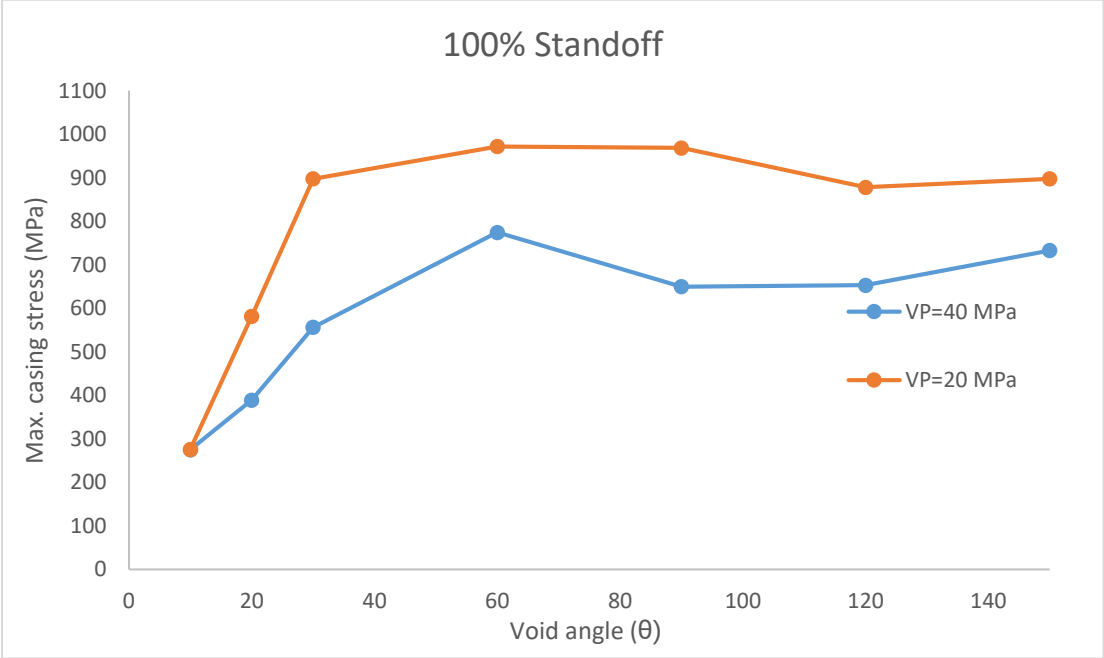

Figure 49. Maximum stress at 100% standoff for a void pressure of 40 MPa and 20 MPa for case 1

Case 2: $\sigma_v = 54\ MPa\ \sigma_H = 54\ MPa$

A maximum stress around 974 MPa that would lead to casing deformation in a TP140 casing grade occurs at a void angle between 30º and 90º for a void pressure of 20 MPa. 837.5 MPa is the highest maximum stress obtained for a void pressure of 40 MPa at a void angle of 60º. The results are similar for the ones obtained from 100% standoff especially when the void angle is higher than 60º for void pressure of 20 MPa and higher than 90º for void pressure of 40 MPa.

Figure 50 shows the stress distribution in the casing for 10% standoff and VP=20 MPa at void angle of 60º, 90º, and 120º. There are approximately two to three points were casing deformation might occur and they are located in the proximity to the contact area between the void and the casing. Figure 51 shows the cement stress distribution for 10% standoff and VP=20 MPa at void angle of 60º and 120º. 525.3 MPa and 416.72 MPa are the maximum stresses for 60º and 120º respectively, and they occur at the intersection between the cement and the void formed in the cement sheath. The location of maximum stress in the cement is the same for all the cases.

Figure 50. Casing stress distribution for 10% standoff and VP=20 MPa at void angle of 60º(left), 90º(center), and 120º(right) in case 2

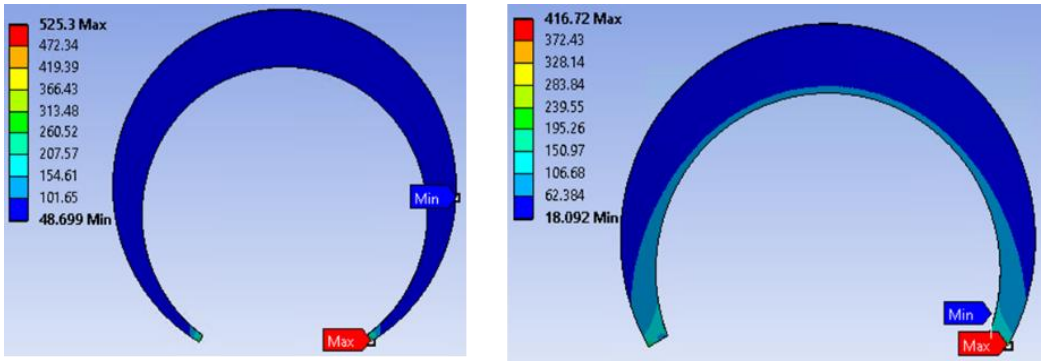

Figure 51. Cement stress distribution for 10% standoff and VP=20 MPa at void angle of 60º(left) and 120º(right) in case 2

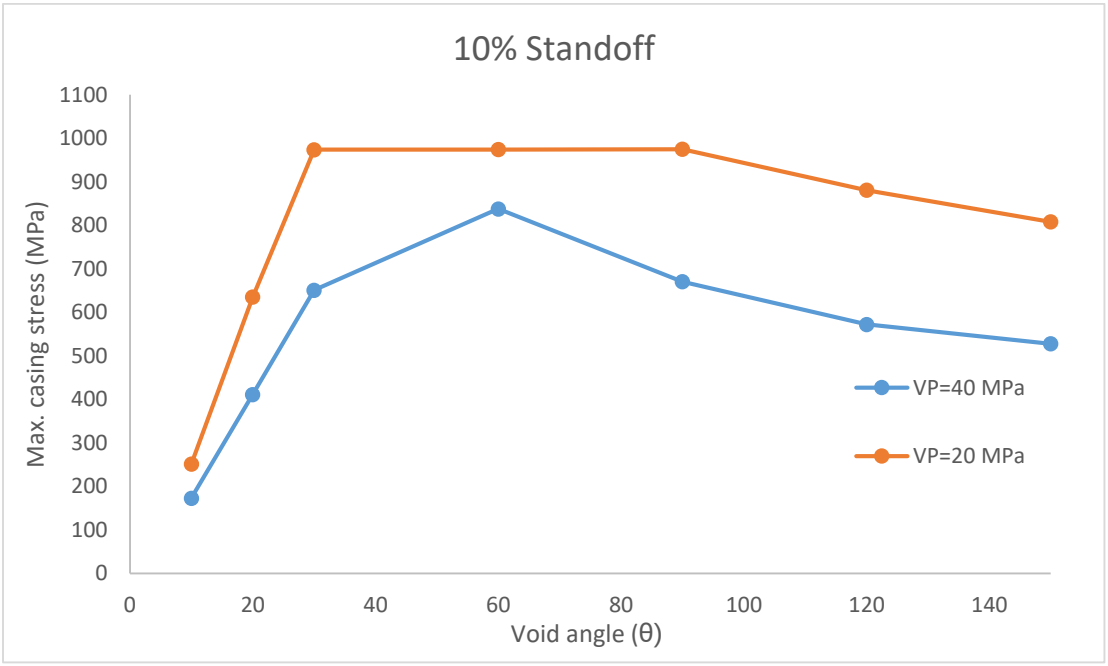

Figure 52. Maximum stress at 10% standoff for a void pressure of 40 MPa and 20 MPa for case 2

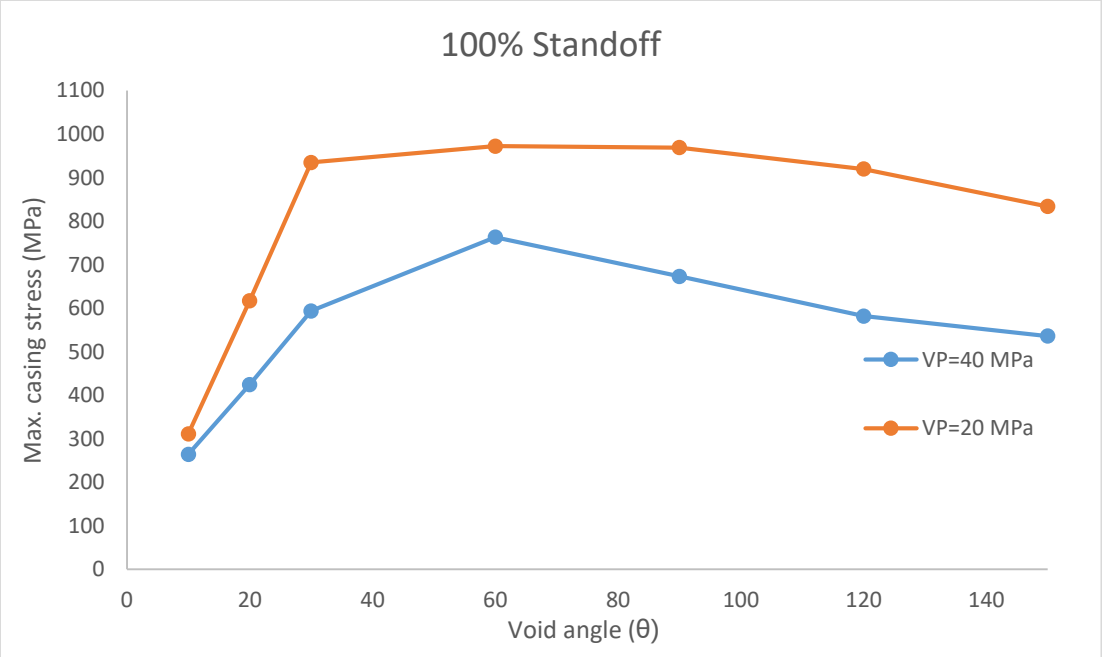

Figure 53. Maximum stress at 100% standoff for a void pressure of 40 MPa and 20 MPa for case 2

Case 3: $\sigma_v = 24\ MPa\ \sigma_H = 52\ MPa$

A maximum stress around 972 MPa that would lead to casing deformation in a TP140 casing grade occurs at a void angle between 30º and 90º for a void pressure of 20 MPa. 823.73 MPa is the highest maximum stress obtained for a void pressure of 40 MPa at a void angle of 60º.

The results are similar for the ones obtained from 100% standoff especially when the void angle is higher than 60º for void pressure of 20 MPa and higher than 90º for void pressure of 40 MPa. There is a representative difference of 60 MPa between 10% and 100% standoff when the void angle is between 30º and 60º for a void pressure of 40 MPa.

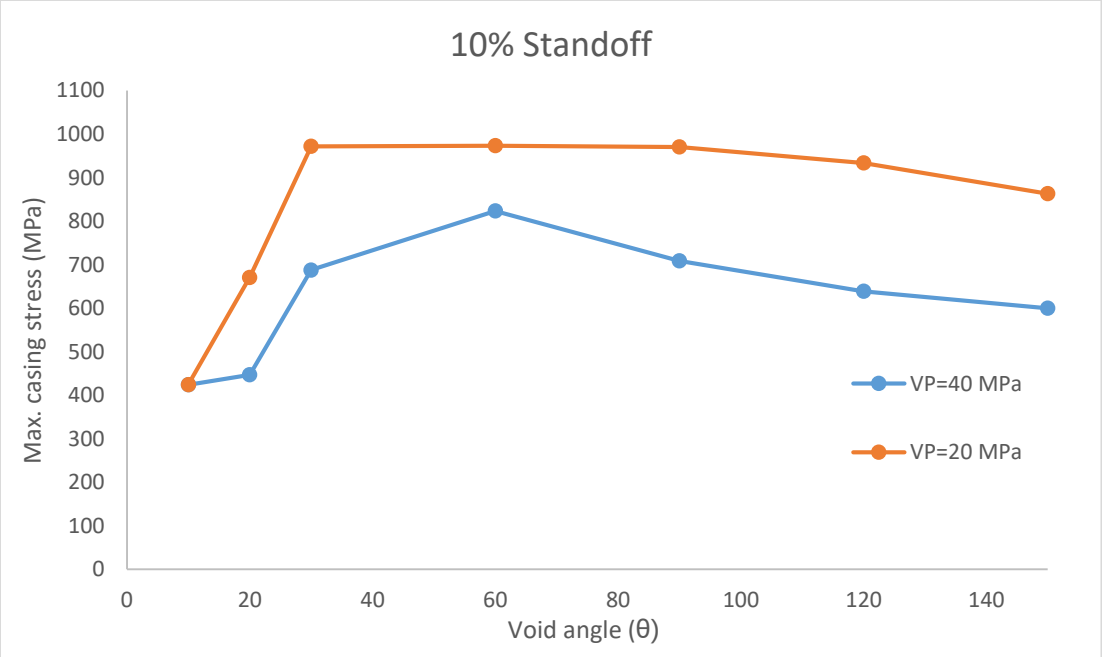

Figure 54. Maximum stress at 10% standoff for a void pressure of 40 MPa and 20 MPa for case 3

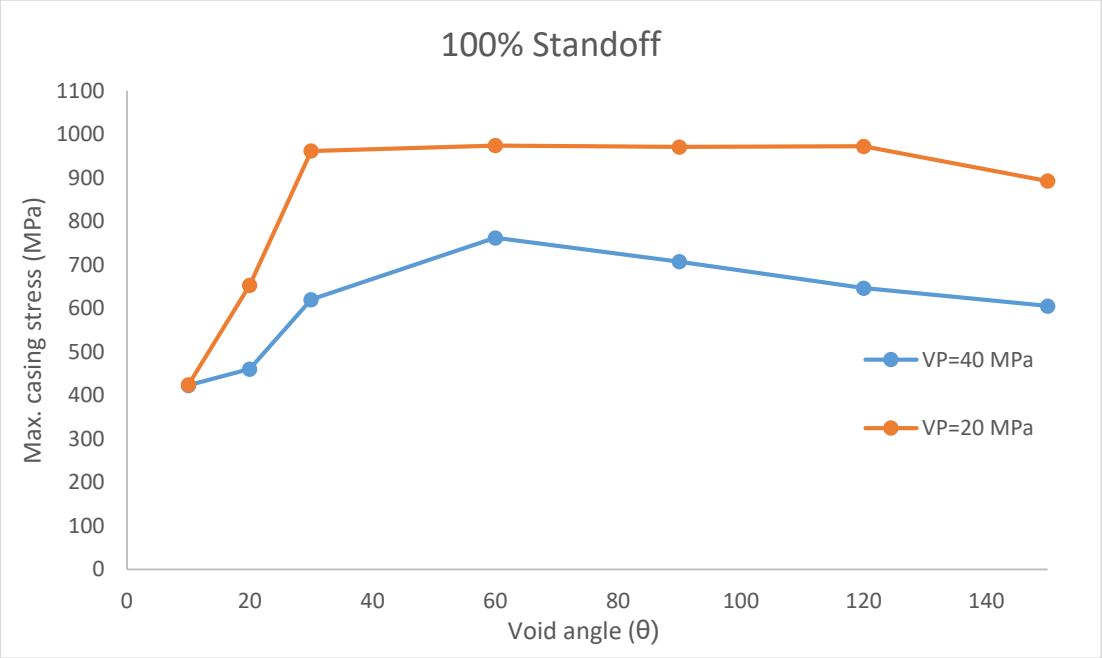

Figure 55. Maximum stress at 100% standoff for a void pressure of 40 MPa and 20 MPa for case 3

Case 4: $\sigma_v = 24\ MPa\ \sigma_H = 52\ MPa$

A maximum stress around 969.75 MPa that might lead to casing deformation in a TP140 casing grade occurs only at a void angle 60º for a void pressure of 20 MPa. 686.87 MPa is the highest maximum stress obtained for a void pressure of 40 MPa at a void angle of 120º.

The results are similar for the ones obtained from 100% standoff especially when the void angle is higher than 60º for void pressure of 20 MPa and higher than 90º for void pressure of 40 MPa. There is a representative difference of 85 MPa between 10% and 100% standoff when the void angle is between 30º for a void pressure of 20 MPa.

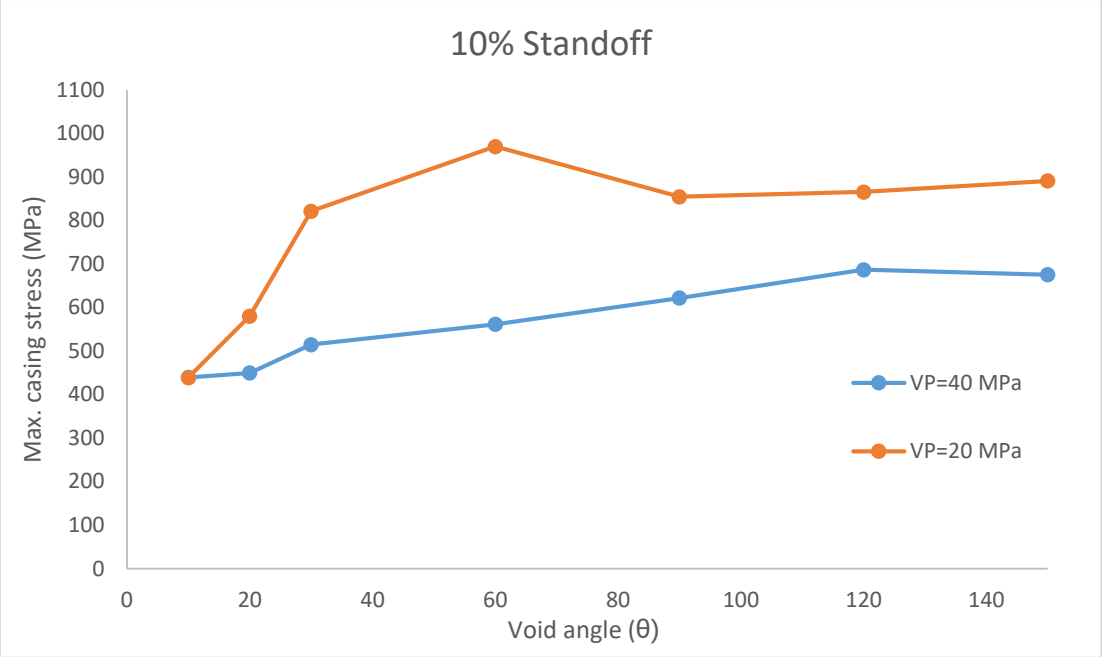

Figure 56. Figure 32. Maximum stress at 10% standoff for a void pressure of 40 MPa and 20 MPa for case 4

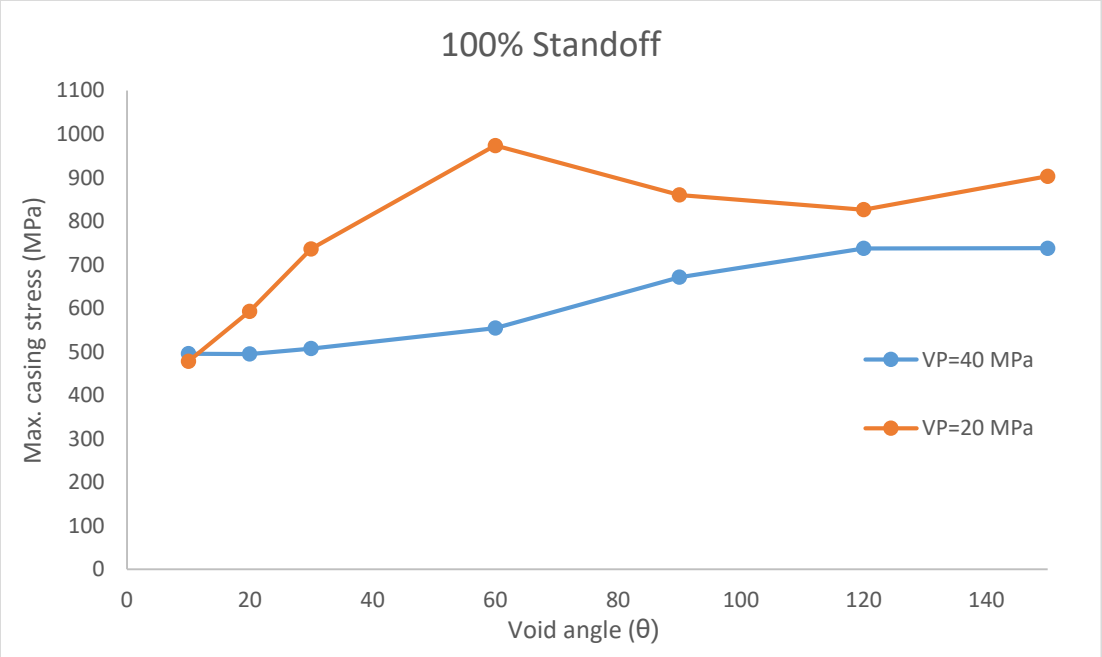

Figure 57. Figure 32. Maximum stress at 100% standoff for a void pressure of 40 MPa and 20 MPa for case 4

4.1.2 Internal Casing Pressure

Complete cement sheath

Figure 58 and Figure 59 show the results of maximum stress on casing at different internal pressure. The values were chosen in a close range to the ones used in the completion operation in Sichuan Basin.

For the concentric case, a higher value of 436 MPa occurs at 120 MPa of internal pressure and a lower of 278.13 MPa occurs at 80 MPa. For the eccentric case (10% standoff), a higher value of 453.48 MPa occurs at 60 MPa of internal pressure and a lower value of 305.64 MPa occurs at 100 MPa. Linear tendency is not observed with the increase of internal pressure in the casing, and there is not a risk of casing deformation under these parameters even for lower grade casing such as P95.

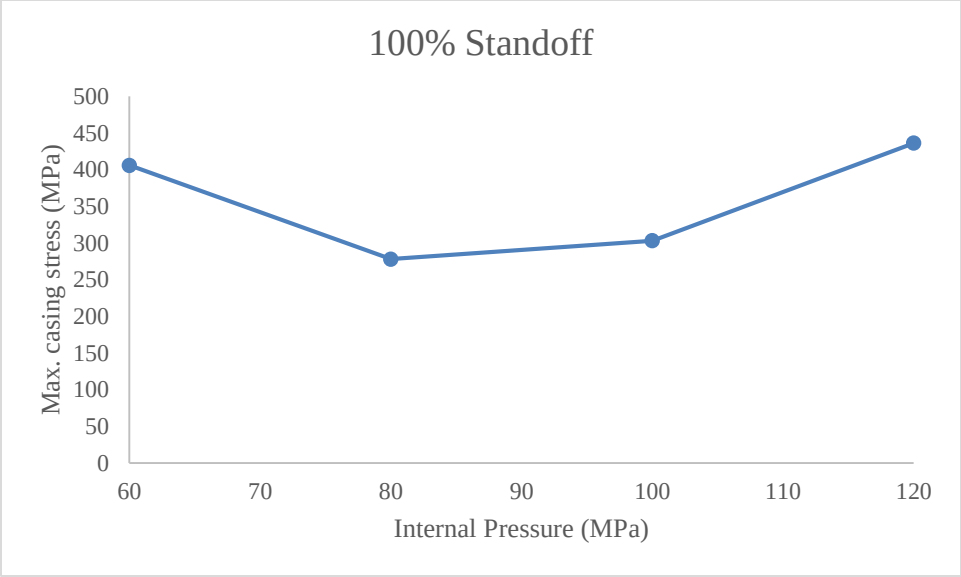

Figure 58. Maximum casing stress under different internal pressure for a concentric case

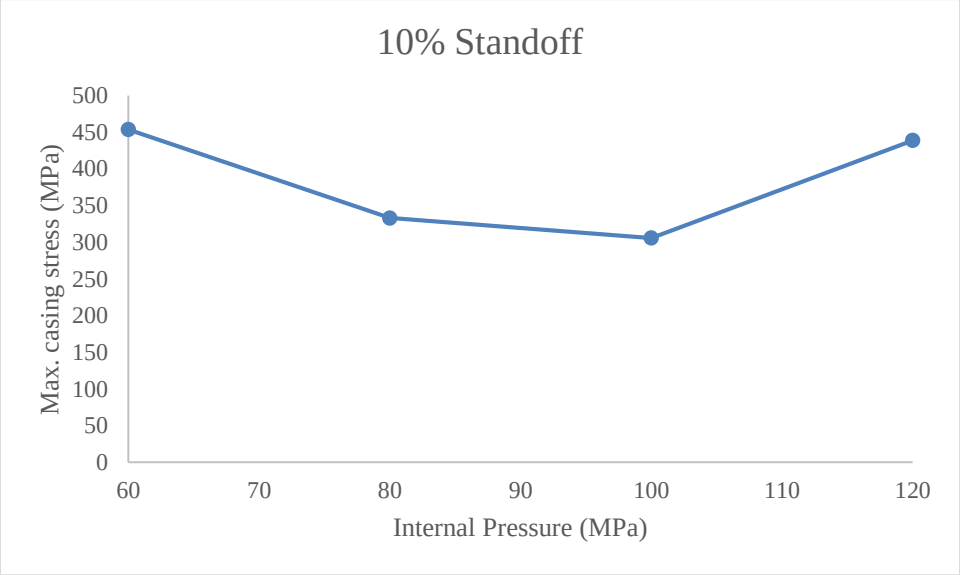

Figure 59. Maximum casing stress under different internal pressure for an eccentric case

Cement sheath with voids

Based on Figure 30, for an eccentric case (10% standoff) and internal casing pressure of 80 MPa, casing deformation occur for void pressures of 40, 20 and 0 MPa. Therefore, in order to analyze more critically the effect of internal pressure, it was chosen a void pressure of 60 MPa that doesn't

experience casing deformation for casing grade of TP140. However, there is still a high risk because casing stress on casing reach 850 MPa at a void angle of 30º.

Figure 60 shows the results of maximum casing stress on casing at different internal pressure for a 10% standoff and a void pressure of 60 MPa. The results of 60 MPa of internal pressure are very similar for the ones of 80 MPa. There is a representative increase of casing stress when the internal pressure goes from 80 MPa to 100 MPa and then to120 MPa at void angles higher than 30º (between 240 MPa and 500 MPa). On the other hand, at void angles lower than 30º, casing stresses at internal pressures of 100 MPa and 120 MPa are lower than 80 MPa.

The most critical results occur at 120 MPa internal pressure since casing deformation will happen even for the highest casing grade available (TP140) for void angles between 30º and 90º. 100 MPa has also important results since it might lead to casing deformation in lower casing grades (P110).

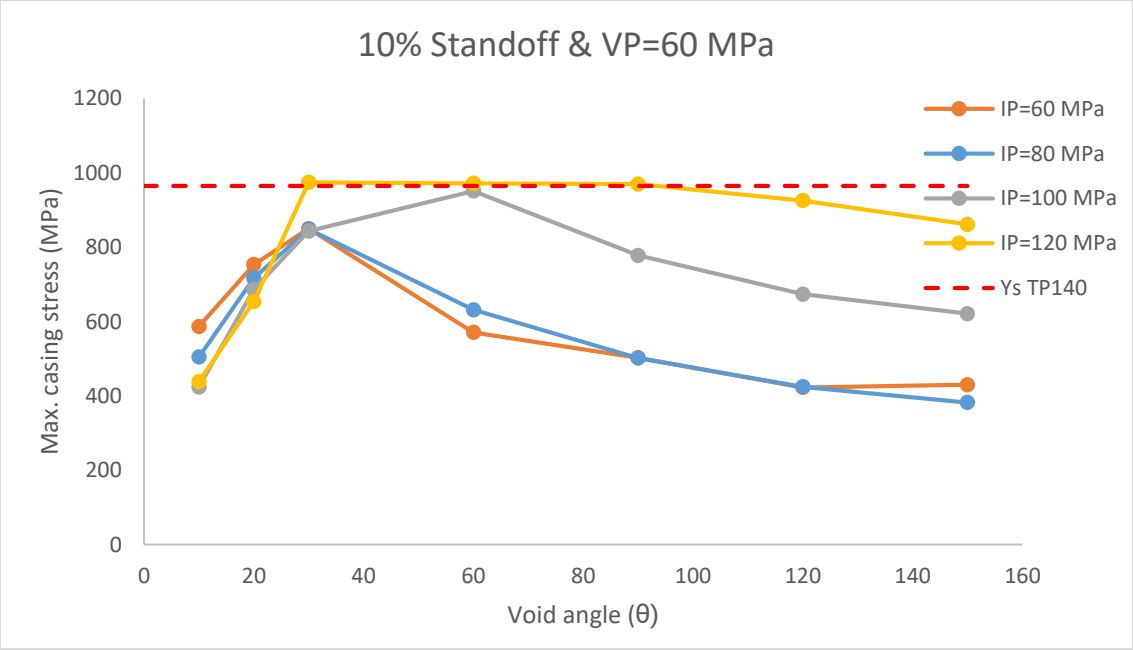

Figure 60. Maximum casing stress for an eccentric case with voids in the cement sheath

4.2 Effect of temperature

Temperature might have a great impact in casing and cement integrity during hydraulic fracturing as discussed before. At high temperatures the casing stress might increase to surpass the yield strength or voids in the cement might shrink creating an addition external load. The location of the maximum casing and cement stress might also rotate in a decrease of temperature. An initial casing designed needs to consider all these variables in order to avoid any wellbore integrity issue.

The effect of temperature was evaluated initially in two simple cases for a concentric casing and complete cement sheath. A heating case were the formation/cement was kept at 22 ºC and the temperature of the casing was increasing progressively to 100ºC. And, a cooling case were the formation/cement was kept at 100 ºC and the casing was cool down to 10ºC. It was also included an analysis with different internal casing pressure during cooling. The cooling case simulates a common case of a hydraulic fracture injection in a hot reservoir, and the heating case was effectuated just for comparison and modeling purposes. Later, the influence of standoff combine with temperature was simulated for a concentric and eccentric casing with a complete cement sheet and a cement sheath with voids.

Same models and input parameters will be used including the in-situ stresses ($\sigma_v = 54\ MPa$ and $\sigma_H = 82\ MPa$) and material properties (Table 7). The bilinear isotropic hardening concept for the casing will be included as mentioned before.

4.2.1 Heating Effect

As shown in Figure 61, the maximum stress increases from 278.1 MPa to 619.9 MPa when there is a 90 ºC increase of casing temperature. The location of the stress doesn't change, but it concentrates more in the upper and lower part of the casing. The maximum cement stress remains in the same location, and it increases around 39% from Δt=0 ºC to Δt=90 ºC.

Figure 63 shows equivalent maximum stress (Von Misses) vs differential temperature. When the temperature increase, the maximum von Mises stress in the casing also increase (linear tendency).

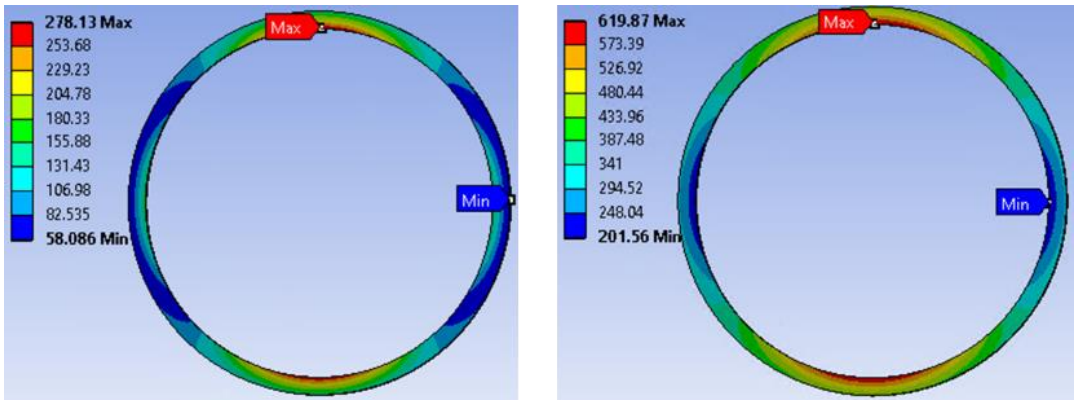

Figure 61. Stress distribution in the casing during heating with ΔT=0ºC (left), ΔT=90ºC (right)

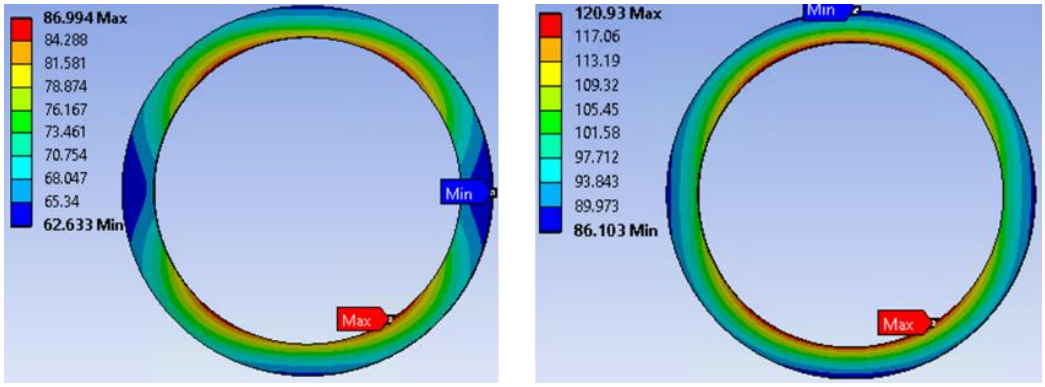

Figure 62. Stress distribution in the cement sheath during heating at ΔT:0ºC (left), ΔT:90ºC (right)

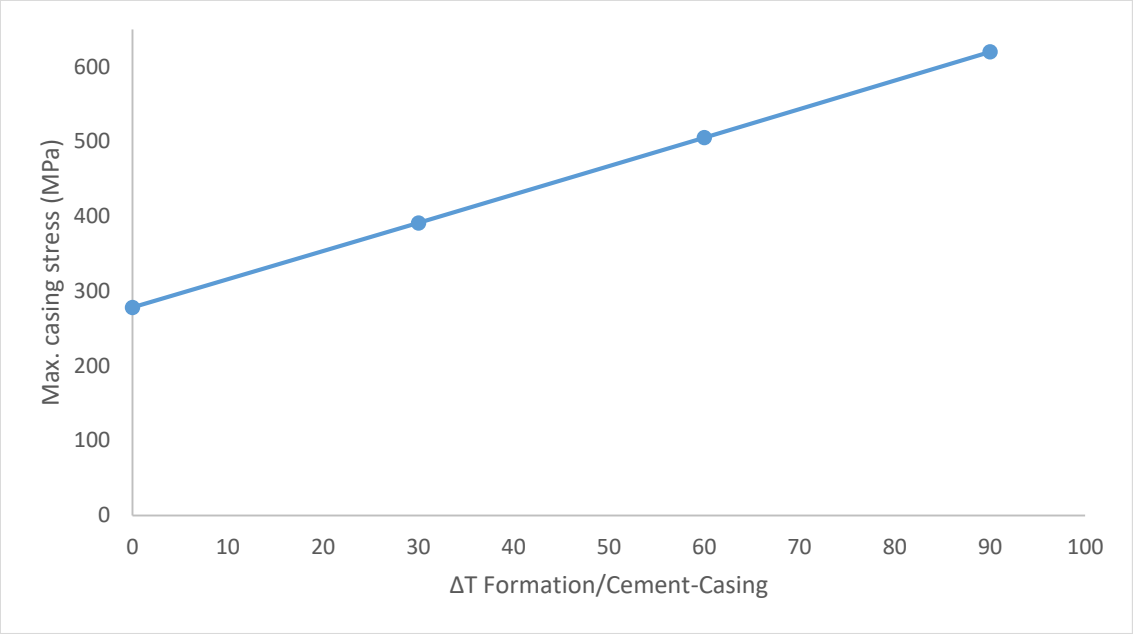

Figure 63. Maximum stress at different differential temperatures (Heating up)

4.2.2 Cooling Effect

As shown in Figure 64, the maximum stress decreases from 557.7 MPa to 230.55 MPa when there is a 90 ºC decrease of casing temperature. There is also a change of maximum stress location in the casing when the casing is cooling down. It starts to concentrate in the upper and lower part, and progressively it starts to distributed around the casing until it rotates to the sides of the casing. The maximum stress in the cement stress remains in the upper and lower part, but it starts to concentrate more in the corners (Figure 65). Maximum stress decreases around 16% from Δt=0 ºC to Δt=90 ºC.

Figure 66 shows equivalent maximum stress (Von Misses) vs differential temperature. When the temperature increase, the maximum von Mises stress in the casing also increase (linear tendency).

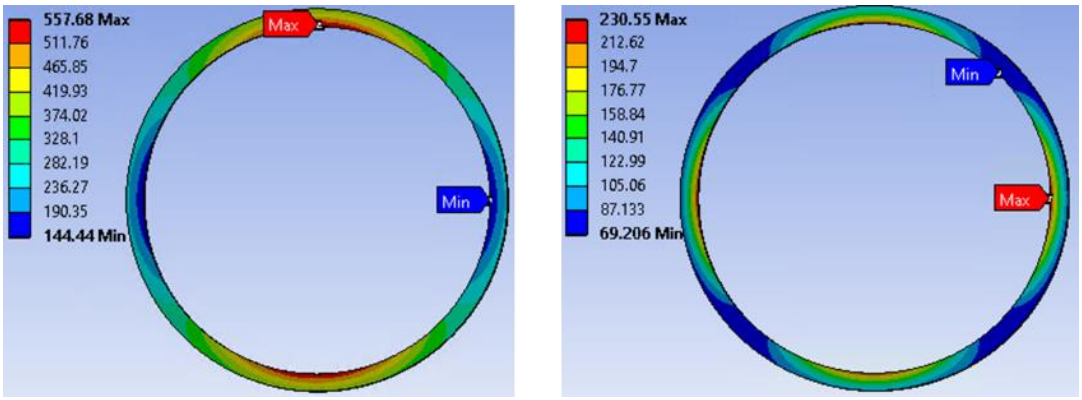

Figure 64. Stress distribution with ΔT=0ºC (left), ΔT=90ºC (right)

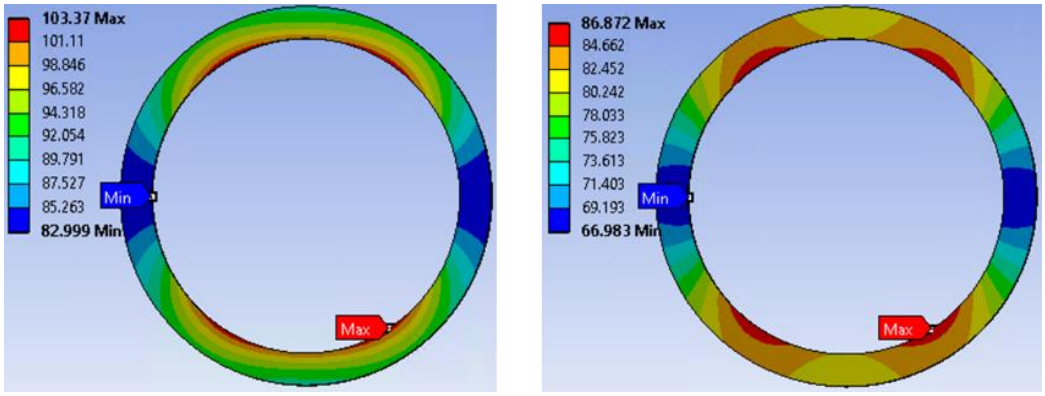

Figure 65. Stress distribution with ΔT=0ºC (left) and ΔT=90ºC (right)

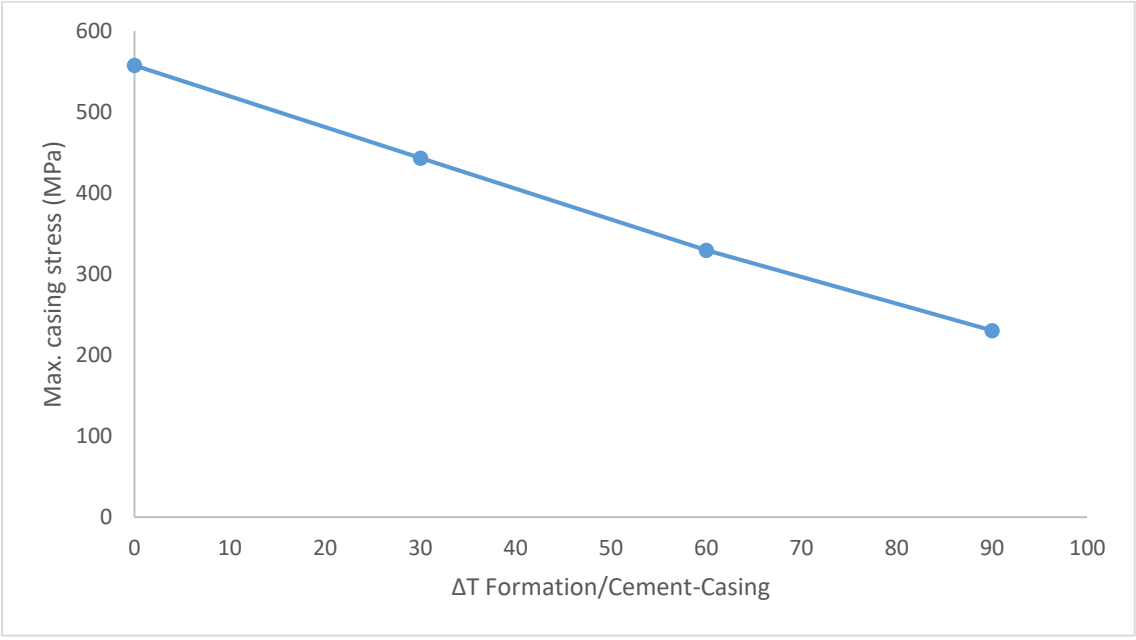

Figure 66. Maximum stress at different differential temperatures (Cooling down)

It is important to consider if this change of location and increase or decrease of maximum stress on casing keeps the same behavior and magnitude at different casing internal pressure.

4.2.3 Cooling effect under different internal pressures

As mentioned previously, the cooling effect is a realistic case because it simulates the impact of the cold hydraulic fracturing fluid entering to the hot formation and cement. The internal pressure chosen for the previous simulations was 80 MPa. It is required to evaluate if the same linear behavior of maximum equivalent stress in the casing occurs at different internal casing pressure under the same in-situ stresses ($\sigma_v = 54\ MPa$ and $\sigma_H = 82\ MPa$). This is done since the depth of the reservoir and formation properties can change between wells thus internal casing pressure.

Five different cases, 60, 80, 100, 110, and 120 MPa were simulated under the same differential temperatures. At 60 MPa when the differential temperature is 0ºC, the highest equivalent stress (688 MPa) is obtained. At this internal pressure when the differential temperature increases the maximum equivalent stress in the casing reduces linearly. This tendency is similar at an internal pressure of 80 MPa. 100 MPa of internal pressure has a similar behavior with the difference that at 30ºC, the slope starts to decrease. As the internal pressure increases (110 MPa, 120 MPa), the slope keeps reducing until it changes from negative to positive, this occurs around 30ºC. Also, the maximum equivalent stress becomes higher when this change of negative to positive happens for the consecutive lower differential temperatures.

In conclusion, cooling down the casing reduces maximum equivalent stress under these conditions for internal pressures of 60 and 80 MPa. For the other cases there is an increase of maximum equivalent stress after the casing has cooled down some temperature. However, this increase of equivalent casing stress doesn't surpass the greatest value obtained at 60 MPa and 80 MPa.

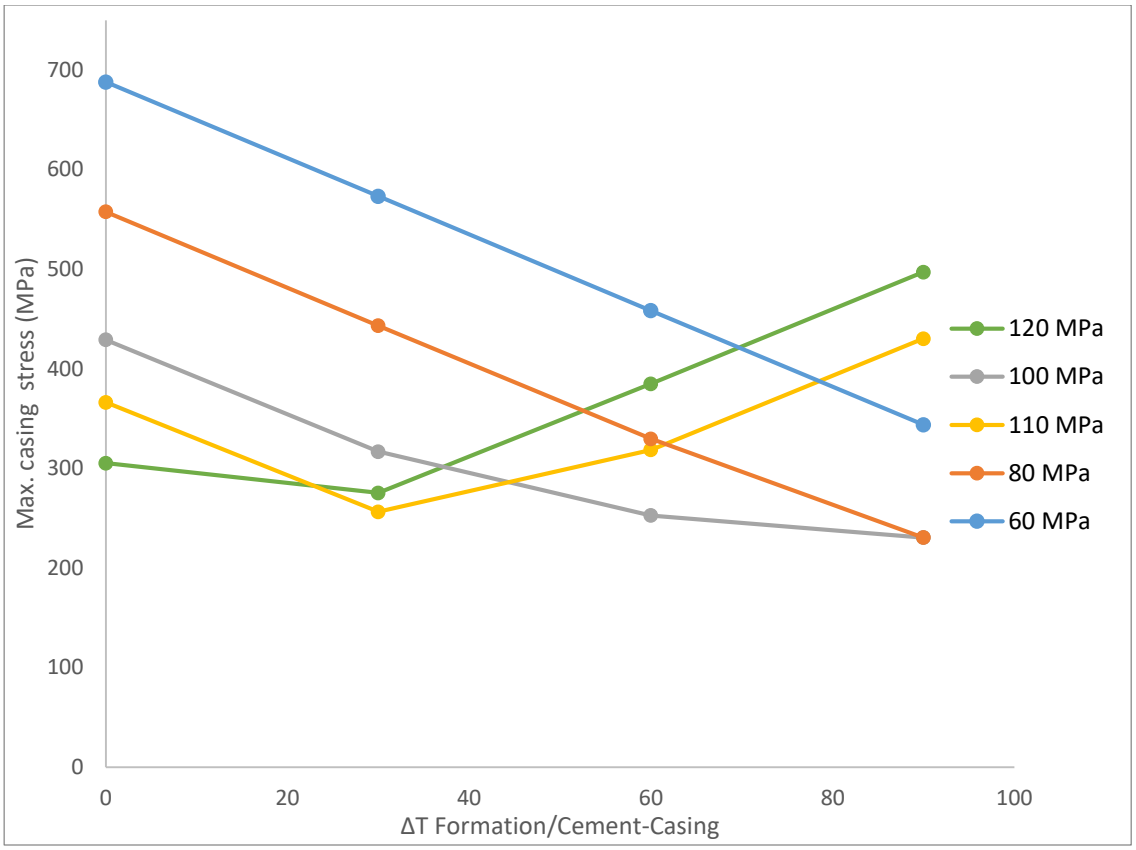

Figure 67. Cooling effect under different internal pressures

4.2.4 Influence of standoff and temperature in casing and cement stress

Complete cement sheath

Now, an analysis of the standoff and temperature influence in casing and cement stress will be performed. It is modeled at an internal pressure of 60 MPa because it is the one that exhibits the greatest equivalent maximum casing stress when the casing is cool and one of the greatest in the cement. Two simulations were run, one when the differential temperature between the formation/cement and casing is 0 C and another when the formation/cement and casing differential temperature is 96 C. A perfect concentric case of 100% an eccentric case of 5% standoff are chosen (Figure 68).

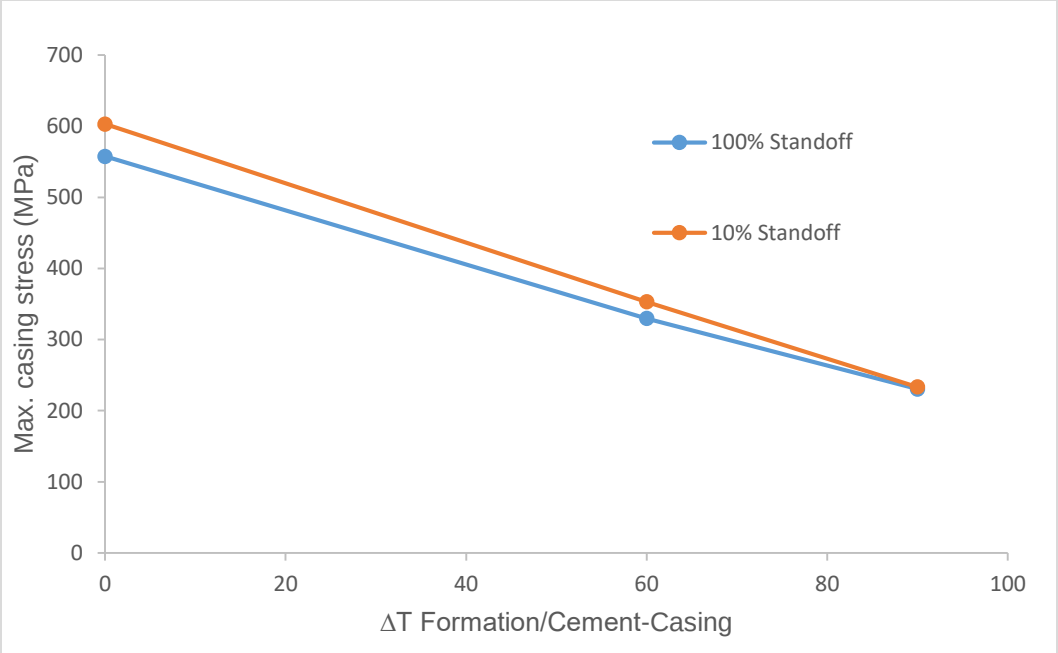

Figure 68. Comparison between a concentric and eccentric case

As it is seen in the Figure 68. the influence of standoff increases maximum equivalent stress in about 6% when there is not differential temperature, but when the differential temperature is 96 ºC, the maximum equivalent stress only increases 1.5%. There is a similar trend for the maximum stress on the cement where it goes form 100 MPa to 105 MPa for a 100% standoff and 88 MPa to 86 MPa for a 5% standoff. As it was discussed before in Figure 26, at lower standoff, a steep stress changes of approximately 18 MPa occurs in the cement within a short distance

Cement sheath with voids

For this model, it was only considered a void pressure of 20 MPa and 60 MPa. Even though, a void pressure of 0 MPa is more critical, it is less likely to occur during hydraulic fracturing operations. The simulations were run for 10% and 100% standoff. Three cases were performed in order to compare to the base case which has the default ambient temperature of 22 ºC. For the first case, it is applied 100 ºC in the formation, cement and casing. For the second one, 100 ºC is maintained in the formation and cement, and the casing is cool down to 60 ºC. And for the last

one, 100 ºC is again maintained in the formation and cement, and the casing is cool down to 20 ºC. As discussed previously, this analysis is made to simulate a common practice performed in several fields around the world, Sichuan, Haynesville and Eagle ford basins, when a cold hydraulic fracturing fluid is injected in a hot formation.

Figure 69 and Figure 70 show the results of casing maximum stress for a void pressure of 20 MPa. As it is seen in the graphs, the effect of temperature at void angles higher than 20º is insignificantly. Casing deformation will occur at 965 MPa at any void angle higher than 20º and the behavior will no longer be linear.

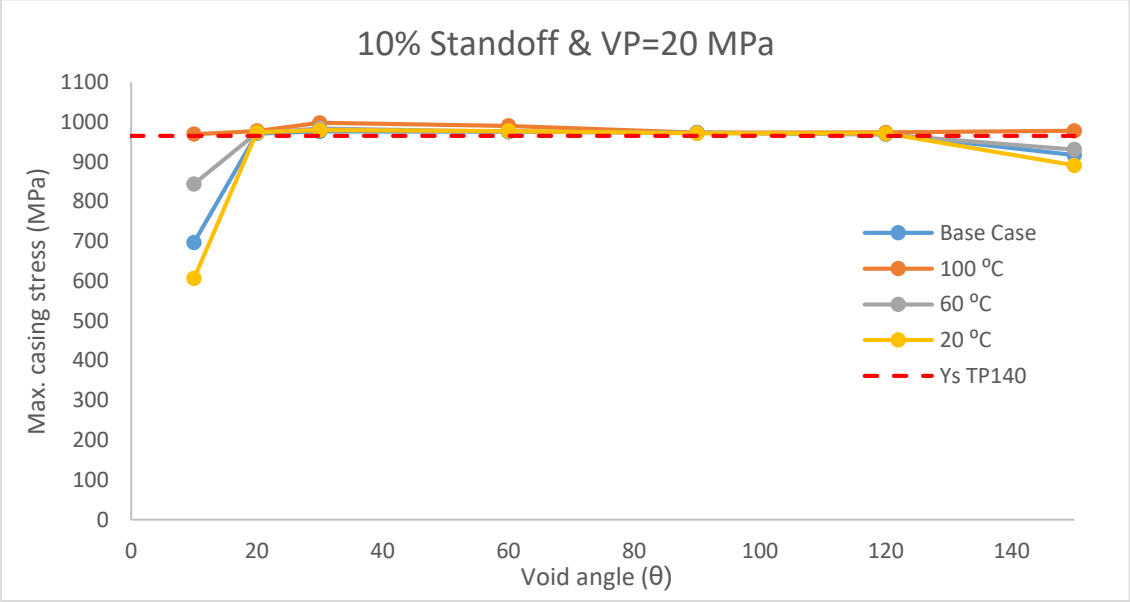

Figure 69. Temperature effect at 10% standoff and void pressure of 20 MPa

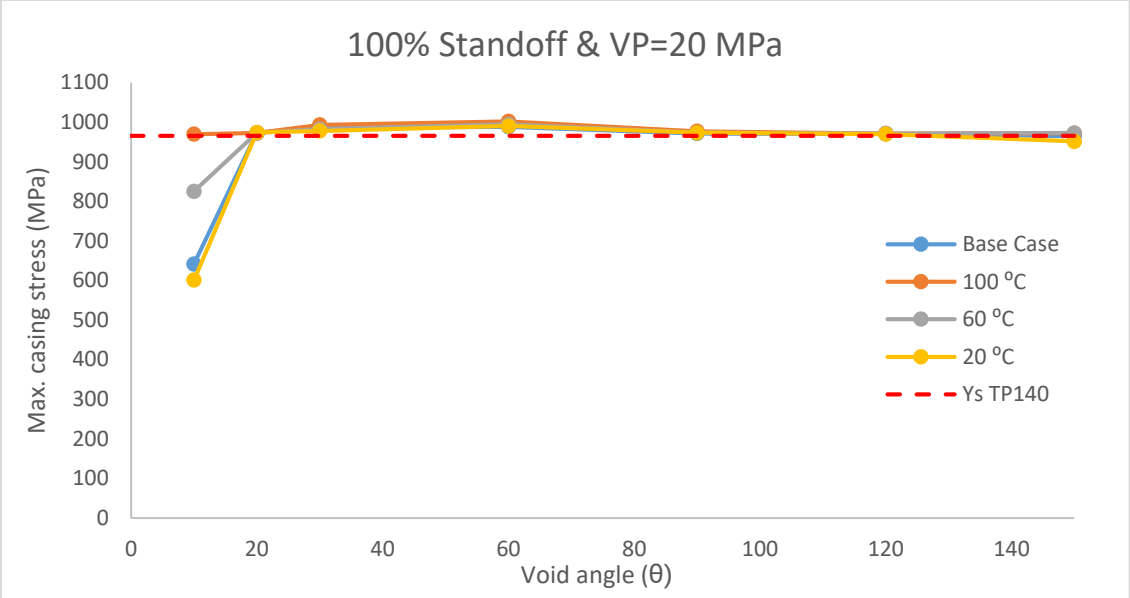

Figure 70. Temperature effect at 100% standoff and void pressure of 20 MPa

Figure 71 and Figure 72 show the results of casing maximum stress for a void pressure of 60 MPa. As it is seen in the graphs, there is a similar tendency for 10% and 100% standoff under a temperature effect. For 10% standoff, the highest values of maximum casing stress occur when 100 ºC is applied to the formation, cement and casing. Casing deformation might occur at void angles between 20º and 60º (values higher than 920 MPa). There are also high values when the casing is cool down to 60º. At void angles between 20º and 30º, the maximum casing stress reach a similar value to the one that has a casing temperature of 100 ºC. On the other hand, when the casing is cool down to 20 ºC, the maximum casing stress decreases even lower than the base case.

For 100% standoff, the highest values of maximum casing stress also occur when 100 ºC is applied to the entire system. However, the chances of casing deformation reduce because it might happen for void angles between 30º and 60º. There are also high values of maximum casing stress when the casing is cool down to 60ºC, and at void angle of 30º reaches a similar value to the

one that has the casing temperature of 100 ºC. The major difference with 10% standoff occurs when the casing is cool down 20 ºC showing higher values of maximum casing stress.

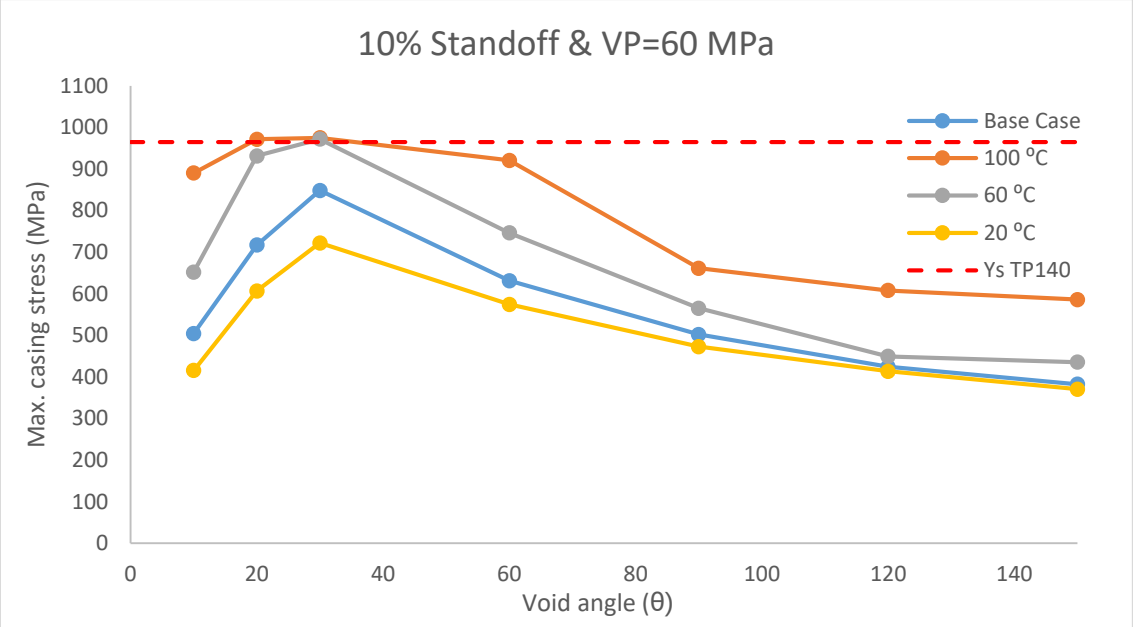

Figure 71. Temperature effect at 10% standoff and void pressure of 60 MPa

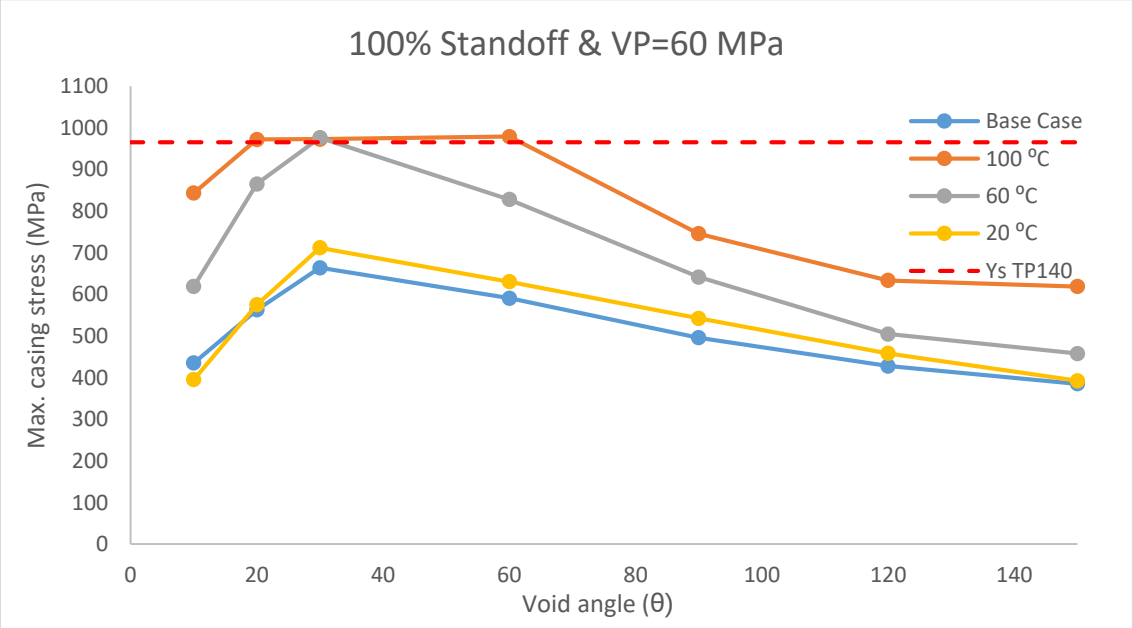

Figure 72. Temperature effect at 100% standoff and void pressure of 60 MPa

5. Discussions

As it is seen throughout the results, there are higher chances of casing deformation when the cement sheath contains drilling fluid voids. The channeling observed in a narrower side of the annulus from a well log of the W-C shale gas field confirms our findings since casing deformation occurs at the same location (Figure 3). Eccentricity also impacts the results in a complete cement sheath with an almost 22% increase of maximum casing stress from the best to the worst centralization, but the greatest value reaches only 340 MPa which is half of the yield strength of a P110 casing.

If we compare the results of maximum equivalent casing stress in a complete cement sheath and a cement sheath with voids (60º void angle) at different void pressure, the results of the cement sheath with voids will be higher. Even if the void pressure is the same as the internal casing pressure (80 MPa) at the moment of the hydraulic fracturing operation, the results are still 100 MPa higher as seen in Figure 73.

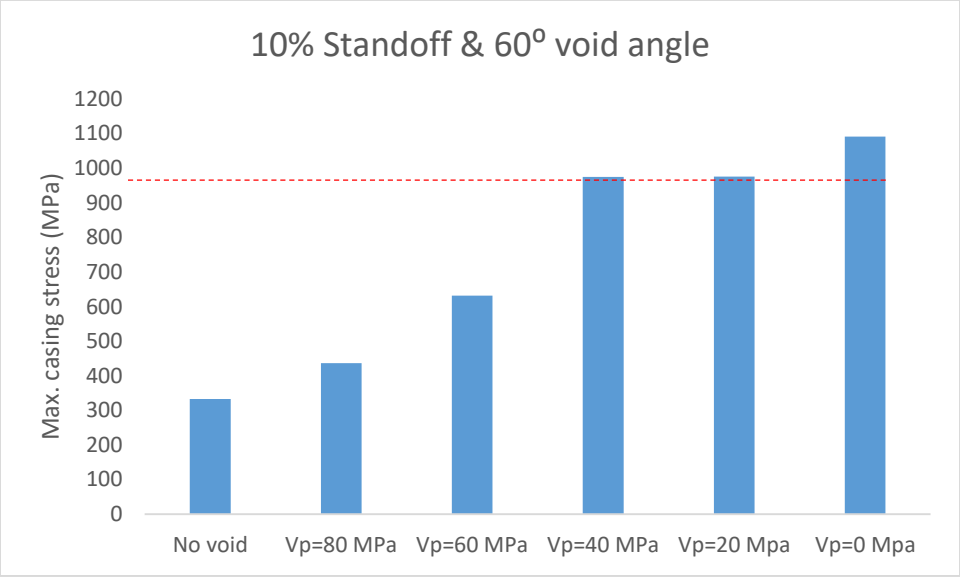

Figure 73. Comparison of maximum casing stress between a complete cement sheath and cement sheath with voids

Although the maximum casing stress results at different standoff for a complete cement sheath are far for the yield strength of a low casing grade (P95), the cement integrity might fail, and the entire system (cement and casing) will be in risk (Figure 26).

The location of the maximum casing stress is quite important since it could help to explain the reason of why casing deformation did occur. For instance, a lead mold printing could be run in the horizontal section of the well and the location of the marks on it will give an idea of the deformation location in the casing. Then, it can be compared these marks with the maximum stress location obtained from our model.

Figure 74 shows the results of the location of the maximum von Mises stress for a complete and incomplete cement sheath in our model. The location is different since three points with a high maximum equivalent stress are visible for the cement sheath with voids and only one for the complete cement sheath. In addition, the location where the maximum stress in the complete cement sheath is, represents a very a low magnitude of casing stress (close to the minimum) for the cement sheath with voids.

The location of the maximum equivalent stress for a cement sheath with voids match quite close with the marks located in a lead mold printing run in a well with casing deformation of the Sichuan Basin. Also, the magnitude of casing stress obtained is higher than the yield strength of a TP140. Therefore, we could confirm that voids in the cement sheath were a cause for the casing deformation.

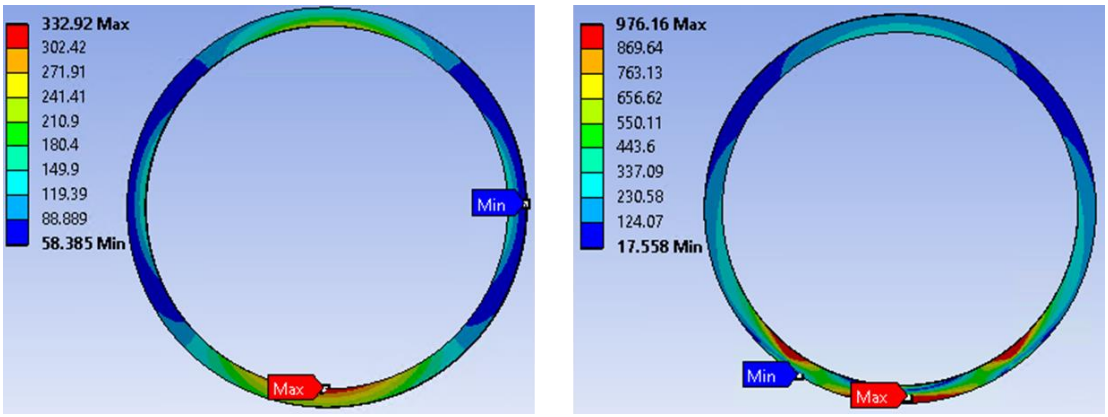

Figure 74. Location of the maximum casing stress in a complete cement sheath (left) and a cement sheath with voids at a void angle of 60^{o} (right)

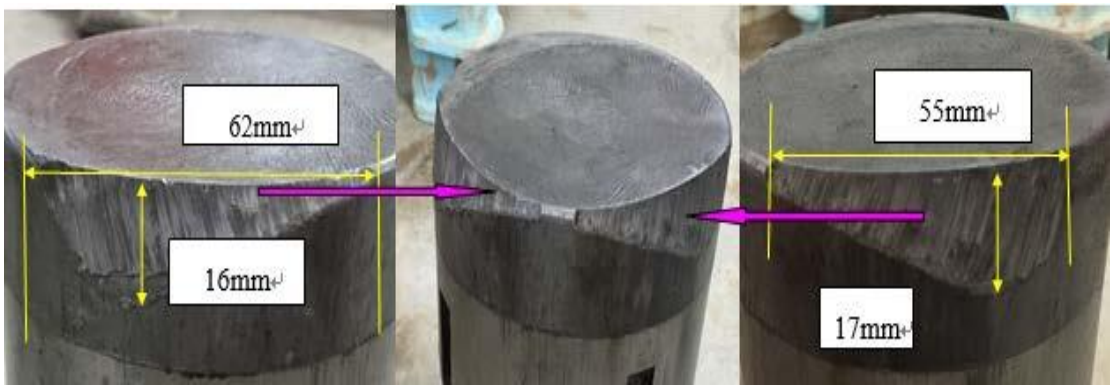

Figure 75. Picture of lead mold printing in deformed casing of well A-6

As mentioned before, we need to validate our model and conclude if the boundary conditions such as in situ stresses and internal pressure have a great impact on the maximum casing stress and if under different boundary conditions the result will be better or worse for the wellbore integrity.

5.1 Influence of standoff at different in-situ stress

Figure 76 shows a comparison of the maximum casing stress vs standoff for the five cases in a complete cement sheath. As it is seen in the graph and discuss previously, only the base case ($\sigma_v = 54MPa$ $\sigma_H = 82\ MPa$) has a noticeable increase of maximum casing stress when the standoff is

decreasing. Even though, the increase of maximum casing stress of the base case is the highest one, the overall maximum stress of case 4 and case 3 is approximately 1.3 times higher. Case 2 is the one who exhibits lower maximum casing stress.

The initial thought was that under higher-geo stress in a complete cement sheath, the maximum casing stress was going to be higher. However, this assumption didn't work for these cases. At lower geo-stresses, the maximum equivalent von Mises stress in the casing was higher than the cases were the in-situ stresses were bigger. It is important to notice that if the stress anisotropy reduces (case 2), the maximum casing stress reduces considerably.

For the cement sheath stress, base case and case 3 are the ones who present a high chance of cement failure since the maximum stress increase around 12% for both cases. There is also a remarkable steep stress changes of the cement within a short distance for the worst centralization (Figure 26, Figure 42) For the other three cases, the cement stress increase is less than 1%.

To conclude, case 1,2 and 4 do not present a risk of casing deformation even for a low grade casing as the P95. There is still a chance of deformation for the base case and case 3 in a complete cement sheath. They might experience a promptly failure of the cement, so casing will be exposed directly to the formation (pore pressure, hydraulic fracturing fluids, and natural fracture slippage).

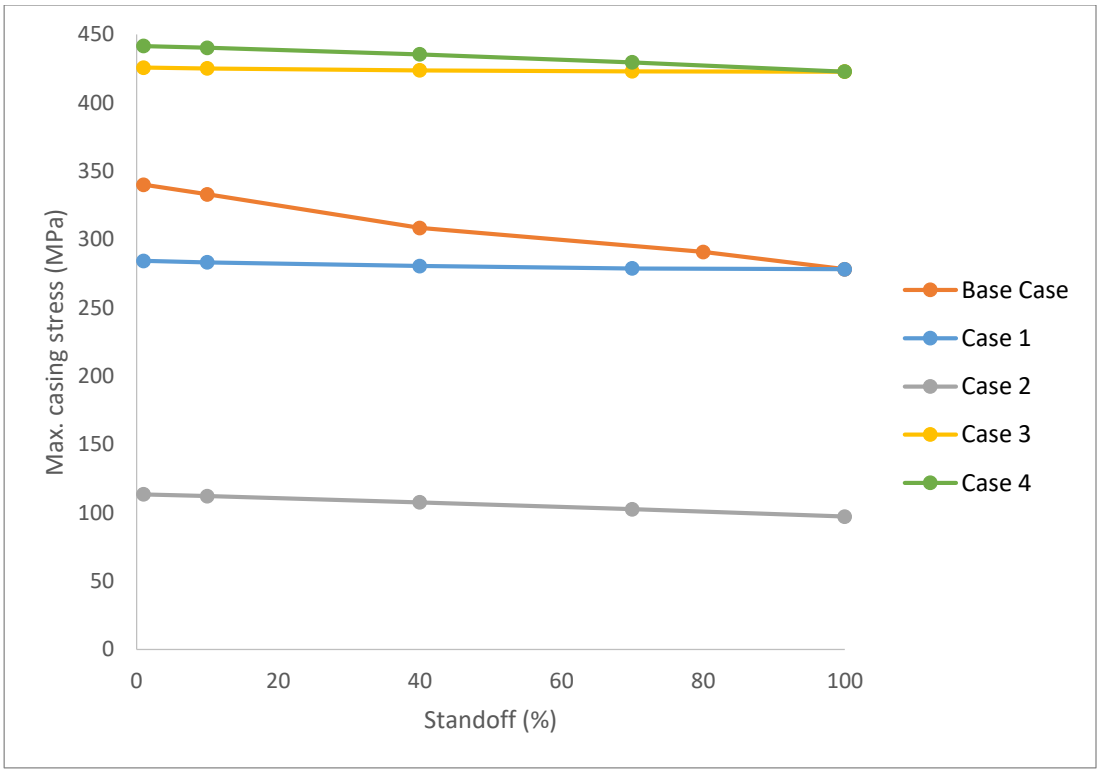

Figure 76. Comparison of the five cases for a complete cement sheath.

In a cement sheath with voids, the differentiation between the cases is completely unlike. Figure 77 shows the comparison among base case, case 1 and 2 and Figure 78 shows the comparison among base case, case 3 and case 4 for 10% standoff and a void pressure of 20 MPa.

The worst case scenario is the base case ($\sigma_v = 54MPa \quad \sigma_H = 82\ MPa$) since casing deformation in a P140 casing grade is happening at void angles between 20º and 120º. There isn't casing deformation at void angles higher than 120º, but the maximum casing stress result (916 MPa) at those angles are close to the yield strength of the casing. Case 1, 2 and 3 exhibit a similar behavior, but their chances of casing deformation reduce since the maximum casing stress exceeds the yield strength at void angles between 30º and 90º. The only case that exhibits a different behavior and the chances of casing deformation are almost zero is the case 4. It would occur at a void angle of 60º. In fact, the maximum casing stress only exceeds in two points the yield strength of a Q125 (862 MPa) grade casing.

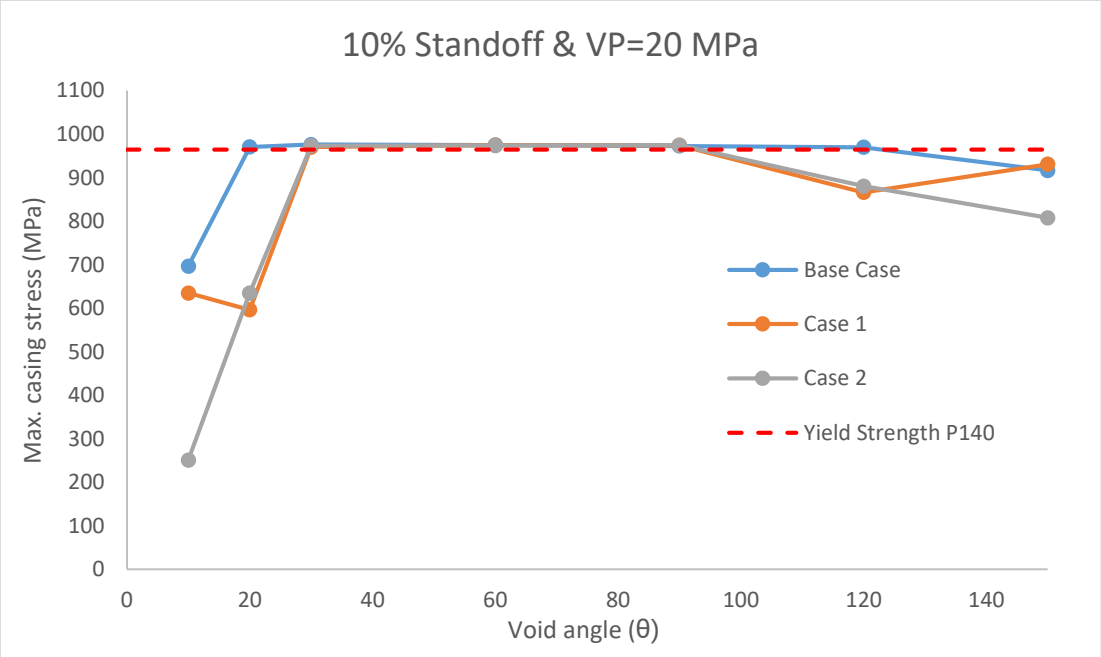

Figure 77. Comparison among base case, case 1 and case 2 for a cement sheath with voids and a void pressure of 20 MPa

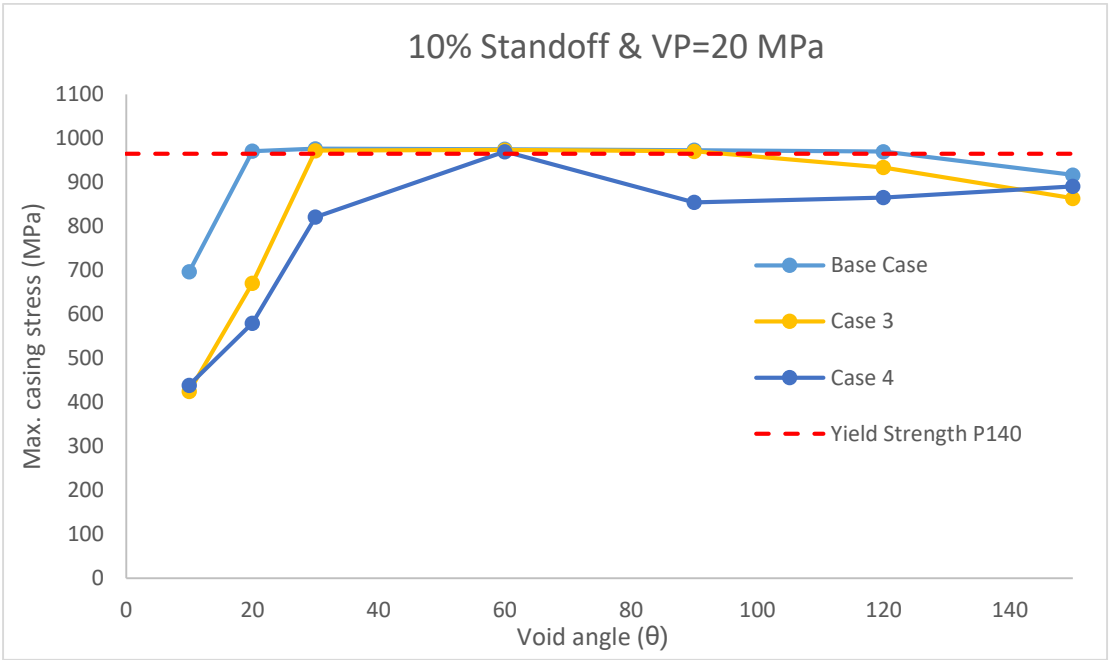

Figure 78. Comparison among base case, case 3 and case 4 for a cement sheath with voids and a void pressure of 20 MPa

As mentioned previously, case 4 represents a Normal fault regime with a lower and common magnitude of in-situ stresses. Based on the literature, a similar magnitude and sometimes lower is seen in some shale fields of the United States were hydraulic fracturing is a necessary activity for every well drilled. Also, centralization is sometimes not properly used or not use at all in some wells, and still cases of casing deformation during hydraulic fracturing are quite uncommon. Therefore, the combination of high geo-stress in a high anisotropy and reverse fault regime with the formation of voids in the cement sheath could be a reason of casing deformation during hydraulic fracturing in the Weiyuan-Changning shale gas field in China.

Figure 79 shows the comparison among base case, case 1 and 2 and Figure 80 shows the comparison among base case, case 1 and case 2 for 10% standoff and a void pressure of 40 MPa.

At this void pressure, casing deformation might only occur for the base case. The only maximum casing stress values that exceeds the yield strength of the casing P140 happens in this case at void angles between 30º and 60º. In fact, a Q125 casing grade will be enough to withstand without deformation during hydraulic fracturing operations. The results between case 2 and case 3 are similar. Case 1 has a similar tendency only at void angles lower than 90º to case 2 and 3. After 90º the maximum casing stress in case 1 starts to increase in compare with the case 2 and 3 which decrease. Case 4 has generally lower values than the other cases, but its tendency is to increase when the void angle becomes higher. A possible reason for this different behavior in case 4 and part of the case 1 is the fact that the location of the maximum stress on casing changes from the internal section to the external one

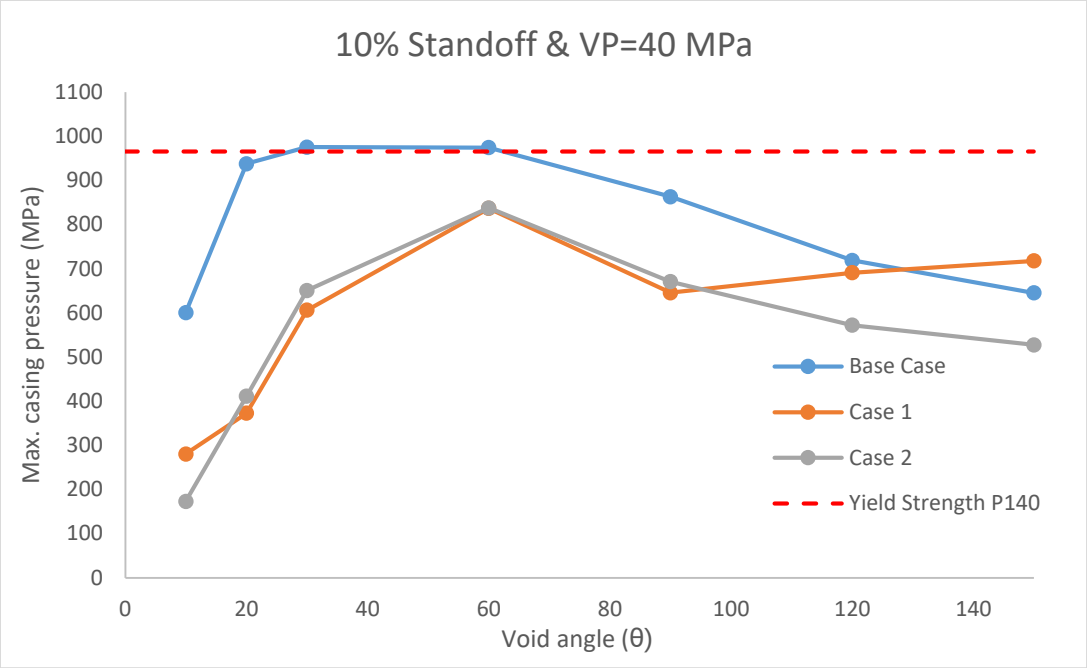

Figure 79. Comparison among base case, case 1 and case 2 for a cement sheath with voids and a void pressure of 40 MPa

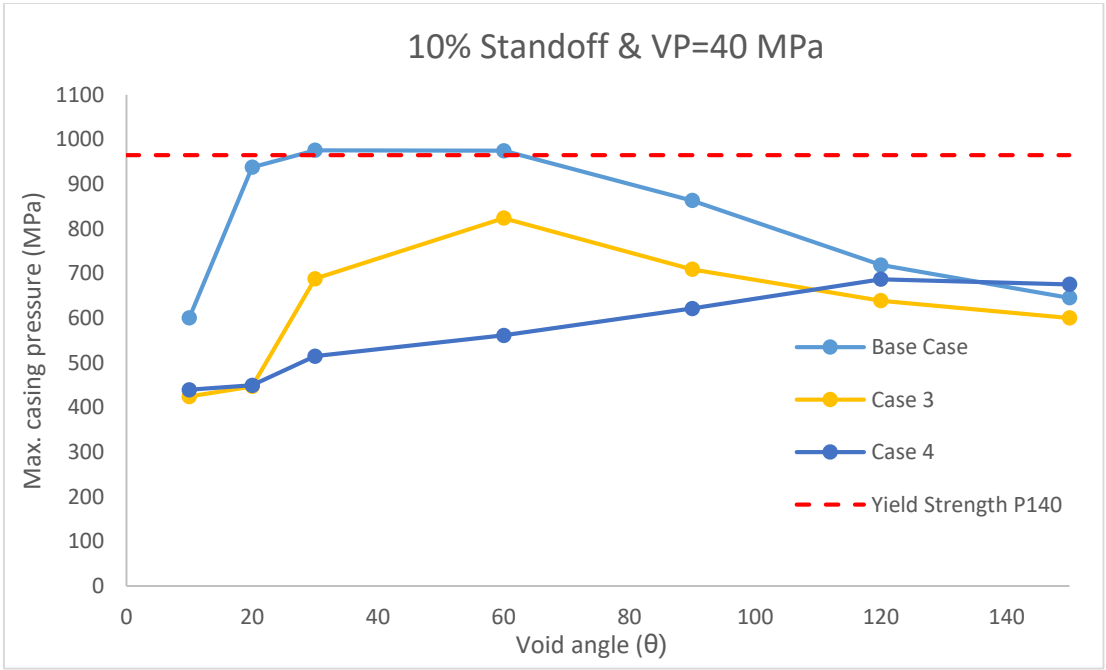

Figure 80. Comparison among base case, case 3 and case 4 for a cement sheath with voids and a void pressure of 40 MPa

Figure 81 shows how the location of the maximum stress in the casing changes from the case 1 to the case 2 at same standoff, void pressure and void angle. It is located in the internal part of the casing for the case 2 whereas it is in the external part of the casing for the case 1.

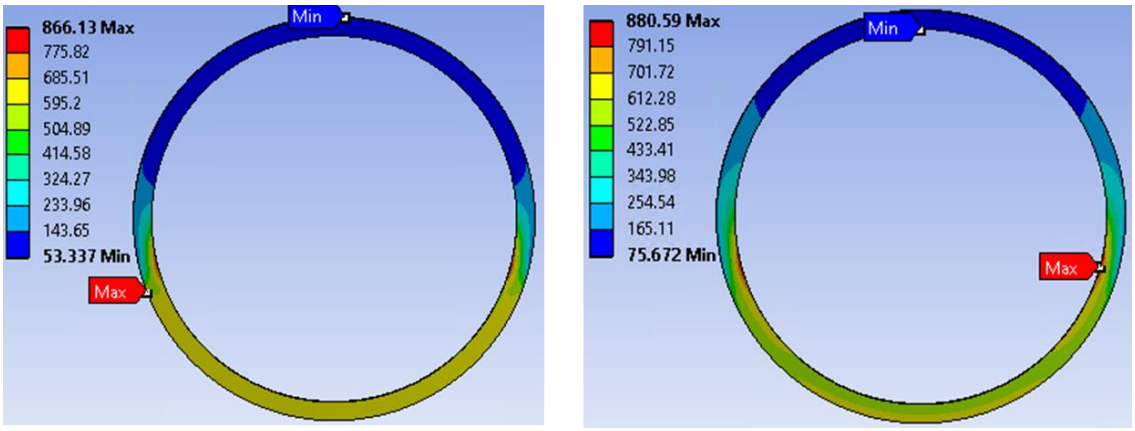

Figure 81. Casing stress distribution for 10% standoff and VP=40 MPa at void angle of 120º for case 1(left) and case 2(right)

The location and stress distribution in the cement sheath is quite similar for all the cases (Figure 47 and Figure 51). The difference lies on the stress magnitude which are higher in the base and first case for the void pressure studied of 20 MPa and 40 MPa. It is important to consider that cement will failed at these high values (100 MPa or more) creating a bigger void length in the cement sheath. These high values are obtained in all the cases.

5.2 Influence of standoff at different internal casing pressures

The tendencies between a concentric and an eccentric case (10% standoff) in a complete cement sheath are quite similar when they under different internal casing pressure (Figure 58 and Figure 59). The difference in magnitude are not significant as well. There is an increase from the best to the worst centralization of 9% when the internal casing pressure is 60 MPa, and less than 1% when the internal casing pressures are 100MPa and 120 MPa. The greatest difference exits when the

internal casing pressure is 80 MPa (base case) which is 20%. The higher value of 436 MPa occur at 120 MPa and it does not represent a risk of deformation for the casing.

On the other hand, voids with a pressure of 60 MPa in the cement sheath will induce casing deformation if the internal casing pressure is increased higher than the established casing pressure of 80 MPa (Figure 60)

60 MPa and 80 MPa of internal casing pressure presents similar results. If the internal casing pressure increase in 20 MPa, casing deformation might occur for a P95 and P110 grade casing since it will exceed their yield strength at void angles between 30° and 90°. And, if the internal casing pressure increase in 40 MPa, casing deformation might occur even in a TP140 grade casing since it will exceed their yield strength for void angles between 30° and 100°.

Figure 82 compares the maximum casing stress at different internal casing pressure for a complete cement sheath at 10% standoff and 100% standoff, and a cement sheath with voids at 10% standoff. The void angle is 60° and void pressure is 60 MPa. It is clearly observed that a cement sheath with voids has a greater impact when the casing internal pressure increases.

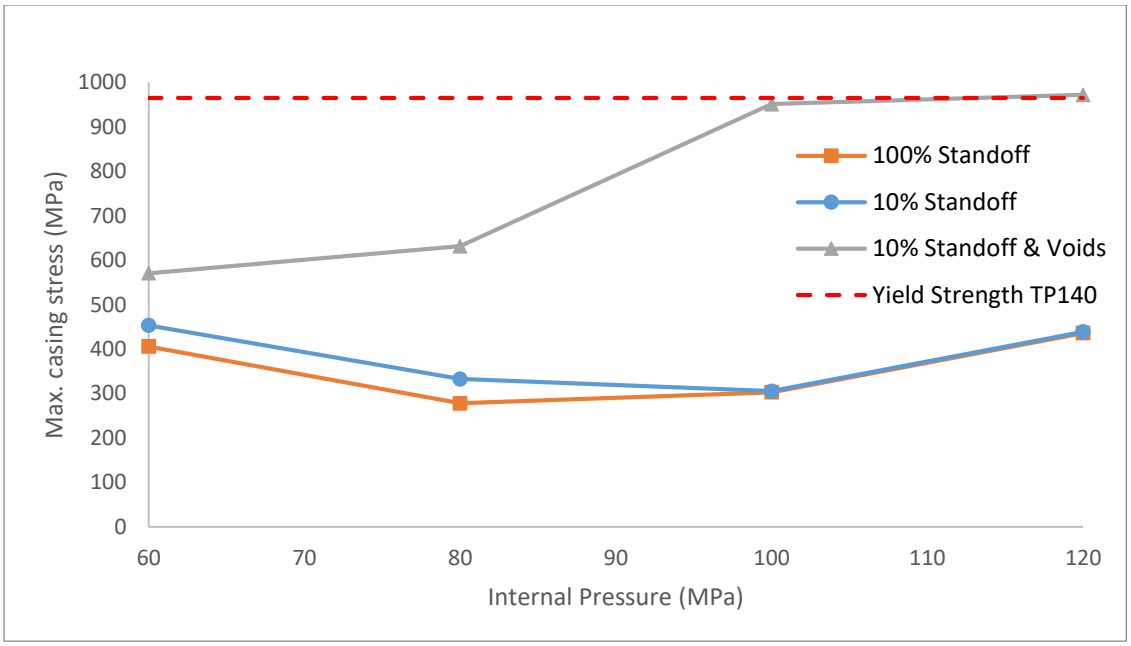

Figure 82. Comparison of a complete cement sheath and a cement sheath with voids at different casing internal pressure

5.3 Temperature effect in wellbore integrity for a concentric and eccentric case

Concentric case

Based on the results in a concentric case, the maximum stress magnitude increases around 123% and decreases around 41% for the heating and cooling cases respectively when a differential temperature of 90ºC is applied to the casing. There is a change of location of the maximum stress for the cooling case.

For the cement sheath. there is not a change of location of maximum stress. It is important to consider that when the casing is cooling down, the maximum stress in the cement will tend to accumulate in two specific points. This might create an instable cement sheath at that location prompting a cement failure.

When different internal pressures are applied to the casing while it is cooling down, the maximum casing stress usually decreases. Indeed, the greatest value obtained is 688 MPa when

the entire system (formation, cement and casing) has a temperature of 100ºC. After 100 MPa, a shift of the slope from negative to positive is observed and the maximum casing stress starts to increase (Figure 67). However, this values are still lower than the yield strength of a low grade casing.

Eccentric case

If we include wellbore eccentricity to the model and the cement sheath is complete, the results won't differ a lot when the casing is getting cold. The difference gets lower when the casing is decreasing in temperature reaching only a 1.5% difference, being the eccentric case the one with a higher value (Figure 68). In other words, cooling down the casing reduces the maximum equivalent stress and the chances of a casing deformation even in an eccentric case.

The big issue is that reducing the temperature of the casing when the formation temperature is hot (100ºC) will decrease the pressure of the voids left by the drilling fluid in the cement because of the poor centralization and/or cement job. And, if the void pressure reaches a value of 20 MPa, it won't matter the casing temperature since casing deformation will occur for all the cases analyzed (Figure 69).

For a void pressure of 60 MPa, the casing temperature will matter (Figure 71). The maximum von Mises casing stress reduces considerable when the casing is cool down from 60ºC to 20ºC until the point that casing deformation won't be a risk anymore. The maximum casing stress location does not change for either a void pressure of 60 MPa or a void pressure of 20 MPa when the casing is cooling down.

Figure 83 compares the maximum casing stress at different differential temperatures (ΔT) for a complete cement sheath at 10% standoff and 100% standoff, and a cement sheath with voids at 10% standoff. The void angles (Va) are 30^{o} and 60^{o} and a void pressure of 60 MPa is kept for

both cases. The tendency when the void angle is 30º is not linear since casing deformation occurs at 965 MPa (TP140 grade) and the behavior becomes plastic instead of elastic as explained previously. It is observed that cooling the casing especially in a cement sheath with voids decreases the equivalent maximum stress.

The great interrogate is to know with a good accuracy how is the heat transfer between the casing and the hydraulic fracturing fluid that is injected at very high pressures. We believe, based on the literature (Sugden et al., 2012 and Xi et al., 2017) that the casing will not reach the same temperature of the hydraulic fracturing fluid at surface. Indeed, it might not go lower than 30ºC after 3 hrs. if a 20ºC fluid temperature is used. This topic will be an interesting to research in more detailed in the future.

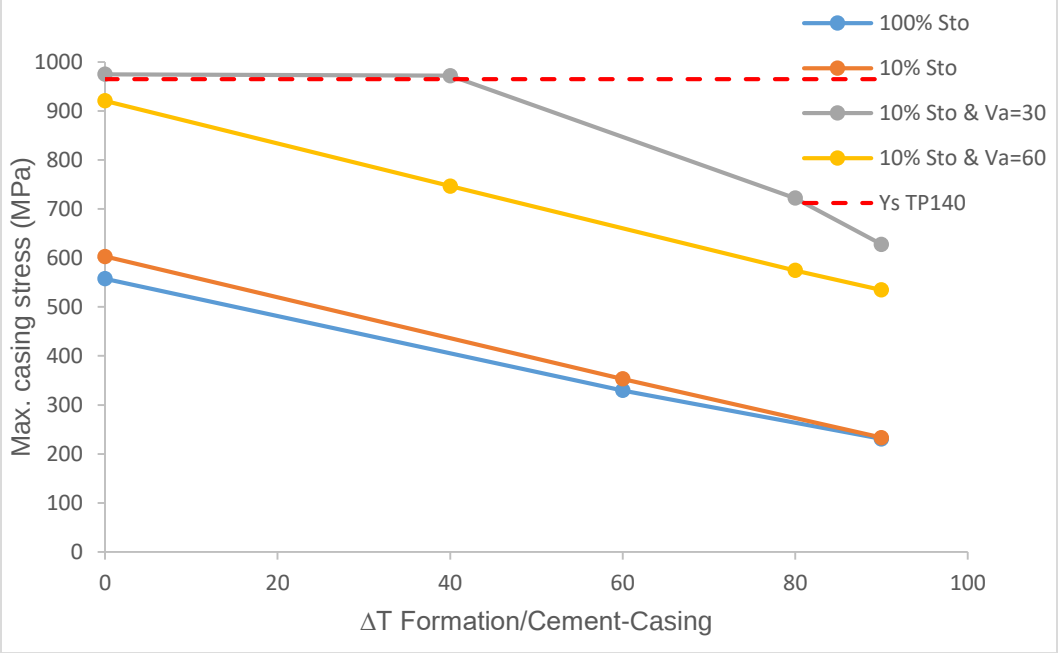

Figure 83. Comparison of a complete cement sheath and a cement sheath with voids at different ΔT between formation/cement and casing

Conclusions, recommendations and future work

In this work, wellbore centralization was studied in order to analyze if a non-proper centralization can be reason for casing deformation during hydraulic fracturing. Finite element analysis was applied with more than 400 simulations. Standoff was the concept used throughout the work where 100% is when the casing and the wellbore are concentric and 0% is fully eccentric what means that the casing is touching the wellbore.

For a complete cement sheath, eccentricity impacts the results with an almost 22% increase of maximum casing stress from the best to the worst centralization, but the greatest value reaches only 340 MPa which is half of the yield strength of a P110 casing. On the other hand, in a cement sheath with voids, eccentricity will exceed under some circumstances (void pressure and void length) the yield strength of a TP140 casing grade which is one of the highest grade available in the industry.

In a high geo-stress environment, especially in a reverse and strike slip fault regime such as the one exhibit in the Sichuan Basin, the chances of casing deformation increases considerably when a non-proper centralization is performed. However, if a void pressure lower than 20 MPa is reached, it will not matter under what magnitude of in situ stress or fault regime the well is exposed.

Temperature has also a great impact in casing deformation since drilling fluid voids in the cement sheath will shrink decreasing their pressure when a cold hydraulic fracturing is injected in a hot shale formation. However, if drilling fluid voids are not formed or their pressure does not decrease, a reduction of casing temperature will decrease equivalent maximum von misses stress.

Eight wells that presented casing deformation were modeled in a concentric casing and an eccentric casing with complete and incomplete cement sheath. The void pressure was 40 MPa. For all of them, the equivalent maximum casing stress exceeds the yield strength of the casing used

during hydraulic fracturing for a cement sheath with voids. It occurs in a range of void angle of at least 30 degrees.

We recommend to improve wellbore centralization since lower standoff increases the casing and cement stress. It will also minimize the formation of drilling fluid voids which is a more crucial factor. Rotating the string while cementing will also help to reduce the formation of voids in the cement sheath since a more homogenous cement will be created. For this purpose, rotating centralizer need to be run in the entire string. Increasing the temperature of the hydraulic fluid before injecting might also work.

For future work, a 3D model with grater formation sizes that includes more parameters such as natural fractures and lithology interfaces is required. Also, the re-orientation of the in-situ stresses after reservoir depletion need to be consider since their magnitude have a high impact under the casing and cement stress distribution as mentioned previously. Lab testing will be also required to prove the findings obtained by numerical analysis.

The heat transfer that occurs between the hydraulic fluid and the system modeled that includes casing, cement and formation requires a more detailed research since there is not accuracy about the temperature that casing and cement will reach after the hydraulic fracturing operation has started.

The temperature cycles when the pumping is stop after a stage is performed was not simulated in this work. It would be interesting to analyze if the variation will impact the casing stress and strength leading to a promptly deformation.

According to our results in a cement sheath with voids, a high stress in the cement and casing was reach even if a deformation does not occur. These high loads might decrease casing

strength or cement resistance. Therefore, it would be interesting to study how this will affect wellbore integrity during the production phase.

Casing failures are near the heel of the horizontal section or in the couplings during hydraulic fracturing are usually mostly found in a P110 casing grade in United States fields as discussed by Magill (2013). High yield strength appears to make the casing vulnerable to brittle failure. For instance, if the H2S content is too high, P110 or higher casing grade might not be appropriate in the well. Information about regarding the failure location in coupling or the pipe was not found, but some casing failures location were found near the heel of the horizontal section. Therefore, this concept might be a reason for casing deformation in geological complex cases and requires a deeper research in the future.

The overall conclusion of this work was not only to provide a reason for casing deformation in the Weiyuan-Changning shale gas field, it was also to perform a general concentric and eccentric model that can adjust to worldwide fields with similar properties to the studied case. Which is another reason of the inclusion of sensitive analysis at different in situ stresses, internal casing pressure and temperatures.

References

Adams, N. J., Services, N. A., Mitchell, R. F., Eustes, A. W., & Sampaio, J. H. (2017). A Causation Investigation for Observed Casing Failures Occurring During Fracturing Operations. In *SPE Hydraulic Fracturing Technology Conference and Exhibition*. The Woodlands, TX.

API Spec 10D. (1995). Casing bow-spring centralizers and centralizer subs. Washington DC. Retrieved from http://mycommittees.api.org/standards/ecs/sc10/Meeting Materials/2014/January - Hebert Spec 10D Revision/API Spec 10D Committee Working Draft 11072013 jh cj.pdf

API Spec 5CT. (2011). Specification for Casing and Tubing. Washington DC.

API TR 5C3. (2008). Technical Report on Equations and Calculations for Casing, Tubing, and Line Pipe Used as Casing or Tubing; and Performance Properties Tables for Casing and Tubing. Washington DC.

Bai, M. (2012). An Innovative Method for Horizontal Well Completion in Tight Shale Gas Reservoirs. In *IADC/SPE Asia Pacific Drilling Technology Conference and Exhibition* (pp. 1–14).

Bellarby, J., Kofoed, S. S., Marketz, F., & Oil, M. (2013). Annular Pressure Build-up Analysis and Methodology with Examples from Multifrac Horizontal Wells and HPHT Reservoirs.

Bonic, Z., Prolovic, V., & Mladenovic, B. (2010). Mathematical modeling of materially nonlinear problems in structural analyses, Part I: Theoretical fundamentals. *Facta Universitatis - Series: Architecture and Civil Engineering*, *8*(1), 67–78. https://doi.org/10.2298/FUACE1001067B

Bonic, Z., Vacev, T., Prolovic, V., Mijalkovic, M., & Dancevic, P. (2010). Mathematical

modeling of materially nonlinear problems in structural analyses, Part II: Application in contemporary software. *Facta Universitatis - Series: Architecture and Civil Engineering*, *8*(2), 201–210. https://doi.org/10.2298/FUACE1002201B

Clark, H. C. (1987). Mechanical Design Considerations for Fracture-Treating Down Casing Strings. In *SPE Drilling Engineering* (Vol. 2, pp. 116–126). Retrieved from http://www.scopus.com/inward/record.url?eid=2-s2.0-0023364083&partnerID=tZOtx3y1

Economides, M. J., Hill, A. D., Ehlig-Economides, C., & Zhu, D. (2013). *Petroleum Production Systems Second Edition*. Pearson Education.

Farahani, R., Lastiwka, M. M., Langer, D. C., Demirdal, B., Matthews, C. M., Jensen, J., … Farahani, A. (2011). Assessment and Prediction of Erosion in Completion Systems under Hydraulic Fracturing Operations Using Computational Fluid Dynamics. *SPE Annual Technical Conference and Exhibition*, (SPE-147514-MS).

Farley, D., & Scott, T. (2011). Field Proven Solutions to the Challenges of Centralizing Solid Expandable Casing. In *SPE Annual Technical Conference and Exhibition*. Denver, CO.

Fry, D., & Pruett, B. (2015). An Analytical Comparison of Wellbore Deviation and its Effects on Proper Centralization in the Bakken. In *SPE Western Regional*. Garden Groce, CA.

Gandossi, L. (2013). *An overview of hydraulic fracturing and other formation stimulation technologies for shale gas production*. *JRC Technical Reports*. https://doi.org/10.2790/99937

Goverment of Western Australia. (2015). *Chemicals used in hydraulic fracture stimulation*. Retrieved from http://www.dmp.wa.gov.au/Petroleum/Chemicals-used-in-hydraulic-20064.aspx

Huang, W., Gao, D., & Liu, Y. (2018). A study of mechanical extending limits for three-section

directional wells. *Journal of Natural Gas Science and Engineering*, *54*(April), 163–174. https://doi.org/10.1016/j.jngse.2018.03.031

J, R., & Coleman, S. (2016). Tubing Length Change due to Ballooning. Retrieved from http://www.drillingformulas.com/tubing-length-change-due-to-ballooning/

Jandhyala, S. R. K., & Chiney, A. (2014). Finite element approach to predict the effect of annular pressure buildup on wellbore materials. In *Offshore Technology Conference Asia* (Vol. 2, pp. 1493–1500).

Kirsh, G. (1898). *Die Theorie der Elastizität und die Bedürfnisse der Festigkeitslehre* (42nd ed.). Zeitschrift des Vereines deutscher Ingenieure.

Lavrov, A., Todorovic, J., & Torsæter, M. (2016). Impact of voids on mechanical stability of well cement. *Energy Procedia*, *86*(1876), 401–410. https://doi.org/10.1016/j.egypro.2016.01.041

Lee, M., Eckert, A., & Nygaard, R. (2011). Mesh Optimization For Finite Element Models of Wellbore Stress Analysis. In *45th US Rock Mechanics / Geomechanics Symposium*. San Francisco, CA. https://doi.org/10.1061/(ASCE)0733-9399(2003)129:11(1295)

Liu, A. F. (2005). *Mechanics and Mechanisms of Fracture: An Introduction*. ASM International.

Liu, G., & Weber, L. (2012). Centralizer Selection and Placement Optimization. In *SPE Deepwater Drilling and Completions* (pp. 20–21). Galveston, TX.

Logan, D. L. (2012). *A First Course In The Finite Element Method* (5th ed.). Cengage Learning.

Lubinski, A. (1950). A Study of the Buckling of Rotary Drilling Strings. In *Presented at the spring meeting,Mid-continent District, Division of Productlon* (pp. 178–214). Oklahoma City, OK.

Magill, J. (2013). Recent Casing Failures in Horizontal Wells. Denver, CO. Retrieved from

http://www.aade.org/chapters/denver/meeting-presentations/

Mendez, M. F., Ichim, A., & Teodoriu, C. (2018). The Effect of Wellbore Centralization in Geothermal Wells, 1–8.

Mills, K. A., Menand, S., & Suarez, R. (2016). Micro Dogleg Detection with Continuous Inclination Measurements and Advanced BHA Modeling Wellbore Trajectory. In *SPE Eastern Regional Meeting* (pp. 1–15). Canton, OH. https://doi.org/10.2118/183299-MS

Mitchell, R. F. (2006). Tubing Buckling–The State of the Art. In *SPE Annual Technical Conference and Exhibition*. San Antonio, TX.

Pearson, M. (2013). Hydraulic Fracturing of Horizontal Wells. Retrieved from http://www.libertyresourcesllc.com/upload/SPE Distinguished Lecture - Horizontal Well Fracturing.pdf

Pollard, D. D., & Fletcher, R. C. (2004). *Fundamentals of Structural Geology*. Cambridge University Press.

SharcNet. (2016). Rate-Independent Plasticity. Retrieved from https://www.sharcnet.ca/Software/Ansys/17.0/en-us/help/ans_thry/thy_mat1.html

Stegent, N. (2016). Choose the Best Completion Strategy for Your Well. Retrieved from https://www.upstreampumping.com/article/well-completion-stimulation/2015/choose-best-completion-strategy-your-well

Sugden, C., Partners, B. E., Johnson, J., Chambers, M., Ring, G., & Suryanarayana, P. V. (2012). Special Considerations in the Design Optimization of High Rate , Multistage Fractured Shale Wells. In *IADC/SPE Drilling Conference and Exhibition* (pp. 1–20). San Diego, CA.

University of North Dakota EERC. (2014). *Completion Technologies*. Retrieved from https://www.undeerc.org/bakken/completiontechnologies.aspx

World Stress Map. (2016). Stress Indicators in the WSM Database. Retrieved from http://www.world-stress-map.org/data/

Xi, Y., Li, J., Liu, G., Cha, C., & Fu, Y. (2017). Numerical investigation for different casing deformation reasons in Weiyuan-Changning shale gas field during multistage hydraulic fracturing. *Journal of Petroleum Science and Engineering*, *163*(November), 691–702. https://doi.org/10.1016/j.petrol.2017.11.020

Xu, Z. (2018). *Numerical Simulation of Hydraulically Induced Casing Deformation in Shale Reservoir*. University of Oklahoma.

Yan, W., Zou, L., Li, H., Deng, J., Ge, H., & Wang, H. (2016). Investigation of casing deformation during hydraulic fracturing in high geo-stress shale gas play. *Journal of Petroleum Science and Engineering*, *150*(April 2016), 22–29. https://doi.org/10.1016/j.petrol.2016.11.007

Yin, F., Han, L., Yang, S., Deng, Y., He, Y., & Wu, X. (2018). Casing deformation from fracture slip in hydraulic fracturing. *Journal of Petroleum Science and Engineering*, *166*, 235–241. https://doi.org/10.1016/j.petrol.2018.03.010

Zhang, J., Standifird, W. B., Adesina, K., & Keaney, G. (2006). Wellbore stability with consideration of pore pressure and drilling fluid interactions. In *The 41st U.S. Symposium on Rock Mechanics (USRMS)*. Golden, CO. Retrieved from https://www.researchgate.net/profile/Jon_Zhang/publication/254542211_Wellbore_stability_with_consideration_of_pore_pressure_and_drilling_fluid_interactions/links/563b781d08aec6f17dd4d2a5.pdf

Appendix A: Different cases simulated in ANSYS

Table A. 1. Simulations run for different Standoff

Case 1=Standoff								
Complete cement sheath	**Case 1.1=Effect of standoff on maximum casing stress**	**1.1.1=100% So**	**1.1.2=70% So**	**1.1.3=40% So**	**1.1.4=10% So**	**1.1.5=1% So**
Cement sheath with voids	**Case 1.2=Effect of standoff at a void pressure of 60 MPa**	**1.2.1=100% So**	**1.2.2=70% So**	**1.2.3=40% So**	**1.2.4=10% So**	**1.2.5=1% So**
		1.2.1.1=10º Va	1.2.2.1=10º Va	1.2.3.1=10º Va	1.2.4.1=10º Va	1.2.5.1=10º Va
		1.2.1.2=20º Va	1.2.2.2=20º Va	1.2.3.2=20º Va	1.2.4.2=20º Va	1.2.5.2=20º Va
		1.2.1.3=30º Va	1.2.2.3=30º Va	1.2.3.3=30º Va	1.2.4.3=30º Va	1.2.5.3=30º Va
		1.2.1.4=60º Va	1.2.2.4=60º Va	1.2.3.4=60º Va	1.2.4.4=60º Va	1.2.5.4=60º Va
		1.2.1.5=90º Va	1.2.2.5=90º Va	1.2.3.5=90º Va	1.2.4.5=90º Va	1.2.5.5=90º Va
		1.2.1.6=120º Va	1.2.2.6=120º Va	1.2.3.6=120º Va	1.2.4.6=120º Va	1.2.5.6=120º Va
		1.2.1.7=150º Va	1.2.2.7=150º Va	1.2.3.7=150º Va	1.2.4.7=150º Va	1.2.5.7=150º Va
	Case 1.3=Effect of standoff at a void pressure of 40 MPa	**1.3.1=100% So**	**1.3.2=70% So**	**Case 1.3.3=40% So**	**Case 1.3.4=10% So**	**Case 1.3.5=1% So**
		1.3.1.1=10º Va	1.3.2.1=10º Va	1.3.3.1=10º Va	1.3.4.1=10º Va	1.3.5.1=10º Va
		1.3.1.2=20º Va	1.3.2.2=20º Va	1.3.3.2=20º Va	1.3.4.2=20º Va	1.3.5.2=20º Va
		1.3.1.3=30º Va	1.3.2.3=30º Va	1.3.3.3=30º Va	1.3.4.3=30º Va	1.3.5.3=30º Va
		1.3.1.4=60º Va	1.3.2.4=60º Va	1.3.3.4=60º Va	1.3.4.4=60º Va	1.3.5.4=60º Va
		1.3.1.5=90º Va	1.3.2.5=90º Va	1.3.3.5=90º Va	1.3.4.5=90º Va	1.3.5.5=90º Va
		1.3.1.6=120º Va	1.3.2.6=120º Va	1.3.3.6=120º Va	1.3.4.6=120º Va	1.3.5.6=120º Va
		1.3.1.7=150º Va	1.3.2.7=150º Va	1.3.3.7=150º Va	1.3.4.7=150º Va	1.3.5.7=150º Va
	Case 1.4=Effect of standoff at a void pressure of 20 MPa	**1.4.1=100% So**	**1.4.2=70% So**	**Case 1.4..3=40% So**	**Case 1.4.4=10% So**	**Case 1.4.5=1% So**
		1.4.1.1=10º Va	1.4.2.1=10º Va	1.4.3.1=10º Va	1.4.4.1=10º Va	1.4.5.1=10º Va
		1.4.1.2=20º Va	1.4.2.2=20º Va	1.4.3.2=20º Va	1.4.4.2=20º Va	1.4.5.2=20º Va
		1.4.1.3=30º Va	1.4.2.3=30º Va	1.4.3.3=30º Va	1.4.4.3=30º Va	1.4.5.3=30º Va
		1.4.1.4=60º Va	1.4.2.4=60º Va	1.4.3.4=60º Va	1.4.4.4=60º Va	1.4.5.4=60º Va
		1.4.1.5=90º Va	1.4.2.5=90º Va	1.4.3.5=90º Va	1.4.4.5=90º Va	1.4.5.5=90º Va
		1.4.1.6=120º Va	1.4.2.6=120º Va	1.4.3.6=120º Va	1.4.4.6=120º Va	1.4.5.6=120º Va
		1.4.1.7=150º Va	1.4.2.7=150º Va	1.4.3.7=150º Va	1.4.4.7=150º Va	1.4.5.7=150º Va
	Case 1.5=Effect of standoff at a void pressure of 0 MPa	**1.5.1=100% So**	**1.5.2=70% So**	**Case 1.5.3=40% So**	**Case 1.5.4=10% So**	**Case 1.5.5=1% So**
		1.5.1.1=10º Va	1.5.2.1=10º Va	1.5.3.1=10º Va	1.5.4.1=10º Va	1.5.5.1=10º Va
		1.5.1.2=20º Va	1.5.2.2=20º Va	1.5.3.2=20º Va	1.5.4.2=20º Va	1.5.5.2=20º Va
		1.5.1.3=30º Va	1.5.2.3=30º Va	1.5.3.3=30º Va	1.5.4.3=30º Va	1.5.5.3=30º Va
		1.5.1.4=60º Va	1.5.2.4=60º Va	1.5.3.4=60º Va	1.5.4.4=60º Va	1.5.5.4=60º Va
		1.5.1.5=90º Va	1.5.2.5=90º Va	1.5.3.5=90º Va	1.5.4.5=90º Va	1.5.5.5=90º Va
		1.5.1.6=120º Va	1.5.2.6=120º Va	1.5.3.6=120º Va	1.5.4.6=120º Va	1.5.5.6=120º Va
		1.5.1.7=150º Va	1.5.2.7=150º Va	1.5.3.7=150º Va	1.5.4.7=150º Va	1.5.5.7=150º Va

So= Standoff, Va = Void angle

Table A. 2. Simulations run for different in-situ stresses

Case 2= In-situ stress	Complete cement sheath	Case 2.1=σv:82 MPa σH:54 MPa	1.1.1=100% So	1.1.2=70% So	1.1.3=40% So	1.1.4=10% So	1.1.5=1% So
		Case 2.2=σv:54 MPa σH:54 MPa	1.1.1=100% So	1.1.2=70% So	1.1.3=40% So	1.1.4=10% So	1.1.5=1% So
		Case 2.3=σv:24 MPa σH:52 MPa	1.1.1=100% So	1.1.2=70% So	1.1.3=40% So	1.1.4=10% So	1.1.5=1% So
		Case 2.4=σv:52 MPa σH:24 MPa	1.1.1=100% So	1.1.2=70% So	1.1.3=40% So	1.1.4=10% So	1.1.5=1% So
	Cement sheath with voids	Case 2.5= σv:82 MPa σH:54 MPa		2.5.1=100%		2.5.2=10%	
				2.5.1.1=40 MPa Vp	2.5.1.2=20 MPa Vp	2.5.2.1=40 MPa Vp	2.5.2.2=20 MPa Vp
				2.5.1.1.1=10º Va	2.5.1.2.1=10º Va	2.5.2.1.1=10º Va	2.5.2.2.1=10º Va
				2.5.1.1.2=20º Va	2.5.1.2.2=20º Va	2.5.2.1.2=20º Va	2.5.2.2.2=20º Va
				2.5.1.1.3=30º Va	2.5.1.2.3=30º Va	2.5.2.1.3=30º Va	2.5.2.2.3=30º Va
				2.5.1.1.4=60º Va	2.5.1.2.4=60º Va	2.5.2.1.4=60º Va	2.5.2.2.4=60º Va
				2.5.1.1.5=90º Va	2.5.1.2.5=90º Va	2.5.2.1.5=90º Va	2.5.2.2.5=90º Va
				2.5.1.1.6=120º Va	2.5.1.2.6=120º Va	2.5.2.1.6=120º Va	2.5.2.2.6=120º Va
				2.5.1.1.7=150º Va	2.5.1.2.7=150º Va	2.5.2.1.7=150º Va	2.5.2.2.7=150º Va
		Case 2.6= σv:54 MPa σH:54 MPa		2.6.1=100%		2.6.2=10%	
				2.6.1.1=40 MPa Vp	2.6.1.2=20 MPa Vp	2.6.2.1=40 MPa Vp	2.6.2.2=20 MPa Vp
				2.6.1.1.1=10º Va	2.6.1.2.1=10º Va	2.6.2.1.1=10º Va	2.6.2.2.1=10º Va
				2.6.1.1.2=20º Va	2.6.1.2.2=20º Va	2.6.2.1.2=20º Va	2.6.2.2.2=20º Va
				2.6.1.1.3=30º Va	2.6.1.2.3=30º Va	2.6.2.1.3=30º Va	2.6.2.2.3=30º Va
				2.6.1.1.4=60º Va	2.6.1.2.4=60º Va	2.6.2.1.4=60º Va	2.6.2.2.4=60º Va
				2.6.1.1.5=90º Va	2.6.1.2.5=90º Va	2.6.2.1.5=90º Va	2.6.2.2.5=90º Va
				2.6.1.1.6=120º Va	2.6.1.2.6=120º Va	2.6.2.1.6=120º Va	2.6.2.2.6=120º Va
				2.6.1.1.7=150º Va	2.6.1.2.7=150º Va	2.6.2.1.7=150º Va	2.6.2.2.7=150º Va
		Case 2.7= σv:24 MPa σH:52 MPa		2.7.1=100%		2.7.2=10%	
				2.7.1.1=40 MPa Vp	2.7.1.2=20 MPa Vp	2.7.2.1=40 MPa Vp	2.7.2.2=20 MPa Vp
				2.7.1.1.1=10º Va	2.7.1.2.1=10º Va	2.7.2.1.1=10º Va	2.7.2.2.1=10º Va
				2.7.1.1.2=20º Va	2.7.1.2.2=20º Va	2.7.2.1.2=20º Va	2.7.2.2.2=20º Va
				2.7.1.1.3=30º Va	2.7.1.2.3=30º Va	2.7.2.1.3=30º Va	2.7.2.2.3=30º Va
				2.7.1.1.4=60º Va	2.7.1.2.4=60º Va	2.7.2.1.4=60º Va	2.7.2.2.4=60º Va
				2.7.1.1.5=90º Va	2.7.1.2.5=90º Va	2.7.2.1.5=90º Va	2.7.2.2.5=90º Va
				2.7.1.1.6=120º Va	2.7.1.2.6=120º Va	2.7.2.1.6=120º Va	2.7.2.2.6=120º Va
				2.7.1.1.7=150º Va	2.7.1.2.7=150º Va	2.7.2.1.7=150º Va	2.7.2.2.7=150º Va
		Case 2.8= σv:52 MPa σH:24 MPa		2.8.1=100%		2.8.2=10%	
				2.8.1.1=40 MPa Vp	2.8.1.2=20 MPa Vp	2.8.2.1=40 MPa Vp	2.8.2.2=20 MPa Vp
				2.8.1.1.1=10º Va	2.8.1.2.1=10º Va	2.8.2.1.1=10º Va	2.8.2.2.1=10º Va
				2.8.1.1.2=20º Va	2.8.1.2.2=20º Va	2.8.2.1.2=20º Va	2.8.2.2.2=20º Va
				2.8.1.1.3=30º Va	2.8.1.2.3=30º Va	2.8.2.1.3=30º Va	2.8.2.2.3=30º Va
				2.8.1.1.4=60º Va	2.8.1.2.4=60º Va	2.8.2.1.4=60º Va	2.8.2.2.4=60º Va
				2.8.1.1.5=90º Va	2.8.1.2.5=90º Va	2.8.2.1.5=90º Va	2.8.2.2.5=90º Va
				2.8.1.1.6=120º Va	2.8.1.2.6=120º Va	2.8.2.1.6=120º Va	2.8.2.2.6=120º Va
				2.8.1.1.7=150º Va	2.8.1.2.7=150º Va	2.8.2.1.7=150º Va	2.8.2.2.7=150º Va

So= Standoff, Va = Void angle, Vp=Void Pressure

Table A. 3. Simulations run for different internal casing pressures

Case 3= Internal Casing Pressure	**Complete cement sheath**	**Case 3.1=Effect of internal casing pressure at different standoff**	**3.1.1=100% So**			
			3.1.1.1=60 MPa IP	3.1.1.2=80 MPa IP	3.1.1.3=100 MPa IP	3.1.1.4=120 MPa IP
			3.1.2=10% So			
			3.1.2.1=60 MPa IP	3.1.2.2=80 MPa IP	3.1.2.3=100 MPa IP	3.1.2.4=120 MPa IP
	Cement sheath with voids	**Case 3.2=Effect of internal casing pressure at 10% standoff and 60 MPa VP**	**3.2.1=60 MPa IP**	**3.2.2=80 MPa IP**	**3.2.3=100 MPa IP**	**3.2.4=120 MPa IP**
			3.2.1.1=10º Va	3.2.2.1=10º Va	3.2.3.1=10º Va	3.2.4.1=10º Va
			3.2.1.2=20º Va	3.2.2.2=20º Va	3.2.3.2=20º Va	3.2.4.2=20º Va
			3.2.1.3=30º Va	3.2.2.3=30º Va	3.2.3.3=30º Va	3.2.4.3=30º Va
			3.2.1.4=60º Va	3.2.2.4=60º Va	3.2.3.4=60º Va	3.2.4.4=60º Va
			3.2.1.5=90º Va	3.2.2.5=90º Va	3.2.3.5=90º Va	3.2.4.5=90º Va
			3.2.1.6=120º Va	3.2.2.6=120º Va	3.2.3.6=120º Va	3.2.4.6=120º Va
			3.2.1.7=150º Va	3.2.2.7=150º Va	3.2.3.7=150º Va	3.2.4.7=150º Va

So= Standoff, Va = Void angle, Vp=Void Pressure, IP=Internal Casing Pressure

Table A. 4. Simulations run for different differential temperatures

Case 4= Temperature	**Complete Cement Sheath**	**Case 4.1=Heating effect at 100% So**		**4.1.1=0ºC ΔT**	**4.1.2=30ºC ΔT**	**4.1.3=60ºC ΔT**	**4.1.4=90ºC ΔT**
		Case 4.2=Cooling effect at 100% So		**4.2.1=0ºC ΔT**	**4.2.2=30ºC ΔT**	**4.2.3=60ºC ΔT**	**4.2.4=90ºC ΔT**
		Case 4.3= Cooling effect under different internal pressures at 100% So		**4.3.1=60 MPa IP**	**4.3.2=80 MPa IP**	**4.3.3=100 MPa IP**	**4.3.4=110 MPa IP** / **4.3.5=120 MPa IP**
				4.3.1.1=0ºC ΔT	4.3.2.1=0ºC ΔT	4.3.3.1=0ºC ΔT	4.3.4.1=0ºC ΔT / 4.3.5.1=0ºC ΔT
				4.3.1.2=30ºC ΔT	4.3.2.2=30ºC ΔT	4.3.3.2=30ºC ΔT	4.3.4.2=30ºC ΔT / 4.3.5.2=30ºC ΔT
				4.3.1.3=60ºC ΔT	4.3.2.3=60ºC ΔT	4.3.3.3=60ºC ΔT	4.3.4.3=60ºC ΔT / 4.3.5.3=60ºC ΔT
				4.3.1.4=90ºC ΔT	4.3.2.4=90ºC ΔT	4.3.3.4=90ºC ΔT	4.3.4.4=90ºC ΔT / 4.3.5.4=90ºC ΔT
		Case 4.4= Influence of temperature at different standoff		**4.4.1=100% So**		**4.4.2=10% So**	
				4.4.1.1=0ºC ΔT		4.4.2.1=0ºC ΔT	
				4.4.1.2=30ºC ΔT		4.4.2.2=30ºC ΔT	
				4.4.1.3=60ºC ΔT		4.4.2.3=60ºC ΔT	
	Cement Sheath with Voids	**Case 4.5= Influence of temperature for a void pressure of 20 MPa**		**4.5.1=100% So**		**4.5.2=10% So**	
			4.5.1.1=20ºC ΔT	**4.5.1.2=60ºC ΔT**	**4.5.1.3=100ºC ΔT**	**4.5.2.1=20ºC ΔT**	**4.5.2.2=60ºC ΔT** / **4.5.2.3=100ºC ΔT**
			4.5.1.1.1=10º Va	4.5.1.2.1=10º Va	4.5.1.3.1=10º Va	4.5.2.1.1=10º Va	4.5.2.2.1=10º Va / 4.5.2.3.1=10º Va
			4.5.1.1.2=20º Va	4.5.1.2.2=20º Va	4.5.1.3.2=20º Va	4.5.2.1.2=20º Va	4.5.2.2.2=20º Va / 4.5.2.3.2=20º Va
			4.5.1.1.3=30º Va	4.5.1.2.3=30º Va	4.5.1.3.3=30º Va	4.5.2.1.3=30º Va	4.5.2.2.3=30º Va / 4.5.2.3.3=30º Va
			4.5.1.1.4=60º Va	4.5.1.2.4=60º Va	4.5.1.3.4=60º Va	4.5.2.1.4=60º Va	4.5.2.2.4=60º Va / 4.5.2.3.4=60º Va
			4.5.1.1.5=90º Va	4.5.1.2.5=90º Va	4.5.1.3.5=90º Va	4.5.2.1.5=90º Va	4.5.2.2.5=90º Va / 4.5.2.3.5=90º Va
			4.5.1.1.6=120º Va	4.5.1.2.6=120º Va	4.5.1.3.6=120º Va	4.5.2.1.6=120º Va	4.5.2.2.6=120º Va / 4.5.2.3.6=120º Va
			4.5.1.1.7=150º Va	4.5.1.2.7=150º Va	4.5.1.3.7=150º Va	4.5.2.1.7=150º Va	4.5.2.2.7=150º Va / 4.5.2.3.7=150º Va
		Case 4.6= Influence of temperature for a void pressure of 40 MPa		**4.6.1=10% So**		**4.6.2=100% So**	
			4.6.1.1=20ºC ΔT	**4.6.1.2=60ºC ΔT**	**4.6.1.3=100ºC ΔT**	**4.6.2.1=20ºC ΔT**	**4.6.2.2=60ºC ΔT** / **4.6.2.3=100ºC ΔT**
			4.6.1.1.1=10º Va	4.6.1.2.1=10º Va	4.6.1.3.1=10º Va	4.6.2.1.1=10º Va	4.6.2.2.1=10º Va / 4.6.2.3.1=10º Va
			4.6.1.1.2=20º Va	4.6.1.2.2=20º Va	4.6.1.3.2=20º Va	4.6.2.1.2=20º Va	4.6.2.2.2=20º Va / 4.6.2.3.2=20º Va
			4.6.1.1.3=30º Va	4.6.1.2.3=30º Va	4.6.1.3.3=30º Va	4.6.2.1.3=30º Va	4.6.2.2.3=30º Va / 4.6.2.3.3=30º Va
			4.6.1.1.4=60º Va	4.6.1.2.4=60º Va	4.6.1.3.4=60º Va	4.6.2.1.4=60º Va	4.6.2.2.4=60º Va / 4.6.2.3.4=60º Va
			4.6.1.1.5=90º Va	4.6.1.2.5=90º Va	4.6.1.3.5=90º Va	4.6.2.1.5=90º Va	4.6.2.2.5=90º Va / 4.6.2.3.5=90º Va
			4.6.1.1.6=120º Va	4.6.1.2.6=120º Va	4.6.1.3.6=120º Va	4.6.2.1.6=120º Va	4.6.2.2.6=120º Va / 4.6.2.3.6=120º Va
			4.6.1.1.7=150º Va	4.6.1.2.7=150º Va	4.6.1.3.7=150º Va	4.6.2.1.7=150º Va	4.6.2.2.7=150º Va / 4.6.2.3.7=150º Va

So= Standoff, Va = Void angle, ΔT=Differential Temperature